ENHANCING NEUROTROPHIC SUPPORT IN HUNTINGTON'S DISEASE VIA AAV-MEDIATED BDNF DELIVERY TO THE THALAMOSTRIATAL SYSTEM

Silvana Cervantes Yepez

Integrated Program in Neuroscience

McGill University, Montreal

Canada

November 2024

A thesis submitted to McGill University in partial fulfillment of the requirements of the degree of Doctor of Philosophy

© Silvana Cervantes Yepez 2024

DETAILED TABLE OF CONTENTS

ABSTRACT IN ENGLISH

This study investigates the potential therapeutic effects of overexpression of striatal brain-derived neurotrophic factor (BDNF) delivered via Adeno-associated viral (AAV) vectors in the parafascicular thalamic nucleus (PF) in the context of Huntington's disease (HD), using the R6/2 mouse model. We initially visualized the thalamostriatal system in C57BL/6J mice using biotin dextran amine (BDA) anterograde tracer, followed by evaluating AAV5-GFP gene expression and axonal transport from the PF to the striatum. Subsequently, we examined the impact of the AAV5-BDNF-GFP vector on motor behavior in R6/2 mice. Behavioral assessments included clasping, open field, and elevated plus maze tests, coupled with histological analysis through immunohistochemistry and stereology to evaluate morphological changes. Our research highlights that the AAV5-GFP vector exhibits effective GFP expression in the PF and anterograde transport to the striatum, but results indicated that our initial AAV5-BDNF-GFP construct does not significantly alter BDNF levels in the PF or TrkB receptor activation in the striatum.

Further evaluations in collaboration with the National Research Council Canada focused on the comparison between plasmid candidates pCMV-hBDNF-IRES2-hrGFP and pCMV-hBDNF-2A-eGFP, with findings suggesting that pCMV-hBDNF-2A-eGFP enhances BDNF expression and secretion *in vitro*. Additionally, we explored AAV9 vectors in C57BL/6J mice, demonstrating improved stability, BDNF overexpression and anterograde transport of AAV9-BDNF-GFP compared to AAV5 vectors. Delivery of AAV9-

BDNF-GFP vector at high titers in R6/2 mice revealed an increased incidence of sudden death. However, survival analysis showed that the diluted AAV9-BDNF-GFP vector resulted in a significant increase in median survival time compared with the non-diluted vector.

Our results suggest that the AAV9-BDNF-GFP viral construct effectively overexpresses BDNF in the PF and increases striatal BDNF levels. Utilizing PF axonal transport of the viral vector enables the dissemination of therapeutic BDNF throughout brain circuitry, thus requiring a lower viral load and providing the physiological support mechanism for thalamostriatal neurotrophic support. This approach holds promise as a therapeutic strategy for developing effective treatments for neurodegenerative diseases.

RÉSUMÉ EN FRANÇAIS

Cette étude explore les effets thérapeutiques potentiels de la surexpression du facteur neurotrophique dérivé du cerveau (BDNF, pour ses sigles en anglais) strié, délivré via des vecteurs viraux associés à l'adénovirus (AAV, pour ses sigles en anglais), dans le noyau thalamique parafasciculaire (PF) dans le contexte de la maladie de Huntington, en utilisant le modèle murin R6/2. Nous avons d'abord visualisé le système thalamostriatal chez les souris C57BL/6J en utilisant le traceur anterograde biotine dextran amine (BDA, pour ses sigles en anglais), suivi de l'évaluation de l'expression génique AAV5-GFP et du transport axonal du PF au striatum. Par la suite, nous avons examiné l'impact du vecteur AAV5-BDNF-GFP sur le comportement moteur chez les souris R6/2. Les évaluations comportementales comprenaient des tests de clasping, open field et elevated plus maze, accompagnés d'une analyse histologique par immunohistochimie et stéréologie pour évaluer les changements morphologiques. Nos recherches soulignent que le vecteur AAV5-GFP montre une expression efficace de la GFP dans le PF et un transport anterograde vers le striatum, mais les résultats ont indiqué que notre premier construct AAV5-BDNF-GFP n'altère pas significativement les niveaux de BDNF dans le PF ni l'activation du récepteur TrkB dans le striatum.

Des évaluations supplémentaires en collaboration avec le Conseil National de Recherches du Canada ont porté sur la comparaison entre les candidats plasmidiques pCMV-hBDNF-IRES2-hrGFP et pCMV-hBDNF-2A-eGFP, avec des résultats suggérant que pCMV-hBDNF-2A-eGFP améliore l'expression et la sécrétion de BDNF *in vitro*. De

plus, nous avons exploré les vecteurs AAV9 chez les souris C57BL/6J, montrant une stabilité améliorée, une surexpression du BDNF et un transport anterograde de l'AAV9-BDNF-GFP comparé aux vecteurs AAV5. La délivrance du vecteur AAV9-BDNF-GFP à des titres élevés chez les souris R6/2 a révélé une incidence accrue de décès soudains. Cependant, l'analyse de survie a montré que le vecteur AAV9-BDNF-GFP dilué entraînait une augmentation significative du temps de survie médian par rapport au vecteur non dilué.

Nos résultats suggèrent que le construct viral AAV9-BDNF-GFP surexprime efficacement le BDNF dans le PF et augmente les niveaux de BDNF striataux. L'utilisation du transport axonal du vecteur viral dans le PF permet la diffusion du BDNF thérapeutique à travers le circuit cérébral, nécessitant ainsi une charge virale plus faible et fournissant le mécanisme de soutien physiologique pour le soutien neurotrophique thalamostriatal. Cette approche semble prometteuse en tant que stratégie thérapeutique pour développer des traitements efficaces pour les maladies neurodégénératives.

ACKNOWLEDGEMENTS

Academic acknowledgements

This research would not have been possible without the financial support from The National Council for Humanities, Science and Technologies / Consejo Nacional de Humanidades, Ciencias y Tecnologías (CONAHCYT) from Mexico, FRQNT – Merit scholarship program for foreign students (PBEEE) and the annual student stipend from Dr. Abbas Sadikot's lab. I am grateful for their generous funding that enabled me to come to Canada and live in Montreal to pursue my PhD dream.

I would like to express my deepest gratitude to my supervisor, Dr. Abbas Sadikot, for his support and guidance throughout my PhD. Thank you for giving me the opportunity to join your lab and be part of the McGill community.

I am thankful to Dr. Vladimir Rymar for teaching me all the techniques I didn't know in the lab, for always being kind and willing to help with everything! Thank you for all your moral support and encouragement, for always helping me remove the fresh brains and ordering all the materials for my project.

I want to thank Dr. Rénald Gilbert and his team at the National Research Council Canada. I am thankful for their expertise and assistance in engineering the plasmids and viral vectors, their support greatly contributed to the advancement of this project.

I also extend my appreciation to the Animal facility in The Neuro. Thank you for housing and taking care of our research animals. Also thank you for training me in the ethical way to treat experimental animals.

Personal acknowledgements

-Spanish-

Antes que nada, a mi mamá. Gracias por darme el amor y la fortaleza necesaria para llegar hasta donde estoy, por pelear por mí y protegerme. Gracias por venir a verme tantas veces, por escucharme y darme ánimos cuando me siento fracasar. Irme de México y no poder verte ha sido la cosa más difícil que he hecho.

A mi papá. Gracias por apoyarme y siempre echarme ánimos en este camino. Gracias por enseñarme a ponerle ganas a todo lo que hago, a ser perseverante y a buscar maneras de solucionar los problemas.

A mi familia y amigos. Gracias por tener los brazos abiertos a mí, por estar a la distancia apoyándome y demostrándome tanto amor como cuando vivía en México. Son la luz que acompaña mi camino y no pasa un solo día que no los extrañe.

A Eric. Conocerte fue el regalo más bonito de la casualidad. Gracias por amarme y querer cuidarme día a día. Por luchar conmigo para construir un futuro juntos y por escucharme tantas horas mentando madres de lo mismo. Gracias por acompañarme a construir una mejor versión de mí. También por acompañarme en las madrugadas a trabajar y llevarme de comer; por no dejarme sola para salir a correr en la obscuridad y por ir conmigo a

otras ciudades para eventos deportivos. Gracias por impulsarme, por escuchar de mi amor por la ciencia, por creer tanto en mí y por aceptar ponerle más verduras a todo lo que comemos. Te amo.

-English-

I want to express my profound gratitude to the fitness community in Montreal, particularly to the group November Project Montreal. This is where I found my first group of friends when I arrived in Montreal -people who showed me how to dress for winter and encouraged me not to be afraid of being outdoors when the weather is challenging. It's where I finally felt like I belonged in this city. It has been my safe space every time I struggled with my mental health, and it has also been the best source of encouragement and support in general, not just in sports-related situations. Thank you to every person I've met at NP, and through running, you have made my life a million times better. Janick, co-leading, planning international events, and traveling together has been the highlight of this NP journey!

To my lab friends, Jemal, Kaitlynn, Gerardo, Lia and Vlad. This entire experience would not have been the same without you. Thank you for listening to me, supporting me, and distracting me from everything else.

Finally, I want to take a moment to express my gratitude to the animals that contributed to my research, making it possible for me to complete my PhD.

CONTRIBUTION TO ORIGINAL KNOWLEDGE

This study aims to evaluate the impact of bilateral AAV-mediated BDNF overexpression, spanning from *in vitro* studies, comparison of two different AAV serotypes, expression of specific AAV markers in transduced neurons and striatal neuronal counts to behavioral and locomotor outcomes in the R6/2 mouse model, a widely utilized animal model in Huntington's disease (HD) research. Notably, this project explores a distinct approach to AAV delivery. Unlike conventional methods that target the striatum -the most affected area in HD- the AAV vector is administered into a striatal afferent. This strategy leverages the physiological pathway of BDNF synthesis and delivery through the parafascicular thalamic nucleus, which projects predominantly to the striatum. This striatal afferent targeted approach is facilitated by the parafascicular thalamic nucleus's small size resulting in less AAV vector required and accessibility via stereotaxic coordinates, further enhancing its viability as a delivery site.

However, this novel delivery method poses challenges. While BDNF overexpression is planned to occur before symptomatic onset, it remains uncertain whether BDNF synthesis, transport and release mechanisms may already be compromised in the disease state. This could hinder adequate BDNF delivery to the striatum or lead to malfunction of TrkB receptors. In the development of gene therapy treatments, consideration must be given to ensuring the specificity of the treatment towards the targeted cell type, and the level of expression and distribution of the therapeutic protein needed to impact positively to alleviate symptoms and prevent toxic damage. Additionally, it is essential to acknowledge the limitations inherent to animal models, which may not

always fully replicate human disease conditions despite their utility in therapeutic screening.

Ultimately, this study aims to establish new therapeutic avenues using AAV-mediated gene delivery to the afferents of the targeted structure to increase neuronal survival and amelioration of symptoms, not only in HD but potentially in other neurodegenerative disorders.

CONTRIBUTION OF AUTHORS

Silvana Cervantes Yepez, under the supervision of Dr. Abbas Sadikot, performed all surgical procedures, behavioral and locomotor assays, *in vitro* and *in vivo* molecular experiments, data collection, analysis and interpretation of results, and thesis preparation.

Dr. Abbas Sadikot conceived the original idea for the study design and supervised the work.

Dr. Vladimir Rymar helped obtain fresh brains by decapitating mice.

Dr. Rénald Gilbert team at the NRC synthesized the CMV-hBDNF-2A-eGFP plasmid, transfected HEK293 cells and provided the corresponding cell pellets and supernatants. Dr. Gilbert team also produced AAV5 and AAV9 vectors.

Dr. Peter McPherson, Dr. Anne McKinney, and Dr. Abbas Sadikot as the Advisory Committee provided critical feedback and helped shape the research.

Summer student (2019) Chris Valenti performed Stereology counts in the striata of R6/2 WT, CAR and CAR-BDNF mice.

LIST OF ABBREVIATIONS

3’-UTR	3 prime untranslated region
3NP	3-Nitropropionic acid
6-OHDA	6-hydroxydopamine
AADC	Aromatic L-amino acid decarboxylase
AAV	Adeno-associated virus
AMPA	A-amino-3-hydroxy-5-methyl-4-isoxazolepropionic acid
ANOVA	Analysis of variance
AP	Antero-posterior
APC	Antigen-presenting cells
BACHD	Bacterial artificial chromosome
BAD	BCL2 associated agonist of cell death
BBB	Blood-brain barrier
BCA	Bicinchoninic acid
Bcl-2	B-cell leukemia/lymphoma 2 protein
BDA	Biotin dextran amine
BDNF	Brain-derived neurotrophic factor
bGHpA	Bovine growth hormone polyadenylation
BSA	Bovine serum albumin
CBA	Chicken β-actin
ChAT	Choline acetyltransferase
CLIC	Clathrin-independent carriers

GEEC	Glycosylphosphatidylinositol enriched endosomal compartment
CM-PF	Centromedian/Parafascicular complex
CMV	Cytomegalovirus
CNS	Central nervous system
CSF	Cerebrospinal fluid
DAB	Diaminobenzidine
DAG	Diacylglycerol
DD	Death domain
DNA	Deoxyribonucleic acid
DRG	Dorsal root ganglion
dsDNA	Double stranded deoxyribonucleic acid
DV	Dorso ventral
ECD	Extracellular domain
ECL	Enhanced chemiluminescence
EF1α	Elongation factor 1α
eGFP	Enhanced green fluorescent protein
EGFR	Epidermal growth factor receptor
ELISA	Enzyme-linked immunosorbent assay
EPM	Elevated plus maze
ER	Endoplasmic reticulum
FACS	Fluorescence-activated cell sorting assay
FGFR-1	Fibroblast growth factor receptor 1
FKHRL-1	Forkhead in rhabdomyosarcoma 1

FRS-2	Fibroblast growth factor receptor substrate 2
GABA	Gamma-aminobutyric acid
GAD	Glutamic acid decarboxylase
GDNF	Glial derived neurotrophic factor
GFAP	Glial fibrillary acidic protein
GFP-IR	Green fluorescent protein immunoreactivity
GPR108	G protein-coupled receptor 108
GTPases	Guanosine triphosphate
GUSB	B-glucuronidase
HAP1	Huntingtin-associated protein-1
HD	Huntington's disease
HEK293SF	Human embryonic kidney cells serum-free
HGFR	Met/hepatocyte growth factor receptor
HIP-1	Huntingtin interacting protein 1
hrGFP	Humanized renilla green fluorescent protein
HSPG	Heparan sulphate proteoglycan
HTT	Huntingtin protein
IA	Ibotenic acid
ICD	Intracellular domain
IP3	Inositol trisphosphate
IRES	Internal ribosomal entry sites
ITRs	Inverted terminal repeats
JNK	C-Jun N-terminal kinase

JTM	Juxtamembrane domain
KA	Kainic acid
KI	Knock-in models
M1	Primary motor cortex
M2	Secondary motor cortex
MAPK	Mitogen-activated protein kinase
MBP	Myelin basic protein
MHC II	Major histocompatibility complex II
mHTT	Mutant huntingtin protein
ML	Medio lateral
MPTP	1-methyl-4-phenyl-1,2,3,6-tetrahydropyridine
MRI	Magnetic resonance imaging
mRNA	Messenger ribonucleic acid
MSN	Medium spiny neurons
NADPH	Nicotinamide adenine dinucleotide phosphate
NF-kB	Nuclear factor kappa B
NGF	Nerve growth factor
NGS	Normal goat serum
NHP	Nonhuman primate
NIIs	Neuronal intranuclear inclusions
NMDA	N-methyl-D-aspartate
NRC	National research council canada
NSE	Neuron-specific enolase

NT-3	Neurotrophin-3
NT-4/5	Neurotrophin-4/5
NTN	Neurturin
OD	Optical density
OF	Open field
ORFs	Open reading frame
p75NTR	75 kda pan-Neurotrophin receptor
PBS	Phosphate-buffered saline
PDGFR	Platelet-derived growth factor receptor
pENK	Pre-enkephalin
PF	Parafascicular thalamic nucleus
PFA	Paraformaldehyde
PI3K	Phosphatidylinositol-3-kinase
PKC	Protein kinase C
PLC- γ	Phospholipase C-γ
QA	Quinolic acid
R6/2 CAR	R6/2 carrier mice
R6/2 WT	R6/2 wild-type mice
rAAV	Recombinant adeno-associated virus
RE1	Repressor element 1
REST	RE1-silencing transcription factor
RIP2	Receptor-interacting-serine/threonine-protein kinase 2
RIPA	Radioimmunoprecipitation assay buffer

RT-PCR	Reverse transcription polymerase chain reaction
S1	Primary somatosensory cortex
SDS-PAGE	Sodium dodecyl-sulfate polyacrylamide gel electrophoresis
Shc	Src homology and collagen protein family
SMA	Spinal muscular atrophy
SMN1	Survival motor neuron 1 promoter
SNpr	Substantia nigra pars reticulata
STN	Subthalamic nucleus
Syn	Synapsin
TBST	Tris-buffered saline with Tween
TMB	Substrate tetramethylbenzidine
TNF	Tumor necrosis factor
TRAF6	Tumor necrosis factor receptor associated factor 6
Trk	Tyrosine kinase receptors
UBC	Ubiquitin C
vg/ml	Viral genomes per ml
VP	Viral proteins
VTA	Ventral tegmental area
WPRE	Woodchuck hepatitis virus post-transcriptional regulatory element
YAC	Yeast artificial chromosomes

LIST OF FIGURES

LIST OF TABLES

Chapter 1: INTRODUCTION

Clinical aspects of Huntington's disease

Huntington's disease (HD) is an autosomal dominant neurodegenerative disorder that primarily affects the basal ganglia. It is characterized by progressive motor abnormalities, neuropsychiatric symptoms, cognitive decline, and eventual death (Ghosh & Tabrizi, 2015; Landles & Bates, 2004). Motor alterations are marked by involuntary hyperkinetic movements including chorea and sustained muscle contraction which evolve to rigidity and bradykinesia in the later stages of the disease (Ghosh & Tabrizi, 2015). Cognitive deficits may include changes in personality, disinhibition and reduced mental capability, potentially advancing to subcortical dementia. Additionally, psychiatric alterations such as anxiety and depression are common (De Souza & Leavitt, 2015). HD is caused by an expansion of CAG repeats in the exon 1 of the gene encoding the huntingtin protein (htt) located in the short arm of chromosome 4. This expansion leads to the production of long polyglutamine stretches, resulting in mutant huntingtin (mhtt) (Bates, 2005). The wild-type gene contains fewer than 36 CAG repeats whereas individuals with more than 40 repeats develop HD (Ghosh & Tabrizi, 2015). The prevalence of HD varies globally, but there is evidence that it is increasing by 15 to 20% per decade in North America, Western Europe, and Australia (Rawlins et al., 2016), particularly among the Caucasian population (E. R. Fisher & Hayden, 2014).

The most notorious neuropathological features of HD are the drastic loss of the GABAergic medium-sized spiny neurons (MSNs) in the striatum and severe atrophy of the neocortex (Alberch, Pérez-Navarro, & Canals, 2004). MSNs are projection neurons

that constitute 95% of all neurons in the striatum. They are divided into two groups: the direct pathway neurons, which project to the substantia nigra pars reticulata (SNpr) and the internal segment of the globus pallidus; and the indirect pathway neurons, which project to the globus pallidus external segment (Alberch et al., 2004). In HD, neurons of the indirect pathway begin to degenerate in the early to middle stages, while at the most advanced stages, all striatal projections are affected (Reiner et al., 1988). Recent evidence suggests that striatal interneurons co-expressing somatostatin and neuropeptide-Y are spared, whereas cholinergic and parvalbumin striatal interneurons degenerate (Reiner et al., 2013; R. Smith et al., 2006). In advanced stages of the disease, there is a reduction in the number of pyramidal neurons of layers II-III, V and VI of the association and motor cortices, suggesting a significant role for the corticostriatal pathway in striatal impairment (Alberch et al., 2004).

HTT protein

The wild-type htt protein is expressed ubiquitously throughout the body, with the highest levels observed in the brain, including in both neurons and glial cells (Schulte & Littleton, 2011). htt is predominantly a cytoplasmic protein that functions as a molecular center, either facilitating the formation of proteins complexes or promoting their dissociation, depending on a fine coordination of cellular processes (Illarioshkin, Klyushnikov, Vigont, Seliverstov, & Kaznacheyeva, 2018). This protein is crucial during development for gastrulation and neurogenesis; homozygous knockout mice do not survive beyond embryonic day 8.5 (Nasir et al., 1995). In the adult brain, htt is important for neuronal survival (Chiara Zuccato, Ciammola, Rigamonti, Leavitt, & et al., 2001). It associates with cell membranes, vesicles, and the cytoskeleton, and it is involved in various processes

such as endocytosis, intracellular trafficking, synaptic transmission, regulation of autophagy, transcriptional regulation and dynamics of vesicular transport. These functions impact directly the neuronal fate and general signal transduction (Illarioshkin et al., 2018). The CAG expansion in the htt gene causes conformational changes in the protein, altering its interactions with other proteins and its degradation, which results in the formation of intracellular aggregates (Illarioshkin et al., 2018). Given the critical role of wild type htt, any modifications to this protein significantly disrupt cellular functions.

Evidence from both *in vitro* and *in vivo* studies indicate that mhtt is associated with abnormalities in glutamatergic and dopaminergic transmission in the forebrain, altered striatal enriched proteins, microglial activation, neuroinflammation, mitochondrial dysfunction, impaired protein clearance and abnormal axoplasmic transport (Landles & Bates, 2004). Additionally, small mhtt fragments translocate to the nucleus and form intranuclear aggregates, which interfere with the proper regulation of gene expression (Illarioshkin et al., 2018). One of the genes negatively affected by mhtt is the brain-derived neurotrophic factor (BDNF) gene (Chiara Zuccato et al., 2001), a member of the neurotrophin family.

Neurotrophic support

Neurotrophins are secreted proteins that promote neuronal development, plasticity and survival. Four neurotrophins have been abundantly described: nerve growth factor (NGF), brain-derived neurotrophic factor (BDNF), neurotrophin-3 (NT-3) and neurotrophin-4/5 (NT-4/5) (Barde, Edgar, & Thoenen, 1982; Cohen, 1960; Hohn, Leibrock, Bailey, & Barde, 1990; Ip et al., 1992; Levi-Montalcini & Hamburger, 1951). These proteins bind to two types of receptors: Tropomyosin receptor kinases (Trks) and the 75 kDa pan-neurotrophin

receptor (p75NTR). Trk receptors are involved in pro-survival signaling, while p75NTR mediates degenerative signaling pathways (C. Ceni et al., 2010; Claire Ceni, Unsain, Zeinieh, & Barker, 2014; Gibon & Barker, 2017; Illarioshkin et al., 2018; Matusica et al., 2013; P. P. Roux, Colicos, Barker, & Kennedy, 1999; Savolainen, Emerich, & Kordower, 2018; Simmons, 2017; Skaper, 2008). The neurotrophic hypothesis, based on NGF function, posits that neurons responsive to a trophic factor project axons to specific targets that produce the factor to ensure their survival. Upon binding to specific membrane receptors on the neuronal projections' terminals, the factor/receptor complex is internalized. The complex is then retrogradely transported from the terminal to the cell body, where it exerts effects on survival and differentiation. In contrast, neurotrophins like BDNF, are synthetized as pro-neurotrophins, in this case pro-BDNF. Depending on specific regulatory mechanisms, pro-BDNF can be cleaved into mature BDNF or remain as pro-BDNF to then be sorted into large dense core vesicles that follow the regulatory secretory pathway. These vesicles are anterogradely trafficked from the cell body along axonal processes and stored within pre-synaptic terminals. BDNF is released from axon terminals via calcium-dependent exocytosis upon depolarization. Once secreted, mature BDNF binds to its specific membrane receptor, TrkB, on the target neuron. The BDNF/TrkB complex is then internalized and is retrogradely transported to the cell body of the target neuron, where it promotes survival, plasticity and differentiation (Conner, Lauterborn, & Gall, 1998; Gibon & Barker, 2017; Von Bartheld, Byers, Williams, & Bothwell, 1996).

Striatal afferent systems

The striatum receives neurotrophic support from three main afferent systems: the corticostriatal and thalamostriatal glutamatergic pathways and the nigrostriatal dopaminergic pathway. Approximately 90% of corticostriatal synapses are formed with dendritic spines, while the remaining synapses are with dendritic shafts and cell bodies of striatal neurons. Within the thalamus, the parafascicular thalamic nucleus (PF) extensively innervates the matrix compartment of the striatum, with some sparse projections to the subthalamic nucleus (STN) and the cerebral cortex. The majority of PF terminals form synapses on dendritic shafts of striatal neurons (Mandelbaum et al., 2019; Y. Smith, Raju, Pare, & Sidibe, 2004). Conversely, nigrostriatal afferents from the substantia nigra pars compacta (SNpc) primarily form synapses on the neck of dendritic spines, close to cortical inputs, rather than to PF inputs. Based on anatomical structures, it is suggested that dopaminergic afferents modulate glutamatergic inputs, particularly cortical inputs (Y. Smith et al., 2014; Y. Smith et al., 2004). Notably, around 70-90% of projections from the PF reach and cover the striatum from the anterior to the posterior portion, making this nucleus a promising target for delivering therapeutic agents (Gonzalo-Martín, Alonso-Martínez, Sepúlveda, & Clasca, 2024; Mandelbaum et al., 2019; Y. Smith et al., 2014).

BDNF-mediated anterograde neurotrophic support

Striatal neurons express TrkB receptors but do not contain BDNF mRNA. Instead, BDNF protein is synthesized by corticostriatal, thalamostriatal and nigrostriatal afferents. BDNF is then transported anterogradely along these axonal projections to the striatal neurons. Once in the striatum, the BDNF/TrkB complex activates signaling cascades that promote

the survival and maintenance of the neurochemical and morphological properties of these neurons (Altar et al., 1997; Fawcett et al., 2000; Kirschenbaum & Goldman, 1995; Nguyen, Rymar, & Sadikot, 2016; Samadi et al., 2013). The neurotrophic hypothesis of HD suggests that decreased BDNF synthesis, transport and delivery to the striatum contribute to striatal neuronal degeneration (C. Zuccato, Valenza, & Cattaneo, 2010).

BDNF synthesis and transport in HD

In HD patients and animal models, evidence shows that neurotrophin levels and Trk receptors decrease, while p75NTR protein levels and its activation increase. This shift results in a loss of survival signaling and an increase in degenerative pathways (Ferrer, Goutan, Marin, Rey, & Ribalta, 2000; Simmons, 2017; C. Zuccato et al., 2008). Prior to striatal degeneration, there are deficits in TrkB activation and the regulation of downstream molecules in the striatum (Nguyen et al., 2016). Additionally, progressive reduction in BDNF mRNA in the motor cortex and thalamic striatal afferents coincides with motor dysfunction and striatal neuronal loss (Samadi et al., 2013). Consequently, several studies suggest that BDNF acts as a neuroprotective agent in HD models (Benraiss & Goldman, 2011; Kirschenbaum & Goldman, 1995; Nguyen et al., 2016; Samadi et al., 2013).

Reports indicate that BDNF protein production is partially regulated by the action of wild-type htt in the BDNF promoter II. When htt is mutated (HD), it acquires toxic functions that inhibit BDNF transcription and disrupt the motor complex responsible for transporting vesicles along microtubules in both anterograde and retrograde directions (Chiara Zuccato et al., 2001). Congruently, this regulation is lost in the early stages of HD, leading

to reduced BDNF transport to the striatum and resulting in neuronal damage due to insufficient neurotrophic support.

R6/2 mouse model

The R6/2 mouse model is one of the most commonly used for studying HD (Gil & Rego, 2009). This transgenic mouse line carries a 1.9 kb human genomic fragment containing promoter sequences and the exon 1 of the htt gene, which includes approximately 130-140 CAG repeats (Mangiarini et al., 1996). The R6/2 mouse exhibits a progressive neurological phenotype; with early onset of symptoms around 8 weeks of age and rapid progression leading to death generally by 13 weeks. This model effectively replicates many characteristics of juvenile human HD, including choreiform-like movements, epileptic seizures, resting tremor, limb clasping, involuntary stereotypic movements (such as repetitive stroking of the nose and face or hind limb kicking or scratching), and non-movement disorder components like anxiety and depression-like behaviors (Lüesse et al., 2001; Mangiarini et al., 1996). One of the earliest noticeable motor symptoms in R6/2 mice is dyskinesia of the limbs when suspended by the tail; affected mice clasp their limbs together and are unable to change their posture. Additionally, these mice begin to lose weight and muscle bulk around the same time motor symptoms emerge (Mangiarini et al., 1996; Samadi et al., 2013).

R6/2 mice are also characterized by decreased striatal and cortical volume, altered neurotransmitter levels and receptor expression, and a progressive decrease in BDNF mRNA detected in striatal afferents between 6-13 weeks of age, which is associated with impaired motor coordination (Gil & Rego, 2009; Mangiarini et al., 1996; Samadi et al., 2013). At 6 weeks of age, a reduction in neostriatal volume is observed, with neuronal

atrophy beginning by 9 weeks and preceding neuronal loss. Striatal neuronal degeneration progresses rapidly between 6 and 13 weeks of age (Samadi et al., 2013).

Gene therapy

All the evidence above suggests that one of the primary processes affected in HD is the striatal BDNF neurotrophic support (Simmons, 2017). Currently, there are no treatments available that can prevent or slow the disease progression. However, BDNF administration as a therapeutic strategy is supported by solid preclinical data from various animal models. Despite reduced TrkB levels and activity, administering BDNF can improve the neuropathological phenotype (C. Zuccato & Cattaneo, 2009). The challenge with exogenous neurotrophins includes their low stability, short serum half-lives, poor availability through oral routes, and restricted blood-brain barrier (BBB) permeability. Even invasive delivery methods may result in limited neurotrophin diffusion and require repeated administration due to the progressive nature of the disease (Simmons, 2017). A promising alternative involves using viral vectors engineered to encode the BDNF protein. Although this method is invasive because it requires injection into the subcortical target area, it typically requires only a single injection. The viral vector enables continuous production of the neurotrophin by the neuron (Simmons, 2017). Extensive research has been done trying to deliver neurotrophic factors to striatal neurons through gene therapy, taking as an advantage that its production would be constant and local. Furthermore, BDNF long-term expression from adeno-associated viral (AAV) vectors has been successfully developed and has produced encouraging results (C. Zuccato & Cattaneo, 2009).

Adeno-associated viral vectors

AAVs are small (25nm), icosahedral, non-enveloped viruses with single-strand DNA genome of 4.7kb. They require a helper virus, either adenovirus or herpesvirus, for replication (Daya & Berns, 2008). The AAV genome includes 145-bp inverted terminal repeats (ITRs) that flank two open reading frames (ORFs), coding for proteins necessary for the viral life cycle (Daya & Berns, 2008). AAVs bind to specific cell surface receptors and enter the cell via endocytosis. The viral genome is then released from the capsid and transported to the nucleus for transcription (Savolainen et al., 2018). After infection, the virus undergoes a lytic stage followed by a lysogenic stage. Helper viruses regulate cellular gene expression, providing a favorable environment for AAV to function. In the absence of a helper virus, AAV replication is limited, viral gene expression is inhibited, and the AAV genome can integrate into a specific region on chromosome 9 for latent infection (Daya & Berns, 2008). Current AAV vectors are engineered to avoid site-specific integration, although ITRs are retained for genome packaging. These recombinant AAV vectors (rAAVs) persist as extrachromosomal elements (Daya & Berns, 2008; Issa, Shaimardanova, Solovyeva, & Rizvanov, 2023).

rAAVs are widely used in gene therapy for the Central Nervous System (CNS) due to their remarkable efficacy, safety, non-pathogenic nature, and ability to infect both dividing and non-dividing cells, especially neurons (Issa et al., 2023; Michaël, Laura, Mickael, Samantha, & Nathalie, 2016; Savolainen et al., 2018). While AAV2 is the most studied serotype, it has been found less effective than other to other serotypes in transducing neurons and producing a smaller radius of transgene expression (Aschauer, Kreuz, & Rumpel, 2013; Burger et al., 2004; Cearley & Wolfe, 2006). New rAAV types have been

developed by inserting the AAV2 genome into the capsids of other AAV serotypes, resulting in different capsid/cell interactions. In the nomenclature, when a rAAV possesses the AAV5 capsid but the AAV2 genome for example, the abbreviation can be written as follows: rAAV2/5, rAAV5/2 or AAV5. Each AAV serotype has a distinct affinity for specific cell surface receptors, establishing cell tropism (Bell, Gurda, Van Vliet, Agbandje-McKenna, & Wilson, 2012; Hordeaux et al., 2018; Shen, Bryant, Brown, Randell, & Asokan, 2011). Upon binding to its receptor, additional cell surface coreceptors facilitate entry into the cell (Akache et al., 2006; Bell et al., 2012; Issa et al., 2023).

AAVs are abundantly used in gene therapy research. Common serotypes include AAV9, AAV5 and AAV1, with different promoters depending on the targeted cell type. Studies have been conducted in various CNS regions, including the striatum, cerebral cortex, ventral tegmental area (VTA), substantia nigra, thalamus and cerebellum in mice, rats, nonhuman primates (NHP) and humans (Burger et al., 2004; Cearley & Wolfe, 2007; Connor et al., 2016; Davidson et al., 2000; Eslamboli et al., 2005; Kells et al., 2004; Kells, Forsayeth, & Bankiewicz, 2012; Kells et al., 2009; Kells, Henry, & Connor, 2008; S. F. Li et al., 2006; McBride et al., 2003; Pearson et al., 2021; S. Ramaswamy et al., 2009; Watakabe et al., 2015).

AAV vectors offer a significant potential for developing treatment strategies for HD. For example, McBride et al. (McBride et al., 2003) reported histological and behavioral protection in rats treated with 3 nitropropionic acid (3NP) following bilateral striatal injections of AAV-GDNF (glial-derived neurotrophic factor). Connor et al., (Connor et al.,

2016), found that bilateral striatal injections of AAV1-BDNF in homozygous HD rats attenuated impairments in motor and cognitive function. Kells et al. (Kells et al., 2004; Kells et al., 2008) observed increased survival of striatal MSN and interneurons after unilateral injection of AAV1-BDNF in quinolic acid (QA) treated rats. In these studies, AAV effectively transduced small sections of the striatum, resulting in a limited radius of BDNF expression.

This study introduces a novel approach aiming to enhance BDNF distribution throughout the striatal structure. By targeting the PF for AAV-BDNF vector transduction instead of direct striatal injection, our research takes advantage of the natural pathway for BDNF synthesis, anterograde transport, and release to striatal neurons.

Anterograde transport of transgenes

Previous studies have demonstrated the feasibility of delivering an AAV vector into an afferent pathway of a targeted structure. This method allows the vector to express the intended protein, which is then transported to the targeted structure to exert its effects. Cearley and Wolfe (Cearley & Wolfe, 2007) compared the axonal transport of a rAAV9 after delivery to the striatum versus the VTA. They found that the VTA spread the transgene more widely throughout the brain parenchyma due to its extensive efferent and afferent projections. AAV1 and AAV10 were also transported anterogradely from the VTA, though at lower expression levels than AAV9. Bankiewicz and colleagues reported widespread expression of GDNF in targeted cortical regions following a single AAV2-GDNF injection in the primate thalamus (Kells et al., 2009). In another study, GDNF was transported anterogradely to the SNpr and STN following AAV2-GDNF injection into the

striatum of 1-methyl-4-phenyl-1,2,3,6-tetrahydropyridine (MPTP) treated primates, resulting in recovery of dopamine activity and motor function (Kells et al., 2012). The same group administered AAV2-AADC (aromatic L-amino acid decarboxylase) into the SN and VTA of children with AADC deficiency, leading to clinical improvement through increased dopamine metabolism in the midbrain and striatum (Pearson et al., 2021). Eslamboli et al. (Eslamboli et al., 2005) observed anterograde transport of GDNF to the globus pallidus and recovery of dopamine metabolism following AAV2-GDNF injection into the 6-hydroxydopamine (6-OHDA) treated primate striatum. Ramaswamy et al. (S. Ramaswamy et al., 2009) reported anterograde transport of NTN (neurturin) to the SNpr and globus pallidus, along with amelioration of HD symptoms, after AAV2-NTN injection into N171-82Q mice.

To date, no studies have explored this anterograde approach using AAV-mediated BDNF overexpression in gene therapy interventions for Huntington's disease.

RESEARCH GOALS

HYPOTHESIS

BDNF overexpression in striatal afferents may lead to increased neuronal survival and maintenance of phenotype in the striatum of R6/2 mice.

Bilateral overexpression of BDNF in the Parafascicular thalamic nuclei could potentially improve the behavioral and general locomotor alterations present in R6/2 mice.

GENERAL AIMS

- Determine if BDNF can be overexpressed in C57bl/6J mice using AAV-BDNF-GFP constructs in the thalamostriatal system including neurons at the injection site and functional release at the striatum.
- Determine if BDNF can be overexpressed in R6/2 mice using AAV-BDNF-GFP constructs in the thalamostriatal system including neurons at the injection site and functional release at the striatum.
- Determine whether AAV-BDNF-GFP constructs can protect striatal neurons.
- Determine whether the effect is functionally relevant using behavioral and locomotor activity assays, such as Open Field, Elevated Plus Maze and Clasping test.

SPECIFIC AIMS

- Visualize the thalamostriatal system in C57BL/6J mice using the anterograde neuronal tracer biotin dextran amine (BDA)
- Determine AAV5-GFP expression and axonal transport timeline
- Build a baseline of R6/2 model behavior and locomotor activity
- Evaluate changes in behavior and locomotor activity in AAV5-BDNF-GFP treated R6/2 mice
- Analyze AAV-induced changes in striatal neuronal number using Stereology
- Evaluate gene expression after bilateral injection in the PF with AAV5-BDNF-GFP in the striatum and at the injection site of C57BL/6J mice
- Select a preclinical overexpression plasmid candidate

- Select a preclinical AAV viral vector candidate
- Evaluate gene expression after bilateral injection in the PF with AAV9-BDNF-GFP in the striatum and at the injection site of C57BL/6J mice

RELEVANCE STATEMENT

Huntington's disease is a hereditary neurodegenerative disorder primarily affecting the basal ganglia, leading to progressive motor abnormalities, neuropsychiatric symptoms, cognitive decline, and ultimately death. Currently, there are no treatments capable of halting its progression, and its prevalence in North America is rising by 15 to 20% per decade. Extensive research has focused on the neuroprotective effects of BDNF in striatal neurons. With advancements like rAAV-mediated gene therapy, there is now potential to administer neurotrophins directly to striatal afferents, facilitating their anterograde transport to the striatum in a physiological manner. If administered early in the disease course, this approach may aim to slow symptom progression and potentially improve the quality of life for affected individuals. Moreover, success in the R6/2 mouse model of HD suggests this therapeutic strategy might hold promise for treating other currently untreatable neurodegenerative diseases as well.

Chapter 2: COMPREHENSIVE REVIEW OF THE RELEVANT LITERATURE

Neurotrophins and Gene Therapy in Huntington's Disease: A Comprehensive Review

Huntington’s disease (HD) is an autosomal dominant neurodegenerative disorder that predominantly affects the basal ganglia leading to significant neuronal death and dysfunction in the brain. HD is characterized by progressive motor abnormalities including chorea, dystonia and incoordination; mood disturbances such as increased anxiety and depression; cognitive decline accompanied by personality changes and dementia; and eventually, death. It is caused by a repeat expansion mutation in the gene IT15, which codes for the huntingtin protein (htt) resulting in abnormally long polyglutamine tracks of more than 36 CAG repeats and the formation of cytoplasmatic and intranuclear inclusions. The length of the expansion is correlated with the onset and severity of the disease; expansions of approximately 70 glutamines or more are observed in juvenile HD cases. Symptoms typically begin in middle age, but the disease can develop at any time between infancy to senescence (Landles & Bates, 2004; Rangone, Humbert, & Saudou, 2004; Walker, 2007). Moreover, the onset of the disease tends to occur earlier in successive generations due to the instability of the CAG repeats during germline transmission, a phenomenon known as genetic anticipation (Rangone et al., 2004).

The precise pathological mechanisms are not fully understood. However, one of the most significant neurodegenerative changes in HD is the selective loss of GABAergic medium

spiny neurons (MSN) in the striatum (Landles & Bates, 2004; Rangone et al., 2004; C. Zuccato & Cattaneo, 2009). Some of the pathogenic mechanisms involved include 1) altered vesicular transport, 2) neuronal intranuclear inclusions, 3) excitotoxicity due to increased input from glutamatergic afferents, 4) transcriptional dysregulation with disrupted metabolic processes, and 5) impaired neurotrophic support from striatal afferents (DiFiglia et al., 1995; Landles & Bates, 2004; Reiner, Dragatsis, & Dietrich, 2011; C. Zuccato & Cattaneo, 2009). Despite the known genetic mutation, there is currently no effective therapy for this neurodegenerative disease.

Huntingtin vs mutated huntingtin

Htt protein is expressed at high levels throughout the brain, in both the nucleus and cytoplasm of cells. During embryonic development, neurogenesis, and in adult life, htt is essential as an antiapoptotic protein. This is likely related to its role in regulating the transcription of brain-derived neurotrophic factor (BDNF), a neurotrophin critical for the differentiation and maintenance of neurons in the brain (Rangone et al., 2004; Chiara Zuccato et al., 2001). Additionally, the association of htt with factors like huntingtin interacting protein 1 (HIP-1) forms a complex involved in endocytosis. However, when HIP-1 is not associated with the complex due to structural changes in mhtt, HIP-1 induces caspase-8 activation through its death effector domain (Gervais et al., 2002; Metzler et al., 2001).

Impaired vesicular transport by mhtt

Within the cytoplasm, htt is present in neuronal cell bodies, dendrites and axons and is associated with vesicular structures such as clathrin-coated vesicles, caveolae, endosomes and microtubules. This suggests its significant role in the secretory pathway, exo- and endocytosis, intracellular transport, microtubule-dependent transport of organelles, and membrane cycling throughout the neuron (DiFiglia, 2002; DiFiglia et al., 1995; Velier et al., 1998). Vesicular transport in both anterograde and retrograde directions along microtubules is htt-dependent and requires the involvement of molecular motors with dynactin and dynein, respectively. The different structure of mhtt results in a loss of interaction with the motor complex, microtubules, and vesicles (Gauthier et al., 2004; Liot et al., 2013).

Neuronal intranuclear inclusions

The mutation in htt alters protein structure, causing a loss of normal functions and acquisition of toxic functions. mhtt can be proteolytically cleaved and translocated to the nucleus. Within the nucleus, htt plays an active role in regulating transcription factors by transporting them between the nucleus and cytoplasm or directly affecting transcription (Rangone et al., 2004; Chiara Zuccato et al., 2001). Although neuronal intranuclear inclusions (NIIs) are a pathological hallmark of HD, NIIs may reflect a cellular mechanism to protect against soluble mhtt-induced cell death. Studies of striatal neurons transfected with mhtt showed induction of apoptotic mechanisms; however, the presence of NIIs did not correlate with mhtt-induced death. Inhibition of ubiquitin-mediated proteolysis blocked the formation of NIIs and an increased mhtt-induced death. Nonetheless, NIIs disrupt

intracellular homeostasis by inhibiting the proteasome, dysregulating synaptic activity and transport, and inducing neurite degeneration (Rangone et al., 2004; Saudou, Finkbeiner, Devys, & Greenberg, 1998). mhtt aggregates also disrupt mitochondrial homeostasis early in the disease progression, leading to the release of cytochrome C, which promots energy metabolism dysfunction, activation of caspases, and disruption of calcium flux, thereby increasing oxidative stress, contributing to excitotoxic processes, and activating proteases such as calpain. Calpain and caspases are among the proteases that cleave mhtt in smaller fragments facilitating translocation to the nucleus (DiFiglia, 2002; Rangone et al., 2004).

Excitotoxicity related to glutamatergic afferents

Alterations are present in synaptic transmission, particularly in the cortical-basal ganglia-thalamic circuits. One of the early features of HD is increased cortical excitability, accompanied by alterations in neurotransmission in the thalamostriatal projections and reduced modulation of excitatory input by dopaminergic projections (Holley et al., 2022; Kolodziejczyk & Raymond, 2016). In two mouse models of HD, R6/2 and YAC128 mice, age-dependent changes in neurotransmission occur. Before the appearance of behavioral symptoms, synaptic currents and glutamate release are elevated with a higher intracellular Ca^{2+} flux (P. R. Joshi et al., 2009). During the early symptomatic stage, transient and highly synchronized cortical synaptic events of large amplitude converge on striatal neurons, exerting excessive spontaneous excitatory neurotransmitter release, possibly due to a lack of dopaminergic regulation. Large events of enhanced and synchronized cortical activity produce cortical epileptogenicity in R6/2 animals (Cepeda

et al., 2003; P. R. Joshi et al., 2009). Additionally, increased glutamate exposure could trigger alterations in postsynaptic neurons. Compensation mechanisms include downregulating AMPA–kainate receptors and decreasing the numbers of dendritic spines, which results in progressive deafferentation associated with a loss of presynaptic and postsynaptic marker proteins. Consistent with this, during the late symptomatic stage, evoked synaptic currents and glutamate release are drastically reduced (Cepeda et al., 2003). Similarly, the YAC128 striatal MSN with mhtt are more sensitive to NMDA-induced toxicity, possibly because these neurons express a higher proportion of NMDA receptors at extrasynaptic sites, which trigger cell death signaling. Activation of NMDA receptors at the synaptic site promotes neuroprotective gene transcription (Kolodziejczyk & Raymond, 2016; Milnerwood et al., 2010). Therefore, it is not only the reduced expression of receptors in HD, but also changes in the receptor localization.

Transcriptional dysregulation by mhtt

Microarray studies in the late symptomatic stage of two mouse models of HD, the R6/2 and N171-82Q mice, revealed that mhtt disrupts the transcriptional machinery. Some of the downregulated mRNAs are involved in signal transduction, such as dopamine, glutamate, cannabinoid, and adenosine receptors, the GABA-synthesizing enzyme glutamic acid decarboxylase (GAD), and the neuropeptide precursors for enkephalin and somatostatin. A decrease in mRNAs of many intracellular downstream signaling components was also observed. Calcium-related mRNAs, nuclear hormone receptors, and mRNA of genes related to transcription, metabolism and cell structure, like a-actinin-2, showed decreased expression (Luthi-Carter et al., 2000). Similar results were obtained

from studies using agonist-receptor binding autoradiography in R6/1, R6/2 and R6/5 brains, which showed a severe decrease in receptor expression by the end of their lives, including AMPA, kainate and group II mGluR (but not NMDAR) in the striatum and cerebral cortex, and acetylcholine and dopamine receptors (D1 and D2) in the striatum (Cha et al., 1999). Specifically, in R6/2 mice, mRNA of A2a adenosine receptors and metabotropic glutamate receptors are reduced in the pre-symptomatic stage at 4 weeks of age, while a reduction in dopamine receptors occurs during the symptomatic stage at 8 weeks, resulting in reduced modulation of the presynaptic terminal (P. R. Joshi et al., 2009). Another gene that is highly influenced by htt is the BDNF-coding gene; the resulting BDNF protein is a member of the neurotrophin family (Gauthier et al., 2004; Liot et al., 2013; Samadi et al., 2013; C. Zuccato & Cattaneo, 2009; Chiara Zuccato et al., 2001).

Neurotrophins, synthesis and signaling cascades

The groundbreaking research of Rita Levi-Montalcini and Victor Hamburger in 1951 (Levi-Montalcini & Hamburger, 1951) led to the discovery of a growth factor secreted by mouse sarcomas. When this factor was implanted into chick embryos, it promoted the differentiation and growth of sympathetic and sensory neurons from the spinal ganglia. Stanley Cohen further purified this growth factor from the mouse submaxillary gland in 1960 (Cohen, 1960), which was later named nerve growth factor (NGF) and earned them the Nobel Prize in Physiology or Medicine in 1986.

Following the discovery of NGF, Barde and colleagues isolated BDNF from pig brains in 1982 (Barde et al., 1982). BDNF was found to support the survival and fiber outgrowth of embryonic chick sensory neurons, which sparked interest in exploring other members of the neurotrophin family based on protein structural similarities and DNA sequences. In

1990, Hohn and colleagues identified Neurotrophin-3 (NT-3) in mice (Hohn et al., 1990), which was subsequently identified in humans by Jones and Reichardt (Jones & Reichardt, 1990). Neurotrophin-4 (NT-4) was discovered and isolated from Xenopus and vipers by Hallböök et al. in 1991 (Hallbook, Ibanez, & Persson, 1991), while Berkemeier et al. identified Neurotrophin-5 (NT-5) in rats (Berkemeier et al., 1991). Nearly simultaneously, Ip and colleagues discovered a neurotrophin they termed Neurotrophin-4 (NT-4) in rats and humans (Ip et al., 1992). The nomenclature for NT-4/5 arose due to overlapping discoveries by Berkemeier and Ip (Berkemeier et al., 1991; Ip et al., 1992).

The neurotrophin family

Neurotrophins constitute a family of secreted growth factors crucial for the development and maintenance of the nervous system. They are categorized into a single family based on their homologous genes, amino acid sequence, and protein structure. Neurotrophins exert their effects through interaction with specific receptors, primarily the tropomyosin receptor kinases (Trks) and p75 neurotrophin receptor (p75NTR), which influence diverse cellular processes including survival, differentiation, growth, and apoptosis (Conner et al., 1998).

Initially synthesized as proneurotrophins of ~30 kDa -pro-NGF, proBDNF, proNT-3, and proNT-4/5- these precursors undergo proteolytic cleavage in the Golgi apparatus to generate mature neurotrophins (~13 kDa). Mature neurotrophins bind to both Trk receptors and p75NTR, whereas proneurotrophins preferentially bind to a receptor complex comprising sortilin or SorCS2 along with p75NTR (Gonzalo-Martín et al., 2024).

Structurally, neurotrophins share similarities in their peptide signal sequences, pro-peptide regions which are involved in correct protein folding and disulfide bond formation, the cleavage site and six conserved cysteine residues. Comparative amino acid sequence analysis reveals significant homology among NGF, BDNF, NT-3, and NT-4/5, highlighting their evolutionary conservation across species, from fish to humans (Hallbook et al., 1991; Hohn et al., 1990; Jones & Reichardt, 1990).

Neurotrophin synthesis and secretion involve intricate intracellular trafficking mechanisms. They are synthesized as preproneurotrophins in the endoplasmic reticulum (ER) and then cleaved to proneurotrophins in the ER lumen. Proneurotrophins are further processed by enzymes like furin and convertases in the Golgi apparatus. Next, they are sorted into the trans-Golgi network and packaged into vesicles to enter either the constitutive secretory pathway or regulated secretory pathways. In the constitutive pathway, vesicles release their cargo by default when they reach the plasma membrane, whereas in the regulated secretory pathway, vesicles are released from axon terminals in response to depolarization.

Neurotrophin release is further regulated by intracellular signaling that modulates vesicle translocation via microtubules to the active zone at the synaptic cleft. Release occurs by exocytosis of presumptive large dense-core vesicles and requires synaptobrevin-like molecules to fuse with the membrane. BDNF predominantly traffics through the regulated secretory pathway, while NGF and NT-3 can utilize both pathways (Costa, Perestrelo, & Almeida, 2018).

Proneurotrophins can be cleaved intracellularly and then secreted as mature neurotrophins; secreted as proneurotrophins with extracellular cleavage by plasmin; or secreted as proneurotrophins without subsequent cleavage. The expression, processing and secretion of proneurotrophins is highly regulated. The ratio between the pro and mature forms of neurotrophins can influence cellular responses, ranging from neuronal survival to cell death (Costa et al., 2018).

Trk receptors

p75NTR was initially identified as the sole receptor for NGF (Johnson et al., 1986). However, it was later found that TrkA, previously known as the *trk* oncogene, also binds and responds to NGF (D. R. Kaplan, Hempstead, Martin-Zanca, Chao, & Parada, 1991; David R. Kaplan, Martin-Zanca, & Parada, 1991). TrkB, discovered shortly thereafter and sharing structural homology with TrkA, is activated by BDNF and NT-4/5 (Berkemeier et al., 1991; R. Klein, Parada, Coulier, & Barbacid, 1989). TrkC, identified by Lamballe et al. in 1991 (Lamballe, Klein, & Barbacid, 1991), was confirmed as the functional receptor for NT-3 through screening of a porcine brain cDNA library. Trk receptors are glycoproteins belonging to a family of cell surface transmembrane tyrosine kinase receptors (Martin-Zanca, Hughes, & Barbacid, 1986). Their general structure includes an extracellular domain (ECD), a transmembrane domain and an intracellular domain (ICD). The ICD of Trk receptors comprises a tyrosine kinase catalytic domain and a short carboxy-terminal tail of approximately 15 amino acids (Barbacid, 1994).

The mouse *trkB* gene locus codes for two receptor isoforms: the full-length receptor $gp145^{trkB}$ ($TrkB.tk^{+}$) and the truncated isoform $gp95^{trkB}$ (TrkB.t1). TrkB.tk+ is a 145 kDa

protein consisting of 821 amino acids, whereas TrkB.t1 is 95 kDa and encodes 476 amino acids. Both isoforms share identical signal peptides, extracellular domains, and transmembrane domains. However, only TrkB.tk+ contains a catalytic tyrosine-protein kinase domain in its ICD (Rüdiger Klein, Conway, Parada, & Barbacid, 1990). This indicates that both TrkB isoforms can bind BDNF and NT-4/5 as ligands (Berkemeier et al., 1991; Ip et al., 1993), but TrkB.t1 lacks catalytic kinase activity. NT-4 shares a close structural resemblance and biological activity with BDNF. Despite their similarities, a distinction arises in the interaction with the $TrkB^{S345}$ mutant receptor variant, which features a $cysteine^{345}$ residue instead of the usual $serine^{345}$ at its extracellular domain. $TrkB^{S345}$ remains responsive to BDNF but not to NT-4/5, suggesting that although mammalian NT-4/5 interacts specifically with TrkB, this interaction is structurally distinguishable from TrkB-BDNF (Ip et al., 1993).

Trk receptors signaling

Activation of Trk receptors by neurotrophins initiates a series of signaling events crucial for neuronal differentiation, mitogenic stimuli, or survival. This activation begins with ligand binding, which induces receptor dimerization at the cell surface. The kinase domains of Trk receptors are then brought into proximity, facilitating auto- and transphosphorylation of tyrosine residues within the kinase domain and other regions of the ICD (Barbacid, 1994; Claire Ceni et al., 2014). Phosphorylated tyrosine residues act as docking sites for downstream signaling enzymes and adaptor proteins. Enzymes are activated via tyrosine phosphorylation, while adaptors facilitate interaction with other

downstream signaling molecules. Subsequently, activated receptors are internalized and transported towards the cell body (Barbacid, 1994; Meldolesi, 2017).

Key tyrosine residues within the Trk intracellular region, such as Y490 and Y785, function as docking sites for adaptor proteins like Shc and FRS2 (Claire Ceni et al., 2014; Meakin, Macdonald, Gryz, Kubu, & Verdi, 1999). When Y490 is phosphorylated, it recruits Shc, which then undergoes phosphorylation and facilitates the recruitment of signaling molecules that activate phosphatidylinositol-3-kinase (PI3K). PI3K, in turn, activates Akt, a central regulator of neuronal survival, which inhibits pro-apoptotic factors such as BAD, caspase 9, and the FKHRL1 transcription factor (Brunet et al., 1999; Claire Ceni et al., 2014; Datta et al., 1997). Activation of Shc can also initiate another pathway by transiently activating MAPK, which is associated with mitogenic and proliferative cell signaling (Meakin et al., 1999). Conversely, activation of FRS-2 at phosphorylated Y490 promotes downstream signaling that induces sustained Erk activity driven by b-Raf kinase. Prolonged MAPK activation stimulates the expression of cell cycle inhibitors, promoting cell cycle arrest and neuronal differentiation. The competition between signaling proteins to bind the Y490 residue regulates the balance between differentiation and proliferation (Meakin et al., 1999).

Additionally, Trk residue Y785 serves as a docking site for phospholipase C-γ (PLC-γ), leading to its activation. PLC-γ hydrolyzes phosphatidylinositol to generate IP3 and DAG, triggering calcium release from intracellular stores and activating PKC. While crucial for neuronal function, this pathway is not essential for neurotrophin-induced survival (Skaper, 2008).

In the context of target-derived neurotrophic factors like NGF, signaling pathways in axons must be transported in signaling endosomes to the cell body through retrograde transport of the NGF-TrkA receptor complex. The Trk receptor embedded in the membrane of the endosome is associated with clathrin and dynein motor machinery that moves along microtubules (Howe, Valletta, Rusnak, & Mobley, 2001; Yano et al., 2001). These endosomes, containing the ligand-Trk receptor complex and associated downstream proteins from PI3K, MAPK, and PLC-γ pathways, act as active signaling platforms during neuronal survival responses (Grimes, Beattie, & Mobley, 1997; Howe et al., 2001; Watson et al., 2001).

p75NTR

p75NTR is a 75 kDa transmembrane protein belonging to the tumor necrosis factor (TNF) receptor superfamily. Its structure includes an ECD characterized by four cysteine-rich domains, a transmembrane domain, and an ICD containing a death domain that lacks catalytic activity (Johnson et al., 1986; Vilar, 2017). All four mature neurotrophins can bind to p75NTR (Hallbook et al., 1991), although this binding occurs with lower affinity compared to proneurotrophins (Meldolesi, 2017). Activation of p75NTR occurs through dimeric neurotrophins, whether in their pro-form or mature form. Binding happens via interactions with the cysteine-rich domains in the ECD, stabilized by hydrophobic interactions, salt bridges, and hydrogen bonds within the ligand-receptor complex (Vilar, 2017).

p75NTR signaling

Upon ligand binding, p75NTR undergoes oligomerization with other p75NTR or homologous receptors, recruiting adaptor proteins such as c-Jun N-terminal kinase (JNK), small GTPases, and the transcription factor NF-kB. This receptor's role is multifaceted and context-dependent. p75NTR signaling is highly regulated by the formation of complexes with various coreceptors and ligands. When p75NTR is associated with the coreceptor sortilin and proneurotrophins, it can trigger apoptotic signaling cascades, including caspase activation, members of the Bcl-2 family, and the JNK pathway (P. P. Roux et al., 1999). This process leads to mitochondrial membrane permeabilization, cytochrome C release, and activation of initiator caspase 9 and executioner caspases 3, 6, and 7 (Claire Ceni et al., 2014). Conversely, binding of NGF to p75NTR leads to interaction with RIP2, influencing NGF's ability to promote cell survival by regulating NF-KB and activating Akt through a PI3K-dependent pathway (Khursigara et al., 2001; Meldolesi, 2017; Philippe P. Roux, Bhakar, Kennedy, & Barker, 2001; Vilar, 2017).

The ICD of p75NTR contains two distinct regions: the Juxta membrane domain (JTM) and the Death domain (DD), each interacting with different proteins involved in various cellular responses, such as caspase and NF-kB activation. TRAF6, a TNF receptor-associated factor, plays a crucial role in activating the survival pathway by binding to a specific region within the JTM of p75NTR (Vilar, 2017). Conversely, another region in the JTM, known as Chopper, induces cell death activity when associated with the plasma membrane (Underwood, Reid, May, Bartlett, & Coulson, 2008). The activation of these pathways is regulated by competitive protein-protein interactions, as downstream signaling molecules bind to overlapping regions in p75NTR (Lin et al., 2015).

Interaction Trk receptors with p75NTR

p75NTR also plays a role in promoting survival through the enhancement of Trk signaling. *In vitro* studies using PC12 cells have demonstrated that co-expression of both receptors increases the rate at which NGF can bind to TrkA by approximately 25-fold, generating high-affinity binding sites that do not require neurotrophin binding to p75NTR. Nevertheless, TrkA binding to p75NTR is necessary to induce enhanced TrkA activation by p75NTR (Mahadeo, Kaplan, Chao, & Hempstead, 1994; Matusica et al., 2013; Underwood et al., 2008; Vilar, 2017). Together, TrkA and p75NTR collaborate in transducing NGF signals, particularly in contexts such as the dorsal root ganglion (DRG), where TrkA is predominantly expressed alongside p75NTR to enhance survival responses to NGF (Vilar, 2017).

Retrograde and anterograde transport of neurotrophins

The neurotrophic hypothesis, primarily based on the function of NGF, proposes that neurotrophins are essential for the survival, growth, and differentiation of neurons, and are expressed in specific target tissues in limited quantities. Responsive neurons extend their axons toward these target tissues where neurotrophins are expressed. Once the axon terminals reach the target tissue, the neurotrophin binds to its Trk receptor, triggering internalization of the neurotrophin-receptor complex into the axon terminals. This complex is then transported retrogradely along the axon toward the neuronal cell body while exerting its signaling effects (Conner et al., 1998).

However, BDNF, NT-3 and NT-4/5 are transported anterogradely along axonal processes and stored within pre-synaptic terminals. von Bartheld et al. (1996) (Von Bartheld et al., 1996) provided the first evidence of exogenous BDNF and NT-3 being transported anterogradely in the developing chick brain from retinal ganglion cells through the developing retinotectal projection, demonstrating neuronal survival in the optic tectum. Zhou and Rush (1996) (Zhou & Rush, 1996) confirmed that endogenous BDNF is transported anterogradely from the dorsal root ganglia towards the dorsal horn of the spinal cord. Neurotrophins also influence synaptic transmission. A study by Torres-Cruz and collaborators (Torres-Cruz et al., 2019) investigated how BDNF and NT-4/5 affect glutamatergic transmission in corticostriatal slices by pharmacologically inhibiting TrkB receptors and downstream signaling pathways. They observed that inhibition of PI3K and MAPK hindered the modulatory effects of both BDNF and NT-4/5 on corticostriatal synapses, indicating that these signaling pathways are directly involved in mediating the effects of neurotrophins on glutamatergic transmission in the corticostriatal circuit.

Neurotrophic support from striatal afferents in HD

Interaction between htt / mhtt and BDNF

Cultured CNS cells overexpressing full-length htt exhibited a 94.6% increase in BDNF mRNA and protein expression as well as subsequent release, compared to parental cells. In contrast, CNS cells overexpressing mhtt, showed a 52.5% decrease in BDNF mRNA and protein expression and release relative to parental cells. Additionally, there is a dosage-dependent reduction in BDNF levels with mhtt (Chiara Zuccato et al., 2001). Reverse transcriptase–polymerase chain reaction (RT-PCR) and RNase protection

experiments revealed that full-length htt positively modulates BDNF gene transcription, while mhtt exerts a negative effect. Both proteins influence the activity of the BDNF gene promoters differently. This pattern was also observed *in vivo* in other HD mouse models, such as the YAC18 and YAC72 mice (Chiara Zuccato et al., 2001). Brain tissue from HD patients showed a 45% decrease in BDNF protein and a 65% reduction in BDNF mRNA levels in the fronto-parietal cortex. These findings suggest that full-length htt enhances BDNF transcription, thereby modulating the production and delivery of cortically derived BDNF to striatal targets and that a cortical dysfunction occurs in HD involving the drastic reduction of huntingtin-mediated BDNF production (Chiara Zuccato et al., 2001).

One mechanism by which htt regulates BDNF transcription involves the transcriptional repressor RE1-silencing transcription factor (REST). REST controls the activity of the silencer, repressor element 1 (RE1), within BDNF promoter II. Full-length htt recruits REST into the cytoplasm, preventing it from binding to and activating the silencing function of RE1. However, in the presence of mutated htt (HD), REST is not retained in the cytoplasm and accumulates in the nucleus, where it binds to RE1 sites in the BDNF gene and reduces BDNF transcription (C. Zuccato & Cattaneo, 2009).

Additionally, mhtt affects the anterograde transport of BDNF vesicles along striatal afferents. BDNF vesicular transport mediated by htt involves huntingtin-associated protein-1 (HAP1) which is transported along axons and acts as a subunit in dynactin protein, an essential component of dynein/dynactin microtubule-based molecular motors. When htt content is reduced or when mhtt interacts with the motor complex instead of htt, HAP1 disrupts the motor machinery, correlating with decreased association with microtubules and impaired BDNF vesicular transport (Gauthier et al., 2004). Upon

BDNF/TrkB complex formation in striatal neurons, retrograde vesicular transport of the complex in striatal dendrites depends on htt and dynein. In mutated conditions, the CAG expansion of mhtt alters the binding of BDNF vesicles to microtubules, impairing their transport (Liot et al., 2013).

BDNF in striatal afferents

Three main striatal afferent systems provide input and neurotrophic support to striatal neurons: the corticostriatal and thalamostriatal glutamatergic pathways, and the nigrostriatal dopaminergic pathway (Mandelbaum et al., 2019). Unilateral ablation studies (Altar et al., 1997) indicate that the frontoparietal cortex contributes 66% of the BDNF protein present in the ipsilateral striatum and 22% in the contralateral striatum. The substantia nigra pars compacta contributes 14% of the BDNF protein in the ipsilateral striatum. Thalamic nuclei, including the PF, are rich in cells containing BDNF mRNA and cells and fibers immunoreactive to BDNF protein (Conner, Lauterborn, Yan, Gall, & Varon, 1997). According to Conner et al., the PF contains a moderate number of cells with BDNF mRNA and a high density of cells with BDNF protein (Conner et al., 1997), suggesting it plays a crucial role in the anterograde transport of BDNF to the striatum. Additionally, excitatory striatal input is approximately 60% from the cerebral cortex and 40% from the thalamus (Kolodziejczyk & Raymond, 2016). Mapping and quantifying cortical and subcortical PF afferents, as well as examining the terminal arborization of PF axons, suggest that the primate Centromedian/Parafascicular (CM-PF) complex is equivalent to the PF nucleus in rodents (Gonzalo-Martín et al., 2024). Axonal mapping revealed that the PF has the highest density of striatum-projecting neurons in the

subcortex (Mandelbaum et al., 2019). About 70-90% of PF projections reach the striatum, covering it from the anterior to the posterior portions, while the remainder project to the STN and cerebral cortex. Despite its small size, the PF contains distinct domains organized into associative, limbic and somatosensory circuits, which are topographically connected to functionally distinct cortical and striatal regions (Gonzalo-Martín et al., 2024; Y. Smith et al., 2014). Lateral PF axons project to the laterodorsal somatosensory circuit of the striatum, the mediodorsal PF projects to the mediodorsal striatal associative circuit, and the medial PF projects to the limbic circuit of the striatum (Gonzalo-Martín et al., 2024; Mandelbaum et al., 2019; Sadikot, Parent, & François, 1992; Sadikot, Parent, Smith, & Bolam, 1992).

Retrograde tracers used to map projections showed that the most predominant PF afferent is the cerebral cortex (> 75%), providing excitatory input, especially from sensorimotor cortical areas (M2, M1, S1), followed by projections from the insular, frontal association, and cingulate cortices (Cornwall & Phillipson, 1988; Gonzalo-Martín et al., 2024; Paré, Smith, Parent, & Steriade, 1988). Each cortical area projects to interconnected PF domains, which are related to specific sensorimotor or cognitive subsystems. Most corticothalamic projections originate from layers 5b and 6b, with the majority being ipsilateral and a small number contralateral. Interestingly, thalamocortical projections from a particular PF domain terminate in the same cortical domains that originate the corticothalamic projections reaching that initial PF domain. These cortical domains also innervate through corticostriatal axons in the same striatal sector where thalamostriatal axons from that PF domain terminate (Gonzalo-Martín et al., 2024).

Approximately 22% of PF input comes from subcortical regions such as the entopeduncular nucleus (known as internal Globus pallidus in primates), SNpr, superior colliculus, the thalamic reticular nucleus, pedunculopontine nucleus, pontine reticular formation, contralateral deep cerebellar lateral nuclei, raphe, locus coeruleus, parabrachial nuclei and periaqueductal gray (Cornwall & Phillipson, 1988; Gonzalo-Martín et al., 2024).

HD rodent models

Animal models are vital for studying HD as they offer a unique opportunity to investigate disease mechanisms and potential treatments on early pathological, cellular and molecular alterations that cannot be measured in human patients *in vivo*. No animal model perfectly replicates human HD, and each model has its own strengths and weaknesses that may influence their performance in trials (Hockly, Woodman, Mahal, Lewis, & Bates, 2003). Key factors to consider include the length of htt transgene (whether full-length, exon 1 or a portion of exon 1), the length of polyglutamine repeats (with CAG repeats greater than 40 typically developing HD, though some models have CAG extensions of up to 180 repeats), the origin of the mutated htt (human or mouse gene), and the levels of mhtt expression compared to the wild-type htt. Additionally, some phenotype may be chemically induced by toxins, and understanding these differences is crucial as they can affect experimental outcomes (Kuhn et al., 2007; L. B. Menalled & Chesselet, 2002; Patrick Pla, Orvoen, Saudou, David, & Humbert, 2014). The genetic background of the model is also significant, as dominant and recessive genetic modifiers can greatly influence the penetrance and progression of the disease (L. Menalled et al., 2009).

Chemically induced HD models

The first chemically induced animal model of Huntington's disease was established in 1976 using kainic acid (KA), based on the vulnerability of striatal neurons to excitotoxicity from excitatory amino acid receptor stimulation (Walker, 2007). Since then, various animal models have been developed to meet specific research objectives.

The QA model generated by intrastriatal infusions of QA induces over-activation of the NMDA receptor exerting excitotoxic, pro-inflammatory and oxidative mechanisms. QA, KA, ibotenic acid (IA) and NMDA are glutamate analogues. Rats treated with QA infused directly into the striatum presented hyperactivity after the lesion, learning deficiency, and significant striatal atrophy and loss of NADPH-diaphorase neurons in regions peripheral to the injection site (Shear, Dong, Gundy, Haik-Creguer, & Dunbar, 1998). BDNF is still present although reduced, whereas very little htt content remains in the ipsilateral cortical layers 5 and 6, which are the layers that project to the striatum. The surviving choline acetyltransferase (ChAT) -expressing neurons contained a moderate amount of BDNF (Fusco et al., 2003). Systemic delivery of QA decreases GABA and substance P levels but spares neuropeptide Y and somatostatin neurons (Shear et al., 1998; Túnez, Tasset, Pérez-De La Cruz, & Santamaría, 2010). Similarly, systemic delivery of KA and IA revealed degeneration of intrinsic striatal neurons along with irreversible reduction of glutamic acid decarboxylase (GAD) and ChAT, enzymes deficient in HD (Borlongan, Koutouzis, Freeman, Cahill, & Sanberg, 1995).

The 3-NP model is created by administering the mitochondrial toxin 3-NP, either directly into the striatum or systemically, as it crosses the blood-brain barrier. 3-NP irreversibly inhibits the enzyme succinate dehydrogenase of the electron transport chain and tricarboxylic acid in the mitochondrial membrane. 3-NP inhibition leads to decreased ATP levels, increased lactate concentrations, and subsequent striatal neuronal death. Rats treated with 3-NP exhibit alterations in grip-strength and learning impairments, as well as deficiencies in the balance beam task. This model creates necrotic cavities in the striatum, accompanied by significant striatal atrophy and neuronal loss, and may more closely resemble the histological dorsal striatal lesions seen in human HD compared to the QA model (Borlongan et al., 1995; Shear et al., 1998; Túnez et al., 2010).

Systemic injections of IA, KA and QA in rats typically result in hyperactivity, whereas administration of 3-NP first induces hyperactivity followed by significant hypoactivity. The IA, KA and QA HD models might better represent the hyperkinetic stages of HD, exhibiting milder behavioral and neuroanatomical effects, while the 3-NP model produces more severe effects, mimicking both later symptoms and the juvenile onset of HD (Borlongan et al., 1995). Notably, microarray studies comparing the 3-NP rat model to a mouse model with conditional BDNF depletion (BDNF +/- and BDNF -/-) specific to the forebrain neurons revealed that the BDNF knock-out model develops striatal transcription profiles more similar to those observed in patients with HD (Strand et al., 2007). It is also important to note that chemically induced HD models may not necessarily reproduce progressive changes in behavior (Carter et al., 1999).

Transgenic HD models expressing mhtt

Transgenic HD models can be categorized based on the type of mhtt expression into three main types: those expressing truncated htt, those expressing full-length htt, and knock-in (KI) models (Carter et al., 1999).

Transgenic models are created by inserting the mutant gene or a portion of it randomly into the mouse genome, resulting in the expression of the mutant protein alongside the endogenous wild-type htt. In contrast, knock-in models involve inserting the mutation directly into the mouse *Hdh* gene (which encodes the mouse htt protein), where it is expressed under its natural promoter and within the appropriate genomic context of the mouse *Hdh* gene (L. B. Menalled & Chesselet, 2002). Models expressing full-length mutant htt such as the YAC mouse lines, typically develop motor deficits later than those expressing truncated htt such as the R6 mouse lines. This allows more time for studying non-motor behaviors (Patrick Pla et al., 2014).

The R6/2 hemizygous mouse model is one of the most studied and widely used models, replicating juvenile HD. It is particularly valuable for evaluating therapeutic strategies aimed at reducing the severity of motor symptoms or slowing disease progression (Cano et al., 2021; Carter et al., 1999). The R6 mouse line with background CBA/J mixed with C57BL/6J was developed by Mangiarini et al., (Mangiarini et al., 1996) by introducing exon 1 of the human HD gene, containing highly expanded CAG repeats into embryos. Htt gene spans a region of 170 kb with 67 exons however the CAG repeat occurs in exon 1. The inserted DNA included a 1.9 kb genomic fragment with approximately 1 kb of

promoter sequences, all of exon 1 and 262 bp of intron 1. This fragment is sufficient to generate a progressive neurological phenotype of HD (Mangiarini et al., 1996).

With the R6/2 mouse line, three more HD mouse lines were created:

1) R6/0: Contains 142 CAG repeats but does not exhibit transgene expression or an HD phenotype due to transgene silencing by the integration site.

2) R6/1: Has 116 CAG repeats with 30% of the transgene expression level compared to wild-type htt and develops a progressive HD phenotype.

3) R6/2: Exhibits 144 CAG repeats with 75% of the transgene expression level, leading to a progressive HD phenotype.

4) R6/5: Contains 128 – 156 CAG repeats with 77% of transgene expression level and develops a progressive HD phenotype, though it requires homozygosity for phenotypic expression.

CAG repeats are unstable upon transmission and therefore it is not appropriate to associate a definitive CAG number to each line, tests should be done each time to confirm (Mangiarini et al., 1996).

The R6/2 model presents a progressive neurological phenotype with motor and behavioral symptoms that start subtly and worsen until death. At 5 – 6 weeks, mice already show difficulty in locomotion. In presymptomatic mice, NIIs are immunoreactive for htt and ubiquitin. Mhtt aggregates are also present in neurites. *In vitro* these are formed through self-aggregation via the polyglutamine repeat into amyloid-like fibrils. By 8 weeks, the locomotor symptomatic stage begins with dyskinesia of the limbs when suspended by the tail, called limb clasping, they also exhibit irregular gait, shudders, stereotypic

excessive grooming, resting tremor and myoclonic jerks. They present vocalizations and chirping noises under stress. Abundant tonic-clonic seizures that last several minutes can lead to death. At the same time, mice start losing weight and muscle bulk and develop nonmovement disorder components like anxiety and depression-like behavior. By the late stage of 12 weeks, mice have a severe movement disorder and typically die by 10 – 13 weeks. Their brains are 19% smaller compared to WT mice, with thinner cortical layers, reduced striatal volume, and enlarged ventricles. This model is particularly suited for evaluating motor symptom treatments due to its quantifiable progression. Due to the early onset and fast progression, R6/2 mice replicate juvenile human HD (Bates, Mangiarini, & Davies, 1998; Carter et al., 1999; Kuhn et al., 2007; Lüesse et al., 2001; Mangiarini et al., 1996).

R6/2 mice are also characterized by altered levels of neurotransmitters and their receptors, signaling molecules and altered gene expression of neurotrophic factors. There is a progressive decrease of BDNF mRNA detected in striatal afferents between 6-13 weeks of age associated with impaired motor coordination. At the age of 6 weeks, neostriatal volume loss is reported but neuronal atrophy occurs until 9 weeks and precedes neuronal loss; striatal neuronal degeneration occurs rapidly over 6-13 weeks of age (Gil & Rego, 2009; Samadi et al., 2013). Transcriptional studies have shown that the striatal mRNA expression in R6/2 mice is not different from the full-length knock-in HD models (Kuhn et al., 2007). This means that the truncated first exon of the human mhtt present in R6/2 does not represent a disadvantage compared to the full-length mhtt gene.

R6/1 hemizygous and R6/5 homozygous mouse lines have a similar progressive phenotype as R6/2 mice but develop symptoms on a slower timescale (Kuhn et al., 2007). R6/1 mice develop symptoms at 4 – 5 months, with mild tremors and involuntary movements emerging by 6 – 7 months. Epileptic seizures have been observed, and the onset is slower compared to R6/2 mice. R6/5 mice show an onset of around 9 months (Bates et al., 1998; Mangiarini et al., 1996). Major differences between R6/2 and R6/1 models include the shorter CAG repeat expansion, (144 vs. 116); and the lower expression rate of the mutant transgene (75% vs. 31%). The N171-82Q model, which expresses 171 residues and 82 CAG repeats, with 10 – 20% transgene expression level, also has a prolonged course of disease. Demonstrating that expression levels and CAG repeat length profoundly impact disease severity. Mice with longer CAG repeats have more widespread neuronal pathology than those with shorter expansions (L. B. Menalled & Chesselet, 2002).

Transgenic mice expressing the full-length human mhtt gene, produced in an FVB/N background, using yeast artificial chromosomes (YAC), include YAC72 and YAC128. YAC72 mice, with 72 CAG repeats, and YAC128 mice, with around 128 CAG repeats, show a slow disease progression with a near-normal life span. They exhibit molecular, cellular, and behavioral characteristics of HD where cell loss is limited to the striatum, partially recapitulating the regional selectivity of adult-onset HD. The mhtt transgene expression level is 30 – 50% with an onset of behavioral symptoms of 7 months of age with hyperkinesia (Kuhn et al., 2007; L. B. Menalled & Chesselet, 2002).

YAC72 mice in the presymptomatic stage exhibit significant reduction in BDNF protein levels in cortical, hippocampal and striatal regions; BDNF exon II mRNA depletion and a decrease in BDNF exon III and IV mRNAs in the cerebral cortex and hippocampus (Chiara Zuccato et al., 2001). YAC128 presents early and selective striatal localization of diffuse nuclear mhtt.

BACHD mouse model expresses full-length human mhtt using a bacterial artificial chromosome (BAC) in an FVB/N background. The BACHD model expresses mhtt exon 1 with 97 CAG repeats under endogenous htt regulatory machinery (L. Menalled et al., 2009). The CAG expansion involves a mixed CAA-CAG repeat which confers stability in the germ line and the cerebral cortex and striatum in the aged brain (Gray et al., 2008). The BACHD model features a robust slowly progressive motor disorder and late-onset pathology, including striatal and cortical atrophy and neuronal loss in the later stages around 18 months (L. Menalled et al., 2009). Neurodegeneration in the BACHD model does not include early nuclear accumulation of aggregated mhtt, inclusions appear in the cerebral cortex and striatum during a more advanced symptomatic stage, exhibiting an adult-onset HD pattern. At two months, BACHD mice exhibit a decrease in rotarod performance, worsening with age. A robust 50% reduction of cortical BDNF transcripts along with decreased synaptic activity in the corticostriatal projections becomes evident at six months (Gray et al., 2008). Similar to YAC mouse lines, BACHD mice present significant weight gain between 2 and 6 months of age. The 12-month-old forebrain was 20% smaller compared to WT mice (Gray et al., 2008; L. Menalled et al., 2009).

Knock-in HD mouse models

Knock-in mouse models most accurately reflect the genetic basis of HD, with the mutation expressed in its natural genomic and protein context. These models provide invaluable insights into the pathogenic mechanisms of the disease (Franich et al., 2019). Among these, the Q140 and *Hdh*Q150 mouse lines are notable. They were created by genetically modifying 129/Sv and 129/Ola embryonic stem cells, respectively, injecting them into C57BL/6J blastocysts, and then backcrossing them to C57BL/6J mice. The *Hdh*Q150 model features an extended CAG repeat inserted into the mouse Htt gene, achieving 50% of the normal transgene expression level. In contrast, the Q140 model replaces mouse exon 1 of the Htt gene with the mutated human exon 1. The Q140 mice exhibit an earlier onset of behavioral symptoms and earlier evidence of striatal htt aggregate deposition in the nucleus at 4.5 months. This model also shows incomplete splicing of mhtt from exon 1 to exon 2, resulting in smaller exon1-intron1 polyadenylated mRNA that encodes a highly pathogenic exon 1 mhtt protein. From 1 to 6 months of age, Q140 mice display hypoactivity with reduced locomotion and lower traveled distance during the open field test. They also exhibit decreased spatial working memory at three months and reduced performance on the running wheel at six months. In contrast, *Hdh*Q150 mice present with htt nuclear aggregates in the striatum at 12 months, indicating that symptoms start much later (Franich et al., 2019; L. B. Menalled & Chesselet, 2002).

The Hdh^{Q111} knock-in model, developed on a CD-1 background with 106 CAG repeats, was created by inserting expanded CAG repeats into the murine HD gene homologue. This model exhibits a mild HD phenotype (L. Menalled et al., 2009). Comparative studies of Hdh(Q111) mice with different genetic backgrounds -C57BL/6, FVB/N and 129Sv-

revealed increased intergenerational and striatal instability of the CAG repeat in the C57BL/6 and FVB/N backgrounds compared to the 129Sv background. This suggests that somatic repeat expansion may be influenced by mismatch repair systems. Additionally, the accumulation of mhtt and formation of NII was fastest in the C57BL/6 background, followed by FVB/N, with the 129Sv background showing the slowest rate. These findings highlight the significant impact of genetic background on HD expression and development, which should be considered when developing treatments and comparing different models (Lloret et al., 2006).

A comparative study of transgenic and knock-in mouse lines, including R6/2, YAC128, BACHD and Hdh^{Q111} models, assessed locomotor and behavioral symptoms in both male and female mice. In the rotarod test, all HD mice showed deficits. R6/2 and BACHD mice displayed progressive, robust deficits starting at 6 and 8 weeks, respectively. YAC128 mice exhibited early deficits with no progression while the Hdh^{Q111} knock-in model showed impairments only at late stages in females. R6/2 mice had deficits in grip strength, more pronounced in males, whereas Hdh^{Q111}, BACHD, and YAC128 mice showed no significant changes. In the open field test, to evaluate general activity determined by distance traveled and rearing, R6/2 and BACHD mice were progressively hypoactive, while YAC128 mice showed mild hypoactivity, and Hdh^{Q111} mice did not differ from wild-type controls. R6/2 females exhibited delayed deficits in general activity compared to males. YAC128 mice on the FVB/n background displayed freezing behavior in the arena, a behavior not observed in YAC128 mice on the C57BL/6J background, indicating background-related differences. R6/2 and BACHD mice showed reduced vertical activity

in the rearing-climbing test. Additionally, robust gait anomalies were noted in R6/2 mice, with minor or no deficits in other lines. Anxiety-like behavior, assessed in the light-dark choice test, was progressive in R6/2 and BACHD mice, while the other lines showed no significant differences. Hdh^{Q111} mice did not display preferences in old age, likely due to blindness in the CD1 albino background. BACHD wild-type mice showed indifference between dark and light, possibly due to limited visual acuity, unlike YAC128 wild-type mice, affecting baseline differences in the groups. Body weight decreased in R6/2 mice but increased in the other lines.

Overall, the full-length models exhibited milder deficits compared to the R6/2 models. Among the full-length models, BACHD mice displayed a stronger phenotype, followed by YAC128 mice with milder phenotypes, and Hdh^{Q111} mice on the CD1 background, which showed a very mild HD phenotype (L. Menalled et al., 2009). The YAC46 and YAC72 mice exhibited almost no behavioral deficits. Within the full-length models, the relationship between behavioral deficits and CAG length (46 and 72 CAGs, respectively) is similar to that observed in humans, at least within a certain range. Strains carrying the Hdh^{Q111} allele may show more pronounced behavioral differences depending on the genetic background, such as the C57Bl/6J background, which influences both nuclear mutant huntingtin deposition and CAG repeat instability intergenerationally and in the striatum (Lloret et al., 2006).

The genetic background strain undeniably affects phenotype severity. Milder effects in the FVB/N strain suggest that the C57Bl/6 background may be more appropriate for drug testing using a behavioral battery of tests. R6/2 and BACHD mice appear to share more similarities in the development of the HD phenotype, though the R6/2 mice have a

considerably shorter lifespan. Testing in BACHD mice could therefore be more expensive. Nonetheless, potential therapies must be evaluated in various animal models before advancing to clinical trials with patients.

Gene therapy

The pursuit of a CNS-directed gene delivery system has been a priority for decades. Delivering naked nucleic acids *in vivo* has proven challenging due to their susceptibility to rapid degradation both extracellularly and intracellularly. For effective cell transduction, DNA must cross the plasma membrane, escape from endocytic vesicles, and ultimately traverse the nuclear membrane. Gene therapy in combination with viral vectors facilitates this process. Gene therapy involves introducing a therapeutic nucleic acid into target cells to: i) replace a defective gene, ii) enhance the expression of a downregulated gene, or iii) reduce harmful levels of a protein through RNA interference or antisense technology (Agbandje-McKenna & Kleinschmidt, 2011; Nonnenmacher & Weber, 2012). Gene delivery vectors encounter a hostile environment upon administration, which is why viruses have evolved mechanisms to overcome these challenges. Viral vectors exploit the virus's ability to infect or transduce mammalian cells and utilize the host machinery to express viral proteins (Hudry & Vandenberghe, 2019; C. R. Joshi, Labhasetwar, & Ghorpade, 2017). A crucial aspect of viral vector construction involves replacing viral genes with the gene of interest.

Gene delivery system investigations are generally categorized into "proof of concept" and "therapy-based" research, depending on the purpose of the study. Proof of concept research often employs reporter genes, such as Green fluorescent protein (GFP), to validate delivery system dynamics and efficiency. Therapy-based research aims to

alleviate disease symptoms or delay disease onset (C. R. Joshi et al., 2017), for example, overexpressing BDNF in HD animal models.

The success of CNS gene delivery is influenced by several factors, including the type of viral vector, vector design, vector titer, the biology of the delivered product, the targeted region, delivery accuracy and the route of administration, all of which vary by disease (Emborg et al., 2014; J. H. Wang, Gessler, Zhan, Gallagher, & Gao, 2024). Administration routes include intraparenchymal, ocular, cochlear, delivery to the cerebrospinal fluid (CSF) via intracerebroventricular, intracisternal, or intrathecal routes, intranasal delivery for brain transduction, intramuscular injection, nerve delivery to the spinal cord, and intravenous delivery for broad, non-invasive CNS transduction (Hudry & Vandenberghe, 2019). Direct and local administration routes maximize transgene concentration and stability near target cells, reducing widespread biodistribution compared to delivery into the venous system or other fluid-filled compartments. Local routes also require less viral vector, minimizing the risk of toxicity or off-target effects (Hudry & Vandenberghe, 2019). Systemic injection of therapeutic viral vectors for CNS diseases faces challenges such as crossing the blood-brain barrier (BBB), peripheral toxicity from non-specific transduction, and immune elimination (Huang et al., 2021). Common viral vectors used in research include adenovirus, lentivirus, herpesvirus and adeno-associated virus (AAV) (Samulski & Muzyczka, 2014). This review will focus on AAV.

Adeno-associated virus

Adeno-associated virus (AAV) is a small, nonenveloped virus with a single-stranded linear DNA genome approximately 5 kb in length. The genome contains inverted terminal

repeats (ITRs) of 145 nucleotides, the first 125 of which form a palindromic sequence (Srivastava, Lusby, & Berns, 1983). AAVs belong to the *Parvoviridae* family and were first discovered in 1965 as a contaminant of adenovirus isolates (Atchison, Casto, & Hammon, 1965). AAVs feature an exceptionally stable capsid, about 25 nm in diameter, composed of 60 subunits of the viral proteins VP1, VP2 and VP3. It is resistant to brief exposure to heat, acidic pH, and proteases (Douar, Poulard, Stockholm, & Danos, 2001). The coding regions of AAV are flanked by ITRs of 145 bases long, which serve as origins for DNA replication and primary packaging signals. These ITRs are the only cis-active sequences required for constructing recombinant AAV vectors (rAAV) and the only AAV-encoded sequences present in AAV vectors (McLaughlin, Collis, Hermonat, & Muzyczka, 1988).

Transgenes cloned into rAAV vectors must be engineered with the appropriate enhancer, promoter, poly(A) sequence, and splice signals to ensure correct gene expression. Wild-type AAVs are defective viruses that require coinfection with a helper virus, such as adenovirus or herpesvirus, to establish a productive infection (Atchison et al., 1965). While this requirement makes AAVs among the safest available viral vectors, it also presents a challenge as rAAV vectors must overcome several biological barriers without a helper virus to effectively transduce cells.

Advantages of AAVs include their non-pathogenic nature, ability to efficiently transduce a broad range of cells, tissues and hosts, and the capacity of some serotypes to cross the BBB. However, AAVs have limitations, such as a cloning capacity of approximately 4.5 kb, preexisting immunity against certain serotypes, and a two-four week delay in transgene expression due to the time required for second-strand DNA synthesis.

AAV serotypes

Wild-type AAVs exhibit rapid evolving changes, resulting in significant genomic diversity classified into viral “clades”. Over recent decades, numerous serotypes and variants have been identified from adenovirus cultures, as well as from primate, human and other mammalian tissues through PCR studies. However, only a few of these are commonly available for packaging rAAV cassettes using AAV2 ITRs. The representative AAV members share approximately 60–99% sequence identity, with AAV4 and AAV5 being the most distinct from each other and from other members (Agbandje-McKenna & Kleinschmidt, 2011; J. H. Wang et al., 2024).

AAV capsid VP perform several functions including protection from nucleases and the immune system, host cell surface receptor recognition, endosomal entry and trafficking, cytoplasmic processing, potential interaction with microtubule-associated proteins for nuclear movement and entry (Agbandje-McKenna & Kleinschmidt, 2011; Hudry & Vandenberghe, 2019). The genomic differences among AAV serotypes are primarily located in the variable loop regions of the virus capsid sequence, especially in VP3. These differences play a crucial role in determining tropism and can significantly alter AAV transduction efficiency (J. H. Wang et al., 2024). Tropism involves receptor affinity, cell entry, trafficking efficiency, DNA uncoating, and post-nuclear gene expression (Agbandje-McKenna & Kleinschmidt, 2011; Samulski & Muzyczka, 2014). Characterization of AAV serotypes has revealed distinct patterns of transduction, tropism, and transgene distribution in various tissues, depending on the specific cell surface receptors required for entry (Burger et al., 2004; Davidson et al., 2000; Issa et al., 2023; Watakabe et al., 2015; Zincarelli, Soltys, Rengo, & Rabinowitz, 2008). For example, rAAV2 binds to

heparan sulphate proteoglycan (HSPG), while AAV3 and AAV6 also bind to heparan sulphate.AAV4 binds to O-linked 2,3-sialic acid; AAV1, AAV5 and AAV6 bind to N-linked sialic acid; and AAV9 binds to N-linked galactose, along with proteinaceous receptors such as FGFR1, integrins, and/or HGFR for AAV2; HGFR for AAV3; EGFR for AAV6; PDGFR for AAV5; and LamininR for AAV2, AAV3, AAV8 and AAV9 for efficient binding and endocytosis (Bell et al., 2012; Huang et al., 2021; Nonnenmacher & Weber, 2012; Pasquale et al., 2003; Shen et al., 2011; J. H. Wang et al., 2024). Recent genome-wide screenings have identified specific host proteins that facilitate rAAV transduction, including KIAA0319L, designated as the AAV receptor (AAVR) (Pillay et al., 2016) and G protein-coupled receptor 108 (GPR108), which plays a role in the transduction of several rAAV serotypes (Dudek et al., 2020).

Cell entry and trafficking

Viruses that replicate in the nucleus have developed mechanisms to overcome two primary cellular barriers: the plasma membrane and the nuclear membrane. AAVs typically enter cells by binding to cell surface glycans on proteoglycans (such as sialic acid, galactose, or heparan sulfate) and interacting with cell surface co-receptors (e.g., fibroblast growth factor receptor or integrin). This binding triggers endosomal uptake through clathrin-coated vesicles and the CLIC/GEEC (clathrin-independent carriers/GPI enriched) endocytic pathway (Agbandje-McKenna & Kleinschmidt, 2011; Nonnenmacher & Weber, 2011). Endosome maturation involves a progressive decrease in internal pH, and the transducing viruses are routed as far as the late endosomal compartment (Douar et al., 2001). Exposure to the acidic pH of the endosomal compartment causes the N-

terminal end of the minor capsid protein VP1 (VP1u) to extrude from the capsid surface (Sonntag, Bleker, Leuchs, Fischer, & Kleinschmidt, 2006). VP1u then facilitates endosome rupture, allowing the AAV capsid to be released into the cytoplasm. In collaboration with VP2, VP1u promotes nuclear entry of the capsid through the nuclear pore complex, where it uncoats the viral DNA (Sonntag et al., 2006). Viral particles may be degraded in the proteasome before reaching their target, limiting transduction efficiency (Douar et al., 2001). Once inside the nucleus, the single-stranded DNA genome is released and converted into double-stranded DNA (dsDNA) through second-strand synthesis, which appears to be a major rate-limiting step for gene expression *in vivo*. Genomic studies of rAAV *in vivo* have shown that transcription begins from the ITR at the 3′ end of the genome (K. J. Fisher et al., 1996). The rAAV double-stranded DNA molecules undergo circularization and concatemerization, persisting stably as episomes in postmitotic cells (Clark et al., 1999; J. H. Wang et al., 2024). This reduces the risk of insertional mutagenesis and provides an additional safety margin for AAV-mediated gene therapy.

Viral vector design

Efforts to enhance AAV efficiency, transduction specificity, and immune evasion through capsid modifications can be categorized into three main strategies: 1) biomining, which involves exploring nature for novel capsid diversity, 2) rational design, which utilizes structural and functional data on capsid domains to manipulate its utility through point mutations, motif insertions, and chemical biology methods; and 3) directed evolution, which involves mutating the wild-type AAV capsid gene to generate capsid libraries that

are then screened to identify new variants with desirable properties (Hudry & Vandenberghe, 2019; Lee, Guenther, & Suh, 2018; Tabebordbar et al., 2021; J. H. Wang et al., 2024).

To customize the rAAV genome, combined strategies include optimizing promoters, incorporating regulatory elements such as enhancers and gene linker sequences, modifying ITRs or introns, adding tissue-specific elements for regulation, using inducible expression systems, optimizing codons, reducing CpG motifs in the transgene cDNA, and employing microRNA (miRNA)-mediated post-transcriptional regulation for retargeting (Ho et al., 2013; Kim et al., 2011; Lewis et al., 2015; J. H. Wang et al., 2024).

Elements of AAV vectors

Promoters in transgene expression cassettes are selected to meet specific needs, such as targeting gene delivery to particular cells and achieving gene expression levels with minimal dosing to avoid off-target effects.

Examples of strong, constitutive, and ubiquitous promoters include the cytomegalovirus (CMV) promoter, chicken beta-actin (CBA) and its derivate CAG, human elongation factor 1α-subunit (EF1α), the β -glucuronidase (GUSB), and ubiquitin C (UBC) (Powell, Rivera-Soto, & Gray, 2015; J. H. Wang et al., 2024). The CMV promoter is shorter (~0.8 kb) and provides strong expression, making it suitable for vectors with packaging constraints like AAV. However, some ubiquitous promoters can be prone to silencing. Tissue-specific promoters are tailored to specific cell markers, such as neuron-specific enolase (NSE), synapsin (Syn) and platelet-derived growth factor (PDGF) for neurons; glial fibrillary acidic protein (GFAP) for astrocytes; macrophage-specific promoters like human CD11b, CD68,

and murine F4/80 for microglia; and myelin basic protein (MBP) for oligodendrocytes and Schwann cells (C. R. Joshi et al., 2017).

Regulatory elements such as upstream enhancers like the Kozak sequence can be engineered to improve expression activity and specificity, thereby reducing the viral load. Other cis- acting post-transcriptional regulatory elements are required for nuclear export of intronless viral RNA, such as the woodchuck hepatitis virus post-transcriptional regulatory element (WPRE), which is added downstream of the transgene to enhance mRNA levels (Powell et al., 2015). Selecting an appropriate polyadenylation signal is critical for nuclear export, translation, and mRNA stability, with examples including SV40 late, beta-globin, or bovine growth hormone (bGHpA) (Powell et al., 2015).

Various strategies have been employed to express multiple transgenes from the same plasmid, including using multiple promoters fused to genes, inserting splicing or proteolytic cleavage signals, creating fusion genes controlled by a single promoter, and inserting internal ribosomal entry sites (IRES) between genes (Kim et al., 2011). The IRES element creates an additional ribosome recruitment site for internal translation initiation, ensuring co-expression of genes upstream and downstream and the possibility of inserting in the downstream gene subcellular localization sequences. However, the translation efficiency of the gene downstream of IRES is typically lower than the upstream gene, around 10-20%, and often exceeds 500 nucleotides in length (Ho et al., 2013; Kim et al., 2011; Lewis et al., 2015). To address this, “self-cleaving” 2A family peptides have been developed. These 18-22 amino acid peptides enable the production of multiple

proteins from the same transcript by causing the ribosome to skip synthesis of a glycine-proline peptide bond at the end of the 2A element, ensuring stoichiometric expression of 1:1 of the adjacent proteins (Kim et al., 2011; Lewis et al., 2015).

Promising results in the CNS

There is substantial evidence supporting the effectiveness of AAV-mediated gene delivery to the CNS over the years. In a study by Ziemlinska et al. (Ziemlińska et al., 2014), completely spinalized rats received AAV-mediated overexpression of BDNF fused with cMyc, which resulted in enhanced excitability in the lumbar spinal network and locomotor recovery. The presence and activity of the fused BDNF protein were confirmed and analyzed through ELISA and Western blotting. Similarly, Wang et al. (J. Wang et al., 2016) used AAV vectors to overexpress BDNF fused with eGFP in a rat model of drug abuse-related behavior. Their findings indicated that the fused BDNF protein activated specific signaling pathways in the VTA mediated by TrkB receptors.

In another study, Han et al. (Han et al., 2019) employed an AAV vector with a 2A linker sequence to overexpress BDNF and eGFP in diabetic mice. The resulting BDNF protein effectively reduced neuroinflammation in the hippocampus by modulating the HMGB1/RAGE/NF-kB pathway. Collectively, these results suggest that AAV-induced overexpression of BDNF, whether as a single protein or in fused forms, maintains its functional integrity.

AAV vectors are also crucial tools for developing treatment strategies for HD. McBride et al. (McBride et al., 2003) demonstrated histological and behavioral protection in rats treated with 3NP following bilateral striatal injection of AAV-GDNF. Connor et al. (Connor et al., 2016) evaluated the effects of bilateral striatal injections of AAV1-BDNF in homozygous HD rats and observed attenuation of motor and cognitive impairments. Similarly, Kells et al. (Kells et al., 2004; Kells et al., 2008) noted increased survival of striatal MSN and interneurons following unilateral injection of AAV1-BDNF in QA-treated rats. Despite these promising results, the extent of the striatum that was transduced and expressed the transgenes was limited. An anterograde approach could potentially achieve a wider distribution in the targeted area.

Previous research has shown that delivering AAV vectors into afferent pathways of targeted structures is feasible. This method allows the vector to express the desired protein, which is then transported to the intended structure to exert its functional effects. Cearley and Wolfe (Cearley & Wolfe, 2007) compared the axonal transport of rAAV9 delivered to the striatum versus the VTA. They found that the VTA showed broader dissemination of the transgene throughout the brain parenchyma due to its extensive efferent and afferent projections to distant brain regions. AAV1 and AAV10 were also transported anterogradely from the VTA, though at lower expression levels compared to AAV9.

In primates, Bankiewicz and colleagues (Kells et al., 2009) achieved widespread expression of GDNF in ipsilateral cortical regions following a single injection of an AAV2-

GDNF vector into the thalamus. Another study found that injecting AAV2-GDNF into the striatum of primates treated with MPTP resulted in anterograde transport of GDNF to the SNpr and STN, leading to recovery of dopamine activity and motor function (Kells et al., 2012). Similarly, administering an AAV2-AADC vector into the substantia nigra and VTA of children with AADC deficiency resulted in clinical improvement through increased dopamine metabolism in the midbrain and striatum that translated into movement (Pearson et al., 2021). Eslamboli et al. (Eslamboli et al., 2005) reported that delivery of AAV2-GDNF into the striatum of primates treated with 6-OHDA led to anterograde transport of GDNF to the globus pallidus and recovery of dopamine metabolism. Ramaswamy et al. (S. Ramaswamy et al., 2009) observed that injecting AAV2-NTN into the transgenic N171-82Q HD mouse model resulted in anterograde transport of NTN to the SNpr and globus pallidus, accompanied by amelioration of HD symptoms. To date, no studies have investigated the anterograde delivery approach using AAV-mediated overexpression of BDNF in gene therapy interventions for HD.

Toxic effects

In a comparative study of various AAV serotypes using a CMV promoter, Watakabe et al. (Watakabe et al., 2015) found that AAV5 and AAV9 effectively transduced neurons and glial cells, resulting in high expression levels of modified hrGFP (hrGFP II). However, they observed a reduction in the NeuN marker in transduced neurons across marmoset, macaque, and mouse cerebral cortex, potentially due to general toxic effects from either high AAV infection levels or CMV promoter-mediated GFP expression. They suggested that maintaining low-level expression could be advantageous for long-term experiments.

Similarly, Eslamboli and Kells (Eslamboli et al., 2005; Kells et al., 2008) highlighted that excessive overexpression of neurotrophins could lead to detrimental effects that undermine their therapeutic potential. They recommended diluting AAV vectors to optimize study outcomes and using cell-specific promoters in rAAV genomes.

AAV-CMV caveats

As more experiments with different AAV vectors in various animal models are conducted, we are uncovering more details about the impact of AAV delivery, particularly with strong AAV vectors like serotype 9 and strong ubiquitous promoters such as CMV. AAV9, AAV5, and AAV1 vectors can successfully transduce neurons, astrocytes, and antigen-presenting cells (APC) like microglia (Ciesielska et al., 2013; Hadaczek et al., 2009; Issa et al., 2023; Lluis Samaranch et al., 2014).

Samaranch and colleagues (Lluis Samaranch et al., 2014) reported in rats and non-human primates (NHP) that delivery of an AAV9-CMV vector encoding a foreign protein, such as GFP, triggered a neurotoxic immune response. They suggested that transduced APCs express GFP peptides conjugated with the major histocompatibility complex II (MHC II), activating a classic adaptive immune response in the injected and connected areas. AAV9 vector with a CMV early enhancer/chicken B actin (CAG) promoter driving GFP expression did not induce the same immune reaction, nor did AAV2, possibly because AAV2 only transduces neurons (Ciesielska et al., 2013; Lluis Samaranch et al., 2014). AAV1-hrGFP injected into monkey brains activated both humoral and cell-mediated immune responses, as evidenced by anti-AAV1 and anti-hrGFP antibodies, infiltration of $CD4^+$ lymphocytes, and upregulation of MHC II (Ciesielska et al., 2013;

Hadaczek et al., 2009). Similarly, human AADC encoded in an AAV9 vector injected into rat brains caused significant inflammation associated with upregulation of MHC II in glia and CD8+ lymphocytic infiltration (Ciesielska et al., 2013). Even when the protein encoded by the AAV is 97% homologous with the host, it can still induce mild gliosis (Forsayeth & Bankiewicz, 2015).

Several strategies have been developed to fine-tune cell or tissue specificity, such as using cell-specific promoters or adding miRNA binding sites in the 3′-UTR to inhibit expression in cells expressing the complementary miRNA. For instance, adding miR-122 binding sites to rAAV9 has been reported to enable CNS expression while avoiding the liver, heart, and skeletal muscle expression (J. Xie et al., 2011). Another option to mitigate transgene immunity is to incorporate APC-specific miRNA binding sites, such as miR-142 and miR-652, into the rAAV expression cassette to prevent transgene expression in APCs (Muhuri et al., 2021; Xiao et al., 2019).

Safety remains a significant consideration in gene therapy, but advancements in gene delivery approaches are improving prospects for managing neurodegenerative diseases and hold strong promise for developing effective, personalized gene therapies.

Clinical rationale

We have developed a strategic approach for delivering AAV5- and AAV9-encoded BDNF to the thalamostriatal system by administering the vector directly into the PF. Although early-stage alterations in thalamostriatal neuronal transmission are observed, the PF was chosen as a therapeutic target in R6/2 mice because neurons within this nucleus and their projections to the striatum remain functional in the early phases of HD and are relatively viable later on due to compensatory mechanisms (81, 82, 174-176). The

psychiatric and cognitive impairments associated with motor dysfunction may partially stem from deficits in the three distinct topographical domains of the basal ganglia: the limbic, associative, and somatosensory circuits, all of which converge in the PF's topographical organization (31).

Additionally, the PF was selected as the target over the striatum due to its smaller size and the fact that approximately 70–90% of PF axonal projections innervate the striatum from anterior to posterior regions, with only a few collaterals extending to the cerebral cortex (32). Consequently, BDNF overexpressed in PF neurons is transported anterogradely and released in the striatum. Direct delivery to the striatum would be less effective as it would not adequately address the three domains due to the striatum's larger volume. Utilizing PF axonal transport of the viral vector enables the dissemination of therapeutic BDNF throughout brain circuitry, thus requiring a lower viral load and reducing the risk of viral toxicity.

Our objective in administering AAV5- and AAV9-BDNF to the PF is to enhance BDNF synthesis, anterograde transport, and release within the striatum, thereby activating its TrkB receptor and providing the physiological support mechanism for thalamostriatal neurotrophic support. The primary aims of this study are to achieve BDNF overexpression in the PF and assess its release in the striatum by evaluating GFP expression, increased striatal BDNF levels, and TrkB receptor activation. Secondary aims include assessing behavioral improvements and motor function following gene delivery.

Chapter 3: METHODOLOGY

Part 1.

Visualize the thalamostriatal system in C57BL/6J mice injecting the anterograde neuronal tracer biotin dextran amine in the Parafascicular thalamic nucleus

Animals:

Animal procedures were done following the Canadian Council on Animal Care guidelines for the ethical use and welfare of animals in research, as determined by the McGill University Animal Care Committee. All surgical experiments performed with C57BL/6J mice used a colony maintained at the Animal Facility for Neurological Disease Models of the Montreal Neurological Institute.

Surgical procedures:

4-weeks old C57BL/6J mice were injected intracranially in the right Parafascicular thalamic nucleus (PF) with the anterograde neuronal tracer Biotin dextran amine (BDA) 10% (NeuroTrace^{TM} BDA-10,000 Neuronal Tracer Kit (N-7167)) following the McGill Standard Operating Procedure #202 “Rodent Stereotaxic Surgery” https://mcgill.ca/research/files/research/202-_rodent_stereotaxic_surgery_-_may_2018_0.pdf). Briefly, animals were deeply anesthetized with isoflurane and positioned in a stereotaxic frame. 0.5ul of BDA 10% was injected using the following stereotaxic coordinates (Franklin & Paxinos, 2008): anterior-posterior (AP) -2.27, medial-

lateral (ML) +0.75, dorsal-ventral (DV) -3.5 at an injection rate of 0.1 μl/min. For a targeted structure, stereotaxic coordinates are calculated relative to two reference points: the Bregma and lambda points situated on the surface of the skull at the junction of different bone plates (Ferry, Gervasoni, & Vogt, 2014).

BDA visualization:

Mice lived a week post-injection, and then they were transcardially perfused with 0.9% heparinized saline followed by 4% paraformaldehyde (PFA) and 0.5% Glutaraldehyde. Brains were cryoprotected with 30% sucrose and then cut coronally in 40 um sections. Free-floating sections were incubated with standard avidin-biotinylated HRP (Vectastain, ABC-HRP kit; LS-J1009) following nickel-enhanced diaminobenzidine (DAB) reaction (Reiner et al., 2000). Finally, to recognize brain regions through histology, sections were counterstained with NeuN (1:500; Sigma-Aldrich, MAB377) and were coverslipped using Permount (Fisher Scientific, Whitby, ON, Canada).

Evaluate AAV5-eGFP gene expression and axonal transport

AAV vector:

A recombinant $AAV_{2/5}$ vector (Capsid: AAV-5, ITR: AAV-2) containing green fluorescent protein cDNA sequence regulated by the cytomegalovirus enhancer promoter was used to express GFP (AAV5-CMV-eGFP). Vector produced by Vector Biolabs (Malvern, PA, USA). The titer used was 5.6×10^{12} vg/ml.

Different treatment groups:

Four weeks old C57BL/6J mice were injected unilaterally in the PF with the vector AAV5-eGFP to evaluate GFP expression dynamics in the ipsilateral striatum at 1-, 3-, 5- and 11-weeks post injection (n=3 per week).

Surgical procedures:

Mice injected intracranially in the right PF used the following stereotaxic coordinates (Franklin & Paxinos, 2008): AP -2.27, ML +0.75, DV -3.5. All surgeries were done following the McGill Standard Operating Procedure #202 “Rodent Stereotaxic Surgery” and the protocol reported by Lowery and Majewska (Lowery & Majewska, 2010). As mentioned before, mice were deeply anesthetized with isoflurane and positioned in a stereotaxic frame where 1 μl of the AAV vector was injected at a rate of 0.1 μl/min.

After 1-, 3-, 5- and 11-weeks of the injection, mice were euthanized under deep anesthesia with transcardial perfusion of 0.9% heparinized saline followed by PFA. Brains were cryoprotected with 30% sucrose and then cut coronally into 40 um-thick sections using a freezing microtome. Free-floating sections were collected serially into six vials per brain containing PBS (0.1M, pH 7.4).

GFP immunohistochemistry:

40 um free-floating sections were incubated in blocking solution (PBS with 0.5% triton X-100, 10% normal goat serum (NGS) and 5% bovine serum albumin (BSA)) for 1 hour. Next, sections were incubated with GFP antibody (1:1000, Invitrogen, #A-11122) in

blocking solution overnight at 4 °C. After incubation, sections were washed three times with PBS at room temperature (RT) followed by incubation in goat secondary antibody (1:200, Bio-Rad, Hercules, CA) in blocking solution at RT for 1 hour. Sections were washed 3 times with PBS at RT and then incubated with standard avidin-biotinylated HRP (Vectastain, ABC-HRP kit; LS-J1009). Next, sections were washed three times with PBS at RT and developed with DAB reaction for 10 minutes. DAB step was stopped by six washes of PBS. Finally, to recognize brain regions through histology, sections were mounted onto glass-coated slides, dried overnight and were counterstained with 0.1% cresyl violet (Nissl stain). Slides dried and were coverslipped using Permount (Fisher Scientific, Whitby, ON, Canada).

Determine if the AAV5-BDNF-hrGFP vector produces motor behavior changes in the R6/2 mouse line

Animals:

The behavioral assays were performed with R6/2 mice from a colony maintained at the Animal Facility for Neurological Disease Models of the Montreal Neurological Institute (B6CBA-Tg(HDexon1)62Gpb/3J) following the standards of the Canadian Council on Animal Care. Ovarian transplanted R6/2 females were obtained from a line maintained at the Jackson Laboratory and were crossed with males of the C57bl/6J background. It is important to mention that within the R6/2 mouse line, there are mice that carry the mhtt gene with CAG repeats between 119 and 125, and those will be referred to as “R6/2 carriers (R6/2 CAR)” whereas the other littermates that do not carry the mhtt gene will be

referred to as “R6/2 wild-type (R6/2 WT)”. The pups were genotyped at three weeks old by Laragen (Culver City, CA, USA). For this project, only male mice were used to avoid variability related to sex (L. Menalled et al., 2009).

Baseline of R6/2 model behavior and locomotor activity:

Behavioral tests timeline:

To establish a baseline of the animal model behavior and locomotor activity, R6/2 CAR and age-matched R6/2 WT littermates mice were studied using the Clasping test, Open Field and Elevated plus maze. Clasping tests were performed every week starting at four weeks of age until the mice reached 12 weeks old. Open Field and Elevated plus maze were performed at 4, 6, 9 and 11 weeks of age.

Clasping test:

The Clasping test is used as a marker of disease progression in several mouse models of neurodegeneration (Guyenet et al., 2010). In this test, the mouse tail is grabbed near its base, allowing the mouse to be lifted approximately twenty centimeters from the table, and it is recorded for twenty seconds the times and duration the mouse retracts a limb towards the midline following the protocol from Samadi et al. (Bissonnette, Vaillancourt, Hébert, Drolet, & Samadi, 2013; Samadi et al., 2013). The extent of clasping per limb was graded as follows: None=0; mild=0.25; moderate=0.5, and severe and constant=0.75. The resulting score was added and averaged.

Open field test:

The Open Field is a 1-hour test that focuses on spontaneous locomotor activity in a square arena surrounded by walls that prevent mice from escaping (Gould, Dao, & Kovacsics, 2009; Kumar, Bhat, & Kumar, 2013). The paths traveled by the mice in the arena were recorded with the EthoVision XT software from the Noldus Company. The total distance traveled, and Mean velocity of locomotor activity are measured from the recorded patterns in the arena.

Elevated plus maze:

The Elevated plus maze is an "+" shaped maze with two covered and two uncovered arms elevated fifty centimeters from the ground. This maze represents a dilemma to the mice because of their innate curiosity to explore new environments against the fear they experience of the open and elevated arms (Baldo & Petersén, 2015; Komada, Takao, & Miyakawa, 2008). The test lasted 10 minutes, and the paths traveled by the mice in the arena were recorded with the EthoVision XT software from the Noldus Company. Time spent in closed arms and time spent in open arms were converted into a ratio Time spent in open arms/Time spent in closed arms, where a higher resulting value corresponds to less anxiety. The time spent ratio, and the total distance covered are variables measured from the recorded patterns in the maze.

Weight:

R6/2 CAR and R6/2 WT were weighed each week.

Statistical methods used in this analysis:

The data were expressed as mean ± SE. The significance of the data from the Clasping test, open field and elevated plus maze variables was statistically analyzed by a two-tailed Independent-sample T-test comparing R6/2 WT vs R6/2 CAR mice per week.

Behavior and locomotor activity in AAV-treated R6/2 mice

After establishing a baseline of the R6/2 model behavior, the AAV5-BDNF-hrGFP vector was administered as a therapeutic vector to R6/2 CAR mice:

AAV vector:

Recombinant $AAV_{2/5}$ vector (Capsid: AAV-5, ITR: AAV-2) containing full human BDNF cDNA sequence followed by hrGFP sequence regulated by the CMV enhancer-promoter was used to overexpress BDNF and hrGFP; an IRES element was used as a linker between transgenes (AAV5-CMV-hBDNF-IRES2-hrGFP; expressed here as AAV5-BDNF-GFP). Vector produced by Vector Biolabs (Malvern, PA, USA). The titer used was 5.6×10^{12} vg/ml.

Different treatment groups:

Three different groups were established with R6/2 mice: 1) not injected R6/2 wild-type mice (R6/2 WT), 2) not injected R6/2 carrier mice (R6/2 CAR) and 3) AAV5-BDNF-GFP injected R6/2 carrier mice (R6/2 CAR-BDNF).

Surgical procedures:

R6/2 CAR mice were deeply anesthetized with isoflurane and positioned in a stereotaxic frame. 1 μl of AAV5-BDNF-GFP vector was injected bilaterally in the PF at four weeks of age following these stereotaxic coordinates (Franklin & Paxinos, 2008): AP -2.27, ML +0.75, DV -3.5 at an injection rate of 0.1 μl/min.

Behavioral and locomotor assays timeline:

R6/2 WT, R6/2 CAR, and R6/2 CAR-BDNF mice were studied using Clasping test, Open Field and Elevated plus maze starting at four weeks old before AAV injection. Mice were left to recover, and Open Field and Elevated plus maze were continued at 6, 9 and 11 weeks of age. Clasping test was performed each week from 6 weeks to 11 weeks of age.

Weight:

R6/2 WT, R6/2 CAR, and R6/2 CAR-BDNF mice were weighed each week.

Tissue preparation for immunohistochemistry:

11.5 weeks old R6/2 WT and CAR mice were euthanized under deep anesthesia with transcardial perfusion of 0.9% heparinized saline followed by PFA. Brains were cryoprotected with 30% sucrose and then cut coronally into 40 um-thick sections using a freezing microtome. Free-floating sections were collected serially in six vials filled with PBS (0.1M, pH 7.4). One of the six vials with free-floating sections was used for NeuN

immunohistochemistry (NeuN 1:1000; MAB377, Millipore, Canada) to evaluate morphological changes induced by AAV expression.

Morphological changes of AAV-injected brains:

These results were obtained by Chris Valenti, a summer student in 2019.

Unbiased stereology was carried out on $NeuN^+$ coronal sections using the Stereo Investigator program (Microbrightfield, Willston, VT, USA) and an Olympus BX-40 microscope equipped with a motorized XYZ stage.

Contours of the neostriatum were drawn at a 4x magnification according to defined boundaries using the Paxinos Mouse brain atlas (Franklin & Paxinos, 2008). While the neostriatum is generally anatomically well-defined, its ventral limits rostral to the anterior commissure are arbitrary, as it interfaces with the nucleus accumbens in this region. Following Samadi et al., (Bissonnette et al., 2013; Samadi et al., 2013) the neostriatum was therefore delimited from the nucleus accumbens by a line extending from the most ventral point of the lateral ventricle medially to the tapered external capsule laterally, at an angle of 30 degrees below the axial plane.

The optical fractionator was used as a stereology probe to obtain unbiased estimates of the total number of neurons; counts were conducted at 100x magnification under oil immersion. The systematic random sampling grid size was 500 × 500 μm, and the optical fractionator counting frame was 60 × 60 μm, with guard zones of 1 μm at the top and bottom surface.

Statistical methods used in this analysis:

The Open field and elevated plus maze assays were statistically analyzed with a Two-way mixed ANOVA. For the Clasping test, R6/2 WT mice showed considerably less clasping than the other two groups therefore, for the statistical analysis, only R6/2 CAR and R6/2 CAR-BDNF mice were analyzed using a two-tailed Independent-sample T-test. Regarding Stereology results, data was analyzed using a one-way ANOVA with a Tukey post-hoc test.

Verification of accurate AAV5-BDNF-GFP injection

Another of the six vials with 40 um-thick free-floating sections in PBS was used for GFP immunohistochemistry (GFP 1:1000; #A-11122, Invitrogen) to verify accurate AAV injection in the PF. The behavioural and locomotor assay analysis included only mice properly injected in the PF.

Evaluate if bilateral injection in the PF with AAV5-BDNF-GFP increases GFP and BDNF expression as well as activation of TrkB receptor in the striatum and at the injection site of C57BL/6J mice

Because it was not possible to verify the accurate injection of AAV5-BDNF-GFP in the PF of the R6/2 WT and CAR mice using GFP immunohistochemistry, comparative molecular studies were performed between the expression of AAV5-BDNF-GFP and the control vector AAV5-GFP.

AAV vectors:

Recombinant $AAV_{2/5}$ vector (Capsid: AAV-5, ITR: AAV-2) containing hrGFP-tagged human full BDNF cDNA sequences regulated by the CMV enhancer-promoter and the IRES element was used to overexpress BDNF (AAV5-CMV-hBDNF-IRES2-hrGFP). As a control, vector AAV5-CMV-GFP was used. Vectors were produced by Vector Biolabs (Malvern, PA, USA). The titer used for both was 5.6×10^{12} vg/ml.

Different treatment groups:

Four weeks old C57BL/6J mice were injected **1)** bilaterally in the PF, AAV5-BDNF-GFP on the right hemisphere and AAV5-GFP on the left hemisphere to evaluate GFP expression at the injection site after three weeks (n=4); **2)** bilaterally in the Striatum, AAV5-BDNF-GFP on the right hemisphere and AAV5-GFP on the left hemisphere to evaluate GFP expression at the injection site after three weeks (n=4), **3)** bilaterally in the PF with AAV5-GFP (n=9) or with AAV5-BDNF-GFP (n=13) to compare BDNF, GFP and pTrkB expression at the injection site and in the striatum after five weeks using western blot or **4)** unilaterally in the right Globus pallidus with AAV5-BDNF-GFP (n=4) to compare BDNF and GFP expression in the injected hemisphere versus the not injected hemisphere after five weeks using western blot. The globus pallidus was chosen as a target region in this case due to its reported lack of $BDNF^+$ fibers, cell bodies, and lack of BDNF mRNA (Conner et al., 1997). Not injected mice were included as a negative control in groups 1, 2 and 3.

Surgical procedures:

Mice injected intracranially in the PF used the following stereotaxic coordinates (Franklin & Paxinos, 2008): AP -2.27, ML +0.75, DV -3.5; in the striatum: AP +0.65, ML 2, DV -3 and in the globus pallidus: AP -0.47, ML 1.75, DV 4. All surgeries were done following the McGill Standard Operating Procedure #202 “Rodent Stereotaxic Surgery” and the protocol reported by Lowery and Majewska (Lowery & Majewska, 2010). As mentioned, mice were deeply anesthetized with isoflurane and positioned in a stereotaxic frame where 1 μl of the AAV vectors was injected per side at a rate of 0.1 μl/min.

Groups 1, 2:

AAV-injected mice in groups 1 and 2 were euthanized under deep anesthesia with transcardial perfusion of 0.9% heparinized saline, followed by PFA. Brains were cryoprotected with 30% sucrose and then cut coronally into 40 um-thick sections with a freezing microtome. Sections were collected serially in six vials filled with PBS (0.1M, pH 7.4). One of the vials with the 40 um free-floating sections was used for GFP immunohistochemistry (GFP 1:1000; #A-11122, Invitrogen).

Groups 3, 4:

AAV-injected mice in groups 3 and 4 were decapitated five weeks post-injection to allow the viral vector to reach a plateau of gene expression at the injection site. Not-injected mice were decapitated at nine weeks of age (age-matched with the AAV-injected mice). Brains were obtained and immediately snap frozen at -80 Celsius until used. Following

the Nguyen et al. (Nguyen et al., 2016) protocol, Atlas defined (Franklin & Paxinos, 2008) PF, striatal and globus pallidal tissue samples were obtained using a 1 x 1.5 mm cylindrical micro-punch (Stoelting, IL, USA).

Tissue preparation and protein extraction:

For the determination of protein expression levels, brain punches were homogenized on ice in 100 μl of RIPA protein lysis buffer consisting of 50 mM Tris–HCl (pH 8.0), 150 mM NaCl and 1% Triton X-100 with Halt protease inhibitor cocktail (Thermo Scientific™ Pierce, Rockford, IL). The homogenates were centrifuged at 14,000 rpm for 20 minutes at 4 °C. The resulting supernatants were collected, and protein levels were determined in an aliquot of each sample using the BCA assay kit (Thermo Fisher Scientific Inc., Rockford, IL).

Western blot:

Thirty μg of protein from AAV5-BDNF-GFP and AAV5-GFP injected mice and not-injected mice were denatured by mixing and boiling with 4x Laemmli buffer (Bio-Rad, Hercules, CA) mixed with β-mercaptoethanol (5%). Recombinant BDNF protein (PreproTech, NJ, USA) was also run in parallel as a positive control for the antibody and the migration of endogenous BDNF at 14 kDa. Proteins were separated by electrophoresis on 4-20% gradient gels of SDS-PAGE and transferred to nitrocellulose membranes (Bio-Rad, Hercules, CA). Membranes were blocked with 5% BSA in TBST for 1 hour at RT and then probed overnight at 4°C with primary antibodies diluted in 5% BSA in TBST: total TrkB (1:1000; Cell Signaling Technologies, MA, USA, #4603), phospho-TrkB (Tyr705; 1:500;

Santa Cruz, CA, USA, #sc135645), BDNF (1:500; Millipore, Temecula, CA, #AB1534), GFP (1:2000, Invitrogen, #A-11122) and Tubulin β-3 (1:5000; Biolegend, #802001) as a loading control. After washing with TBST, a secondary HRP-conjugated antibody (Goat Anti-Rabbit IgG; 1:4000; Bio-Rad, Hercules, CA; #1706515) diluted in 5% BSA in TBST was incubated for 1 hour at RT. Following a second wash of membranes with TBST, membranes were developed by ECL (Pierce, IL, USA) and Image-J (NIH software, version 1.47) was used for optical density (OD) quantification of each protein band. Relative protein levels were derived by calculating the OD of the specific band minus the background intensity of the membrane and normalized to the tubulin β-3 band in the same lane, thereby controlling for any effect of unequal total neuronal protein concentrations between lanes (Nguyen et al., 2016; Stael, Miller, Fernández-Fernández Á, & Van Breusegem, 2022).

Statistical methods used in this analysis:

The data were expressed as mean ± SE. An Independent-sample T-test was used to determine significant differences between BDNF, GFP and pTrkB expression in the different regions of injected mice.

Part 2.

Preclinical AAV plasmid candidate selection in collaboration with Dr. Rénald Gilbert's group at the National Research Council Canada (NRC)

R6/2 CAR mice injected with AAV5-BDNF-GFP showed statistically significant changes in the Clasping test and striatal neuronal number. However, it was not possible to verify accurate AAV injection in the PF of R6/2 mice nor evaluate in C57BL/6J mice increase in BDNF or GFP using western blot. Therefore, we approached Dr. Rénald Gilbert from the NRC to genetically study the AAV5-BDNF-GFP vector.

cDNA Plasmids sequence:

Upon request, the genetic material in the AAV5-BDNF-GFP vector was provided separately by Vector Biolabs (Malvern, PA, USA) for further testing. It will be referred to as the plasmid CMV-hBDNF-IRES2-hrGFP. Dr. Gilbert's group at the NRC sequenced the plasmid using the primers mentioned in **Table 1** and compared the amino acids alignment of the resulting GFP with a regular eGFP from a plasmid provided by Cell Biolabs (pCMV-eGFP).

Table 1*. Primers used to sequence Vector Biolabs plasmid elements*

Primers	Sequence
#4 (CMV)	GATTTCCAAGTCTCCACC
#358 (IRES2)	GCTTCGGCCAGTAACGTTAGG
#487 (bGHPolyA)	GCAAACAACAGATGGCTGGC
#662 (IRES2)	CCACCATATTGCCGTCTTTTGG

Next, the group created a plasmid using the hBDNF sequence provided by Vector Biolabs (Malvern, PA, USA) and the CMV promoter and eGFP sequence provided by Cell Biolabs connected by the link sequence 2A: pCMV-hBDNF-2A-eGFP (**Table 2**).

In vitro evaluation of pCMV-hBDNF-IRES2-hrGFP compared to pCMV-eGFP:

HEK293SF cells at P23 grown in BalanCD HEK293 medium (Irvine Scientific, #91165) containing 4 mM L-Glutamine were transfected by Dr. Gilbert's group at the NRC. Using PEIpro® DNA transfection reagent (VWR International), cells were transfected with pCMV-hBDNF-IRES2-hrGFP or pCMV-eGFP. Not transfected HEK293SF cell cultures were used as controls.

GFP fluorescence

Cells were incubated at 37 °C for 24-, 48- and 72-hours post-transfection and then looked at GFP fluorescent signal under an inverted microscope. After GFP signal observation, cell pellets and supernatants were collected and stored at -20 °C until used by our lab. This experiment was conducted three independent times. Cell pellets were collected from each cell culture to be analyzed by our lab using a western blot to evaluate BDNF and GFP expression.

Fluorescence-Activated Cell Sorting (FACS) assay

FACS assay was performed at 48- and 72-hours post-transfection to evaluate the percentage of GFP+ cells as a measure of the proportion of successfully transfected cells in each culture.

In vitro validation of pCMV-hBDNF-2A-eGFP compared to pCMV-eGFP:

Another set of HEK293SF cells at P10 grown in BalanCD HEK293 medium (Irvine Scientific, #91165) containing 4 mM L-Glutamine were transfected by Dr. Gilbert's group. Using PEIpro® DNA transfection reagent (VWR International), cells were transfected with pCMV-hBDNF-2A-eGFP or pCMV-eGFP. Not transfected HEK293SF cell cultures were used as controls. Cell cultures were incubated at 37 °C for 48 hours, and then cell pellets and supernatants were collected and stored at -20 °C until used by our lab. This experiment was conducted three times. Cell pellets were analyzed by western blot to evaluate GFP expression, and the supernatants were analyzed by our lab using enzyme-linked immunosorbent assay (ELISA) to evaluate BDNF secretion.

***Table 2**. Plasmids used during in vitro testing*

Plasmid	Produced by
pCMV-hBDNF-IRES2-hrGFP	Vector Biolabs
pCMV-hBDNF-2A-eGFP	NRC

Cell pellet preparation and protein extraction:

For the determination of protein expression levels, HEK293SF cell pellets after 48 hours of transfection were homogenized on ice in 100 μl of RIPA protein lysis buffer consisting of 50 mM Tris–HCl (pH 8.0), 150 mM NaCl and 1% Triton X-100 with Halt protease inhibitor cocktail (Thermo Scientific™ Pierce, Rockford, IL). The homogenates were centrifuged at 14,000 rpm for 20 minutes at 4 °C. The resulting supernatants were collected, and protein levels were determined in an aliquot of each sample using the BCA assay kit (Thermo Fisher Scientific Inc., Rockford, IL).

Western blot:

Thirty μg of protein from each transfected cell culture or not transfected, was denatured by mixing and boiling with 4x laemmli buffer (Bio-Rad, Hercules, CA) mixed with β-mercaptoethanol (5%). Recombinant BDNF protein (PreproTech, NJ, USA) was also run in parallel as a positive control for the antibody and the migration of endogenous BDNF at 14 kDa. Proteins were separated by electrophoresis on 4-20% gradient gels of SDS-PAGE and transferred to nitrocellulose membranes (Bio-Rad, Hercules, CA). Membranes were blocked with 5% BSA in TBST for 1 hour at RT and then probed overnight at 4°C with primary antibodies diluted in 5% BSA in TBST: BDNF (1:500; Millipore, Temecula, CA, #AB1534) and/or GFP (1:2000, Invitrogen**,** #A-11122) and Tubulin β-3 (1:5000; Biolegend, #802001) or β-actin (1:10000; Sigma-Aldrich, #A5441) as loading control. After washing with TBST, a secondary HRP-conjugated antibody (Goat Anti-Rabbit IgG; 1:4000; Bio-Rad, Hercules, CA; #1706515) diluted in 5% BSA in TBST was incubated for 1 hour at RT. Following a second wash of membranes with TBST, membranes were

developed by ECL (Pierce, IL, USA) and Image-J (NIH software, version 1.47) was used for OD quantification of each protein band.

Relative protein levels were obtained by calculating the OD of the specific band minus the background intensity of the membrane and normalized to the tubulin β-3 or actin band in the same lane, thereby controlling for any effect of unequal total neuronal protein concentrations between lanes (43).

Enzyme-linked immunosorbent assay (ELISA):

Supernatants of HEK293SF cell cultures transfected with pCMV-hBDNF-2A-eGFP, pCMV-eGFP or no plasmid were analyzed by triplicate using an ELISA kit from Biosensis (#BEK-2211) to evaluate mature BDNF secretion. Supernatants were thawed and centrifuged at 10,000 x g for 5 minutes to remove particulates (all steps were performed at RT). Mature BDNF standard serial dilutions were prepared with BalanCD HEK293 medium (Irvine Scientific, #91165) to create a standard curve with known concentrations. Diluted mature BDNF standards, supernatant samples and positive and negative controls were loaded into a pre-coated 96-well microplate and were incubated on a shaker for 45 minutes at 140 rpm. Five washes with wash buffer followed, and the detection antibody was added. The antibody was incubated for 30 minutes on a shaker at 140 rpm and then washed five times. A streptavidin-HRP conjugate was added and incubated for 30 minutes on a shaker at 140 rpm. The final five washes were done before adding the substrate tetramethylbenzidine (TMB), which was incubated for 5 minutes without shaking in the dark. After stopping the reaction, the visible blue color changed to yellow, and the absorbance was read at 450 nm on a plate reader.

To calculate BDNF protein levels, all values were adjusted for background absorbance by subtracting the OD of the blank value (BalanCD HEK293 medium). The BDNF standard curve was plotted with the adjusted OD of each BDNF standard solution as the Y-axis vs. the known concentration of mature BDNF standard solution as the X-axis. The mature BDNF protein concentration of the supernatant samples was interpolated from the standard curve.

Statistical methods used in this analysis:

The data were expressed as mean ± SE. A One-way ANOVA was used to analyze western blot and ELISA results to determine significant differences between protein expression and BDNF secretion in transfected and control HEK293SF cell cultures.

Preclinical AAV viral vector candidate selection in collaboration with Dr. Rénald Gilbert's group at the National Research Council Canada (NRC)

AAV vectors:

Once the CMV-hBDNF-2A-eGFP plasmid was tested and chosen, Dr. Gilbert's team transfected it into HEK293 packaging cells along with other helper plasmids to construct a BDNF-expressing rAAV (Jalšić et al., 2023). The two ITRs were taken from the AAV2 genome, but AAV5 and AAV9 capsids were used. The result was: AAV2/5-CMV-hBDNF-2A-eGFP (titer 4.95E+12 vg/ml) and AAV2/9-CMV-hBDNF-2A-eGFP (titer 2.99E+13 vg/ml) vectors with their corresponding control vectors, AAV2/5-CMV-eGFP (titer 5.40E+12 vg/ml) and AAV2/9-CMV-eGFP (titer 1.53E+13 vg/ml).

Different treatment groups:

Injected C57BL/6J mice received the following NRC produced vectors: **1)** AAV5-eGFP (n=3), **2)** AAV9-eGFP diluted 1:1 with PBS (n=3), **3)** AAV5-BDNF-eGFP (n=3) and **4)** AAV9-BDNF-eGFP (n=3) to evaluate GFP expression at the injection site and anterograde transport to the ipsilateral striatum after 3.5 weeks post-injection. Another group of mice received **5)** AAV5-BDNF-eGFP (n=3) and **6)** AAV9-BDNF-eGFP (n=3) to evaluate GFP expression at the injection site and anterograde transport to the ipsilateral striatum after nine weeks post-injection.

Surgical procedures:

4-week-old C57BL/6J mice were injected unilaterally in the PF using the previously mentioned stereotaxic coordinates (Franklin & Paxinos, 2008): AP -2.27, ML +0.75, and DV -3.5. Stereotaxic surgeries were done following the McGill Standard Operating Procedure #202 “Rodent Stereotaxic Surgery” and the protocol reported by Lowery and Majewska (Lowery & Majewska, 2010). Mice were deeply anesthetized with isoflurane and positioned in a stereotaxic frame where 1 μl of the AAV vector was injected at a rate of 0.1 μl/min.

GFP immunohistochemistry:

After the specified time of survival post-injection, AAV-injected mice were euthanized under deep anesthesia with transcardial perfusion of 0.9% heparinized saline followed by

PFA. Brains were cryoprotected with 30% sucrose, cut coronally in 40 um-thick sections and processed for GFP immunohistochemistry performed as described above.

Statistical methods used in this analysis:

Comparison of GFP expression at nine weeks post-injection between AAV5-BDNF-eGFP and AAV9-BDNF-eGFP injected mice in the injected PF and in the ipsilateral striatum was measured as pixel intensity by public domain National Institutes of Health Image J analysis software (NIH Image J, v1.45s, Bethesda, MD). The data were expressed as mean ± SE. A Mann-Whitney U test was used to analyze the pixel intensity values because the data obtained failed to meet a normal distribution.

Evaluate if the injection in the PF with AAV9-BDNF-eGFP viral vector increases GFP and BDNF expression as well as activation of TrkB receptor in the ipsilateral striatum and at the injection site of C57BL/6J mice

AAV vectors:

Recombinant AAV2/9 vectors produced by Dr. Gilbert's group at the NRC will be used for the experiments in this section: AAV2/9-CMV-hBDNF-2A-eGFP (titer 2.99E+13 vg/ml) and AAV2/9-CMV-eGFP (titer 1.53E+13 vg/ml) viral vectors. AAV2/9-CMV-eGFP vector had to be diluted 1:1 with PBS to restrict the cellular transduction to cells closer to the site of injection (results not shown here).

Different treatment groups:

Group **1)** was injected with the AAV9-BDNF-eGFP vector in the right hemisphere and the AAV vehicle buffer in the left hemisphere (n=5) to evaluate BDNF anterograde transport to the striatum, GFP expression and pTrkB activation three weeks post-injection; Group **2)** was injected with AAV9-BDNF-eGFP (1:5 diluted with PBS) in the right hemisphere and the AAV9-eGFP (1:1 diluted with PBS) vector in the left hemisphere (n=3) to quantify BDNF protein levels in the striatum three weeks post-injection. Not-injected age-matched mice were included as negative controls (n=3).

Surgical procedures:

Four weeks old C57BL/6J mice were injected bilaterally in the PF using the previously mentioned stereotaxic coordinates (Franklin & Paxinos, 2008): AP -2.27, ML +0.75, and DV -3.5.

Tissue preparation:

After the specified time of survival post-injection, AAV-injected mice were decapitated, and then brains were obtained. Brains were cut in half along the coronal plane at the segment between the caudal edge of the optic chiasm and the last portion of the visible optic nerve (seen ventrally). The anterior block of the brain contained the anterior striatum, whereas the posterior block contained the thalamic portion.

GFP immunohistochemistry:

The thalamic block was immediately immersed for 24 hours in PFA, then cryoprotected with 30% sucrose and finally cut coronally in 40 um-thick serial sections. Thalamic free-floating sections were used to verify accurate AAV injection in the PF using the GFP immunohistochemistry protocol described above.

Protein extraction:

The striatum block was immediately snap frozen at -80 ºC, and following Nguyen et al. (Nguyen et al., 2016) protocol, Atlas-defined (Franklin & Paxinos, 2008) striatum tissue samples were obtained using a 1 x 1.5 mm cylindrical micro-punch (Stoelting, IL, USA). Striatal punches from brains in group 1 and group 2 were homogenized and processed for western blot and ELISA.

Western blot:

Thirty μg of protein from striatum lysates of AAV9-BDNF-eGFP and AAV buffer vehicle-injected mice in group 1 was run in 4-20% gradient gels of SDS-PAGE and transferred to nitrocellulose membranes. Membranes were incubated with BDNF, phospho-TrkB, GFP and tubulin β-3, followed by a secondary HRP-conjugated antibody and developed by ECL. The protocol is described above in detail. Relative protein levels were calculated by the OD of the specific band minus the background intensity of the membrane and normalized to the tubulin β-3 band in the same lane.

Enzyme-linked immunosorbent assay (ELISA):

Striatum lysates from mice in group 2 injected with AAV9-BDNF-eGFP and AAV9-eGFP and not injected mice were analyzed by triplicate using an ELISA kit from Biosensis (#BEK-2211) to evaluate mature BDNF protein levels. Lysates were thawed and diluted 1:5 with Biosensis assay diluent A (all steps were performed at RT). Mature BDNF standard serial dilutions were prepared with RIPA buffer to create a standard curve with known concentrations. Diluted mature BDNF standards, lysate samples and positive and negative controls were loaded into a pre-coated 96-well microplate and were incubated on a shaker for 45 minutes at 140 rpm. Five washes with wash buffer followed, and the detection antibody was added. The antibody was incubated for 30 minutes on a shaker at 140 rpm and then washed five times. A streptavidin-HRP conjugate was added and incubated for 30 minutes on a shaker at 140 rpm. The final five washes were done before adding TMB, which was incubated for 5 minutes without shaking in the dark. After stopping the reaction, the visible blue color changed to yellow, and the absorbance was read at 450 nm on a plate reader.

To calculate BDNF protein levels, all values were adjusted for background absorbance by subtracting the OD of the blank value (RIPA buffer). The BDNF standard curve was plotted with the adjusted OD of each BDNF standard solution as the Y-axis vs. the known concentration of mature BDNF standard solution as the X-axis. The mature BDNF protein levels of the striatum lysate samples were interpolated from the standard curve and then multiplied by the dilution factor.

Statistical methods used in this analysis:

The data were expressed as mean ± SE. To analyze the western blot results, an Independent-sample T-test was used to determine significant differences between BDNF, GFP and pTrkB expression in the striatum of AAV9-BDNF-eGFP and AAV buffer vehicle-injected mice. To analyze the ELISA results, not-injected mice were not considered because there were no differences with the AAV9-eGFP control vector. Therefore, an Independent-sample T-test was used to determine significant differences in BDNF protein levels anterogradely transported to the striatum of AAV9-BDNF-eGFP and AAV9-eGFP injected mice.

Part 3.

After verifying that injection of AAV9-BDNF-eGFP in the PF induces BDNF overexpression and anterograde transport to the striatum in brains of C57BL/6J mice, AAV9-BDNF-eGFP vector was administered to R6/2 CAR mice as a therapeutic vector:

Different treatment groups:

R6/2 mice were injected at four weeks of age establishing six separate groups: **1)** AAV9-BDNF-eGFP injected R6/2 WT mice (R6/2 WT-BDNF) (n=15), **2)** AAV9-BDNF-eGFP injected R6/2 CAR mice (R6/2 CAR-BDNF) (n=8), **3)** AAV9-eGFP (dilution 1:1) injected R6/2 WT mice (R6/2 WT-GFP 1:1) (n=5), **4)** AAV9-eGFP (dilution 1:1) injected R6/2 CAR mice (R6/2 CAR-GFP 1:1) (n=4). At a subsequent time, **5)** AAV9-BDNF-eGFP vector was diluted 1:5 with PBS and was injected bilaterally in the PF of R6/2 CAR mice (R6/2 CAR-

BDNF 1:5) (n=10). Following that, **6)** AAV9-BDNF-eGFP vector was diluted 1:10 with PBS and was injected bilaterally in the PF of R6/2 CAR mice (R6/2 CAR-BDNF 1:10) (n=6).

Surgical procedures:

R6/2 WT and R6/2 CAR mice were injected bilaterally in the PF with the NRC-produced AAV9-BDNF-eGFP or AAV9-eGFP viral vectors. 1 μl of AAV vector was injected bilaterally using the following stereotaxic coordinates (Franklin & Paxinos, 2008): AP -2.27, ML 0.75, DV -3.5 at an injection rate of 0.1 μl/min.

Comparison of survival curves of AAV-injected R6/2 mice:

The Kaplan-Meier method was used to calculate the survival distribution of R6/2 CAR mice injected with AAV9 vectors. Survival time refers to the weeks after AAV delivery until death.

R6/2 CAR mice injected with AAV9-BDNF-eGFP (groups 2, 5 and 6) and AAV9-eGFP vector (group 4) were left to survive without any manipulation. AAV-injected R6/2 WT mice (groups 1 and 3) were euthanized at 11.5 weeks of age under deep anesthesia with transcardial perfusion of 0.9% heparinized saline followed by PFA.

Statistical methods used in this analysis:

To test if the survival functions are equal between the different dilutions of the AAV9-BDNF-eGFP vector, the Breslow test was used, and a Bonferroni correction was made

with statistical significance accepted at the p< .0167 level (since we have three comparisons to be made, the alpha level was divided by 3 (0.05 / 3 = 0.0167)).

***Table 3**. Viral vectors used throughout the project*

Viral construct	Titer (vg/ml)	Dilution (PBS)	Produced by	Mentioned in text as:
AAV2/5-CMV-hBDNF-IRES2-hrGFP	5.6×10^{12}	-	Vector Biolabs	AAV5-BDNF-GFP
AAV2/5-CMV-eGFP	5.6×10^{12}	-	Vector Biolabs	AAV5-GFP
AAV2/5-CMV-hBDNF-2A-eGFP	4.95×10^{12}	-	NRC	AAV5-BDNF-eGFP
AAV2/5-CMV-eGFP	5.40×10^{12}	-	NRC	AAV5-eGFP
AAV2/9-CMV-hBDNF-2A-eGFP	2.99×10^{13}	-	NRC	AAV9-BDNF-eGFP
AAV2/9-CMV-hBDNF-2A-eGFP	2.99×10^{13}	1: 5	NRC	AAV9-BDNF-eGFP 1: 5
AAV2/9-CMV-hBDNF-2A-eGFP	2.99×10^{13}	1: 10	NRC	AAV9-BDNF-eGFP 1: 10
AAV2/9-CMV-eGFP	1.53×10^{13}	1: 1	NRC	AAV9-eGFP

Chapter 4: RESEARCH FINDINGS

Part 1.

A) Verification of target and anterograde transport

BDA anterograde transport through thalamostriatal projections

To determine if the striatal afferents, such as the PF, can be used to deliver proteins to the striatum anterogradely, we first used the anterograde tracer BDA to visualize the thalamostriatal system following the stereotaxic coordinates AP: -2.27, ML: +0.75, DV: -3.5 (**Fig.1**).

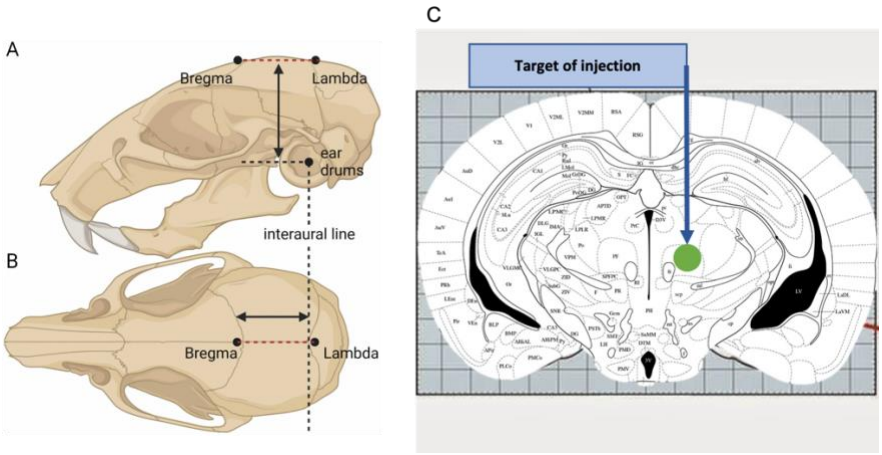

Figure 1*. Rodent skull landmarks considered for stereotaxic surgery. A. lateral view, B. dorsal view. Taken from Cecyn and Abrahao (Cecyn & Abrahao, 2023). C) Slide taken from Paxinos Mouse Atlas (Franklin & Paxinos, 2008) pointing at PF stereotaxic coordinates AP: -2.27, ML: +0.75, DV: -3.5.*

For this study, we used high molecular weight BDA (10k) because it labels axons and terminals selectively, whereas BDA (3k) shows retrograde labeling of neuronal cell

bodies. **Figure 2** shows a representative picture of a PF intracranial BDA-10k injection made at the correct stereotaxic coordinates given that the axonal labeling apparent as black Ni-DAB^{+} axonal stains stem from the PF (red dotted circle) and cover the neostriatum. Among subcortical structures, the PF has been shown to have the highest density of projections to the neostriatum, and at the same time, the PF contains distinct neuronal populations that project in a specific topographical manner to and from the cerebral cortex (Mandelbaum et al., 2019). With this experiment, it was confirmed that stereotaxic coordinates are correct and that if the PF is injected with an agent that is taken by those thalamic neurons and is transported anterogradely, it can be visualized and measured along the PF axons reaching the ipsilateral striatum. Some expected thalamic projections to the somatosensory cortex are observed too. In one week, BDA-10k was transported 3.87 mm anterogradely (**Fig. 2**).

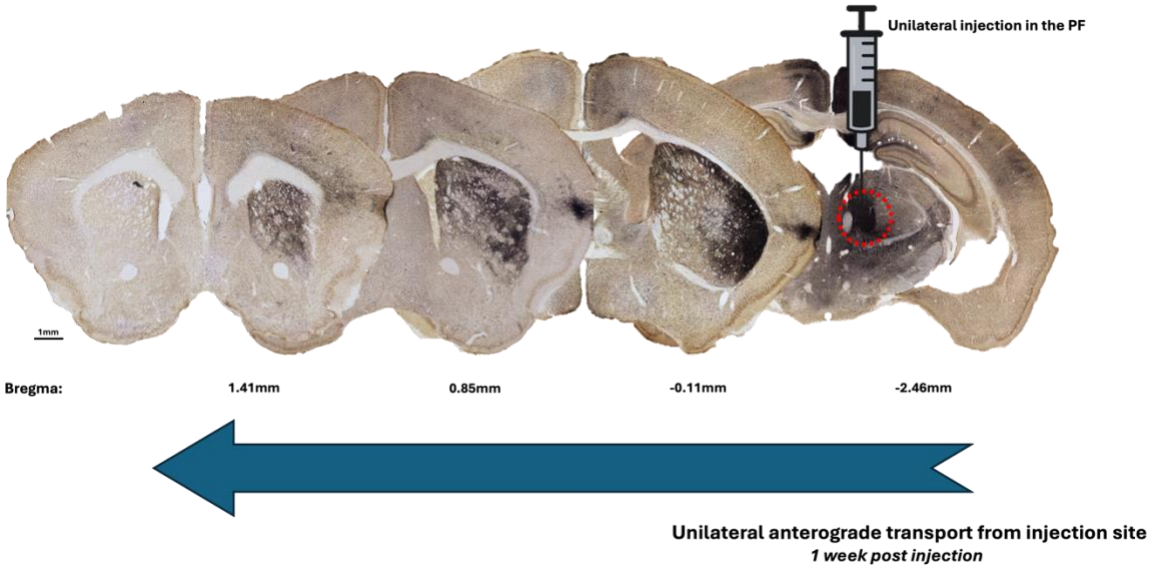

***Figure 2**. Representative pictures of coronal sections of C57BL/6J mice showing anterograde BDA neuronal tracing (black) counterstained with neuronal marker NeuN (brown).*

AAV5- GFP expression and anterograde transport

After the thalamostriatal afferents were visualized through BDA-10k injection in the PF, 1 μl of AAV5-GFP control vector was injected unilaterally into the same nucleus to evaluate how soon GFP expression appeared at the injection site and at which week GFP was transported to the ipsilateral striatum anterior to the anterior commissure (**Fig. 3**). Studying AAV5 gene expression dynamics is important to establish the experimental plan to know when the peak of transgene expression and transport is since it is not the same as the BDA transport (Aschauer et al., 2013).

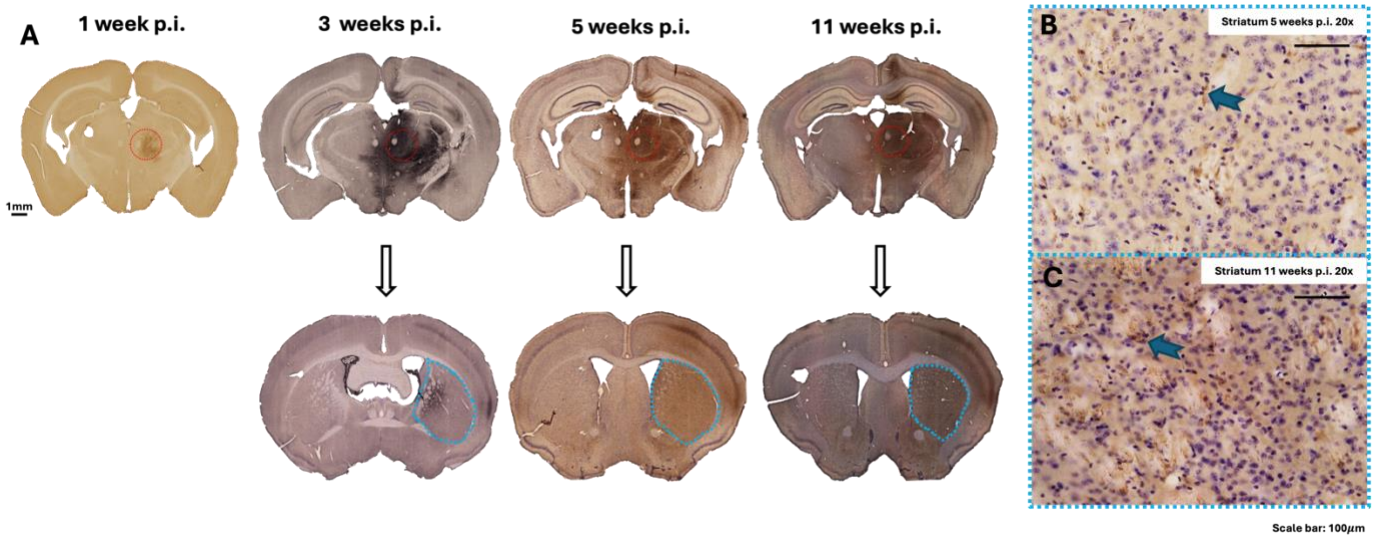

***Figure 3**. Representative pictures of coronal sections of C57BL/6J mice showing GFP expression at the injection site and transport to the ipsilateral striatum at different weeks post-injection. A. Injection site highlighted with a red circle and striatal contour in blue. B. Striatum 5 weeks post-injection, C. Striatum 11 weeks post-injection. Blue arrow pointing at GFP⁺ projections reaching striatal neurons.*

GFP expression in the cell bodies at the injected site appeared one week post-injection of the AAV5-GFP vector. However, no GFP⁺ projections towards the striatum nor the

cerebral cortex were observed (**Fig.3**). GFP expression in the cell bodies of the injected site reached its peak at three weeks post-injection and remained stable until 11 weeks after viral injection. GFP^+ projections to the striatum and cerebral cortex appeared at three weeks and remained stable until week 11 post-injection. No cell bodies in the striatum appeared to be GFP^+, only thalamic axons.

Another important aspect of studying AAV5-GFP gene expression dynamics is the amount of anterograde transport observed as opposed to retrograde transport (**Fig.4**). The viral vector transduced the cell bodies in the PF (**Fig.4E**) causing GFP synthesis in the cytosol and passive anterograde transport along the axons to the PF projection terminals, in this case the striatum, the nucleus accumbens and the cerebral cortex can be observed (**Fig.4B, C, D**). However, the PF receives projections from other regions that could pick up the AVV5-GFP vector through axon terminals present in the PF, such as other cortical regions, the pedunculopontine nucleus, the pontine reticular formation, the superior colliculus, or various regions in the brain stem that could retrogradely transport the viral vector to their cell bodies where GFP is synthesized. In **Fig.4,** there are only a few GFP^+ cell bodies in the pedunculopontine nucleus and the pontine reticular formation (**Fig.4F, G**), which suggests that there is considerably more anterograde than retrograde transport.

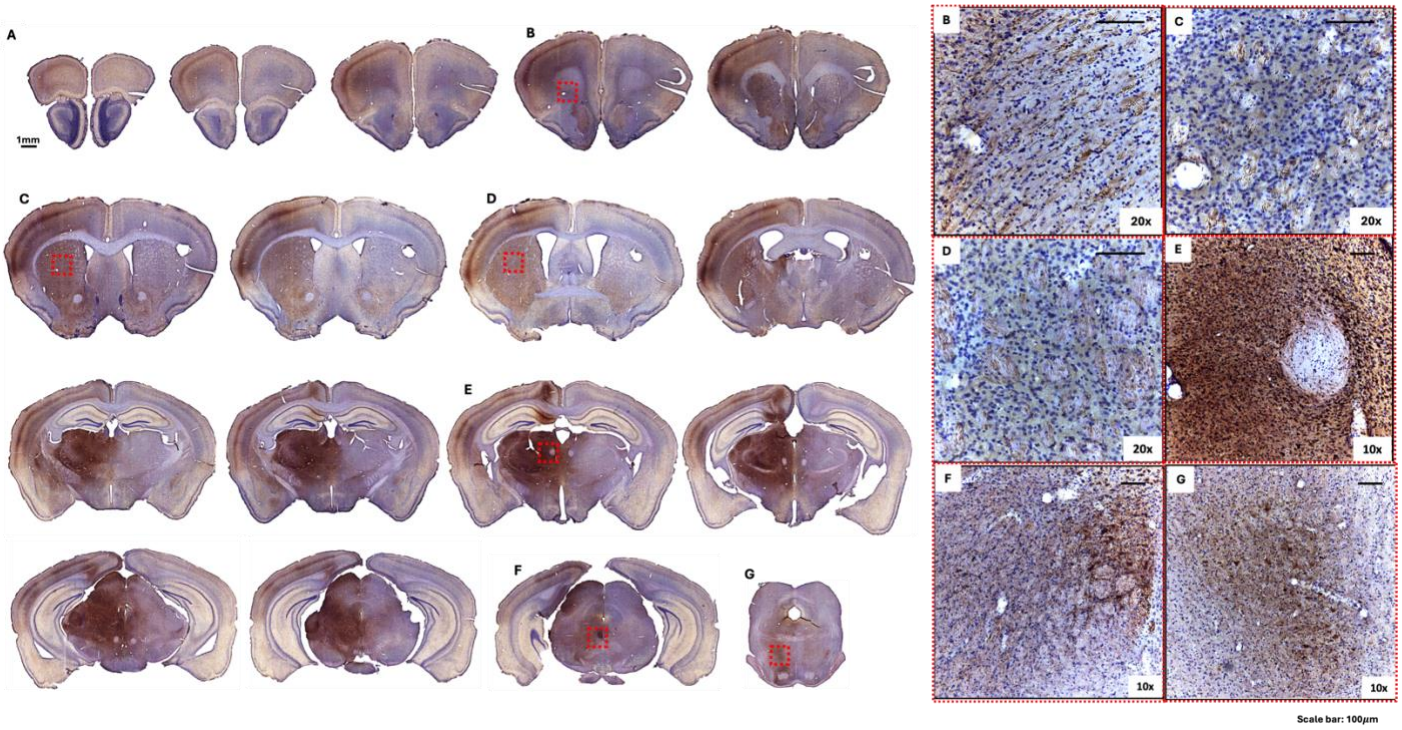

***Figure 4**. Representative pictures of coronal sections of C57BL/6J mice showing GFP expression in afferent and efferent connections of the AAV5-GFP injected PF 11.5 weeks post-injection. B, C. Anterior striatum with GFP⁺ axons. D. Striatum at anterior commissure level with GFP⁺ axons. E. GFP⁺ cell bodies at the injection site. F, G. Few GFP⁺ cell bodies at PF afferent sites.*

B) Effects of AAV5-BDNF-GFP on the behavior of R6/2 mouse model of Huntington's disease

Once we learned the peak in AAV-induced GFP expression was at three weeks post-injection and GFP transport dynamics in AAV5 transduced brains, the AAV5-BDNF-GFP vector was used to determine if a BDNF-expressing AAV construct could increase BDNF synthesis in the PF and influence its anterograde transport to the striatum. To determine if overexpression of BDNF induced by the AAV5-BDNF-GFP vector has a therapeutic

effect on locomotor activity and anxiety-like behavior, the AAV5-BDNF-GFP vector was tested in the R6/2 mouse model of Huntington's disease.

R6/2 mouse line behavior baseline

Before testing the therapeutic agent, a baseline of the animal model behavior and locomotor activity was established using R6/2 WT mice and their littermates R6/2 CAR mice. R6/2 WT mice do not possess the mhtt gene; whereas R6/2 CAR mice carry the mhtt gene and develop the disease, as opposed to R6/2 WT mice. Tests for clasping, spontaneous locomotion in an open field (OF) and anxiety-like behavior using an elevated plus maze (EPM) were performed following this schedule (**Fig.5**):

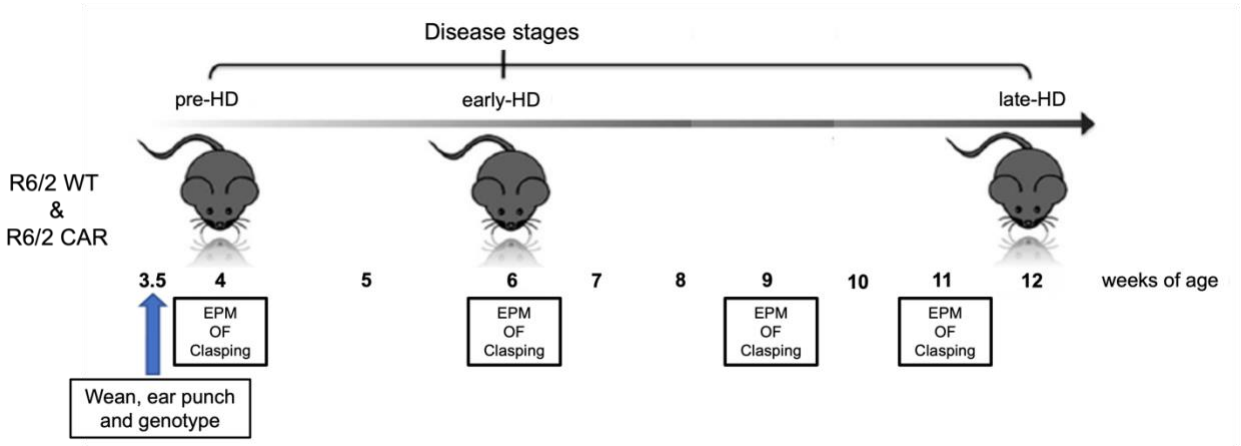

***Figure 5**. Timeline of behavior and locomotor activity assays scheduled for R6/2 mice. Elevated plus maze (EPM), Open Field (OF) and Clasping tests were performed at 4, 6, 9 and 11 weeks of age in R6/2 WT and CAR mice. In R6/2 CAR mice, the pre-HD stage is considered to be around 4 weeks old, early-HD around 6 weeks and late-HD around 12 weeks.*

Clasping test

The severity of the involuntary movements will determine the score given (**Fig.6A**) (Crevier-Sorbo, Rymar, Crevier-Sorbo, & Sadikot, 2020; Samadi et al., 2013). A two-tailed independent-sample t-test statistical analysis was performed. R6/2 WT mice rarely presented involuntary movements like clasping throughout their lives, whereas R6/2 CAR mice started showing mild signs of clasping at 4 weeks old [t= -2.368, df= 25.532, *p= 0.026]. The score increased very significantly at 6 weeks of age [t= -6.310, df= 23.062, p<0.001] and continued to rise more slowly at 9 and 11 weeks [t= -15.297, df= 10.138, p<0.001 and t= -14.305, df= 18, p<0.001, respectively] (**Fig.6B**).

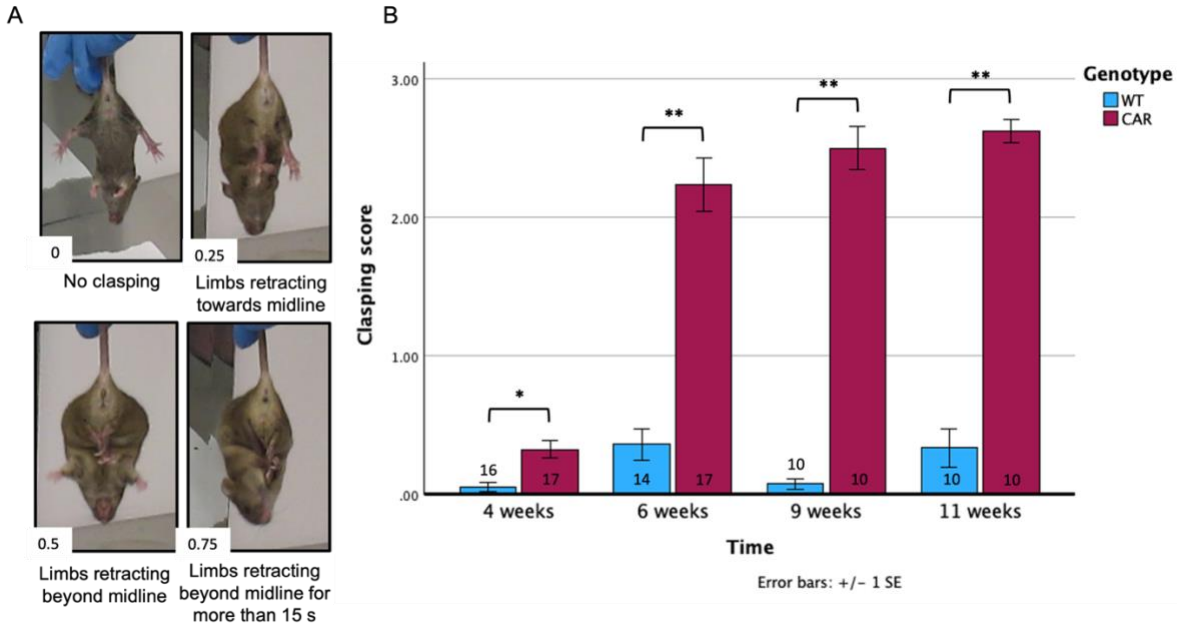

***Figure 6**. Clasping score between R6/2 CAR mice compared to R6/2 WT mice at different disease stages A. Pictures of mice showing the criteria and score to evaluate clasping test. B. As the disease progressed, there was a statistically significant increase in clasping score in R6/2 CAR mice compared to R6/2 WT littermates. A two-tailed independent-samples t-test statistical analysis was performed ("n" per group specified at the bottom of each graph bar) (*p= 0.026; **p< 0.001).*

Open field test

The open field test is used as a measure of spontaneous locomotor activity (Gould et al., 2009; Kumar et al., 2013) (**Fig.7**). Using an overview video camera and Ethovision software activity traces were recorded and analyzed. Traces showed intense activity in all directions at 4 and 11 weeks in R6/2 WT mice. In contrast, R6/2 CAR mice appeared to have increased activity in the arena at 4 weeks of age compared to R6/2 WT mice followed by a marked decrease at 11 weeks (**Fig.7A**). In agreement with the activity traces, a two-tailed independent-samples t-test revealed that total distance traveled and velocity in the arena in R6/2 CAR mice appeared to be increased at 4 and 6 weeks however it was not a significant change. At 9 and 11 weeks, there was a statistically significant reduction in R6/2 CAR mice compared to R6/2 WT mice [total distance traveled at 9 weeks: t= 2.474, df= 16.071, p= 0.025 and 11 weeks: t= 3.998, df= 7.371, p= 0.005; mean velocity at 9 weeks: t= 2.412, df= 15.761, p= 0.012 and 11 weeks: t= 3.892, df= 7.161, p= 0.006] (**Fig.7B, C**).

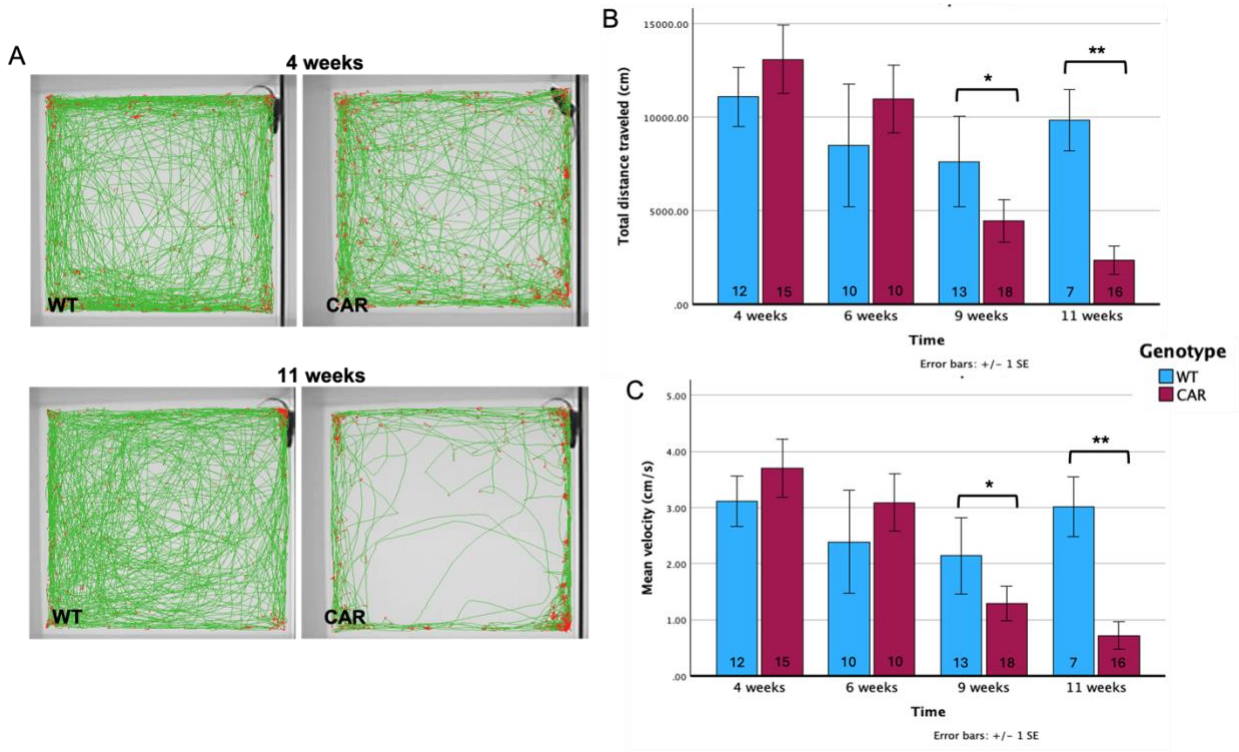

***Figure 7**. Open field test with R6/2 CAR mice compared to R6/2 WT mice at different stages of the disease. A. Representative activity traces recorded from R6/2 WT and CAR mice at 4 and 11 weeks of age. B. The total distance traveled in R6/2 CAR mice declined progressively as the disease advanced compared to R6/2 WT mice. C. Mean velocity in R6/2 CAR mice was reduced as the disease progressed compared to R6/2 WT mice. A two-tailed independent-samples t-test statistical analysis was performed ("n" per group specified at the bottom of each graph bar) (*p< 0.03; **p< 0.006).*

Elevated plus maze

Anxiety-like behavior, total distance traveled along the maze and velocity were the variables measured (**Fig.8**) (Baldo & Petersén, 2015; Komada et al., 2008; Kumar et al., 2013). A two-tailed independent-samples t-test was used to evaluate statistically significant differences between groups. Activity in the maze was recorded with an overview camera and analyzed using Ethovision software by drawing activity traces. In

the R6/2 WT mice group, traces reflected activity predominantly in closed arms with some open-arms exploration. Traces in the R6/2 CAR mice group at 9 weeks showed considerably more activity in open arms; however, 11 weeks traces of R6/2 CAR mice suggested less activity overall (**Fig.8A**). Time spent in the open and closed arms was analyzed by calculating the ratio; the higher the ratio, the less anxiety observed. That is because spending more time in the open arms reflects less anxiety and fear in the open and elevated spaces; more anxiety is observed by staying in the secured closed arms. Statistical results indicate that as the disease progressed, R6/2 CAR mice appeared to have less anxiety compared to their R6/2 WT littermates by spending more time in the open arms [t= -2.510, df= 20.491, #p= 0.021]. Total distance traveled and mean velocity measured by the activity traces in the maze, showed a progressive decline in the R6/2 CAR mice as the disease advanced compared to R6/2 WT mice [total distance traveled at 6 weeks: t= 4.444, df= 27, p< 0.001; 9 weeks: t= 4.543, df= 27, p< 0.001; 11 weeks: t= 5.400, df= 12.906, p< 0.001 and mean velocity at 6 weeks: t= 4.086, df= 27, p< 0.001; 9 weeks: t= 4.514, df= 27, p< 0.001; 11 weeks: t= 5.409, df= 12.883, p< 0.001] (**Fig.8B, C**).

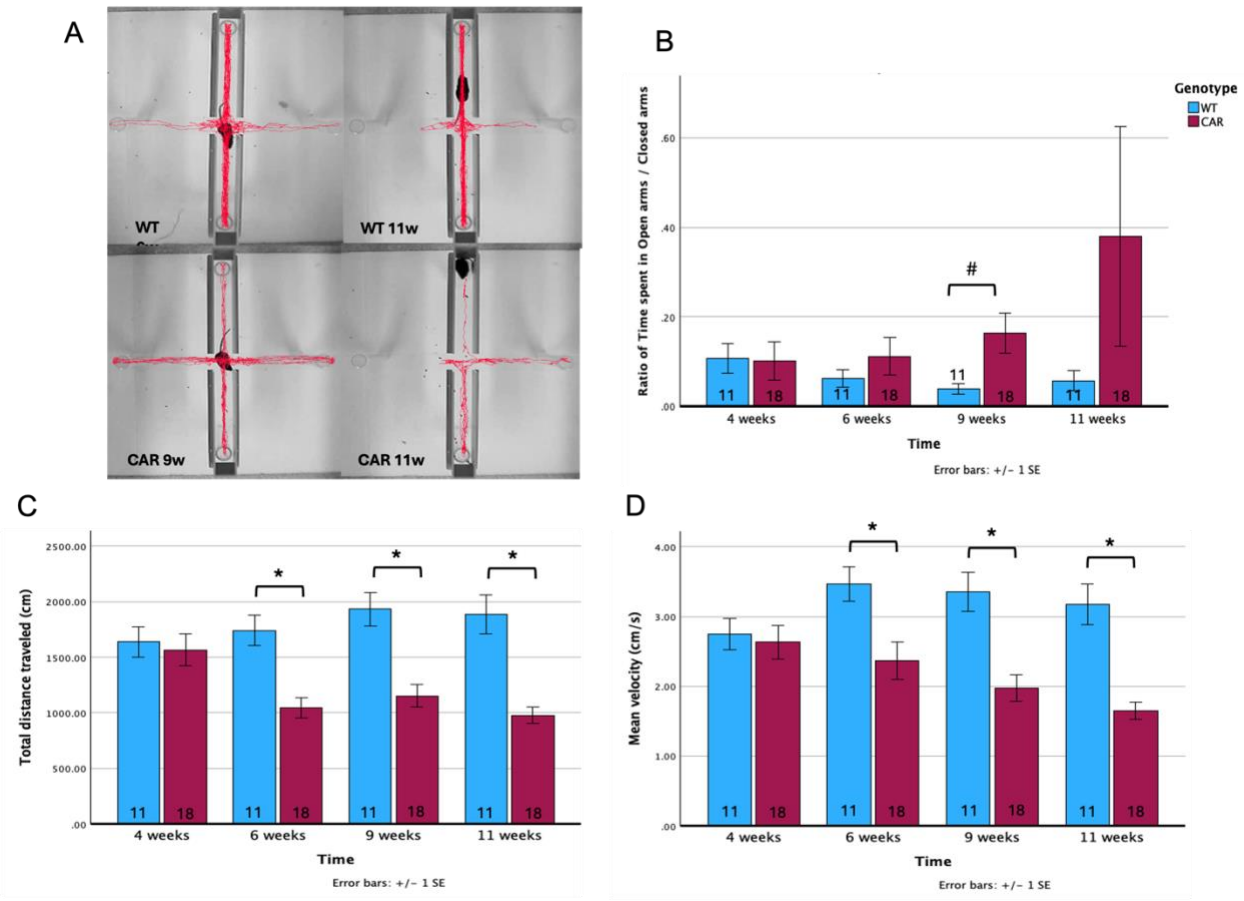

***Figure 8**. Elevated plus maze analysis of R6/2 CAR mice compared to R6/2 WT mice at different stages of the disease; a two-tailed independent-samples t-test statistical analysis was performed. A. Representative activity traces recorded from R6/2 WT mice at 6 and 11 weeks of age and R6/2 CAR mice at 9 and 11 weeks of age. B. The ratio of time spent in open arms divided by closed arms means higher ratios and less anxiety. As the disease progresses, R6/2 CAR mice appear to have less anxiety compared to their R6/2 WT littermates (#p= 0.021). C. Total distance traveled in R6/2 CAR mice declined progressively as the disease advanced compared to R6/2 WT mice (*p< 0.001). D. Mean velocity in R6/2 CAR mice was reduced as the disease progressed compared to R6/2 WT mice (*p< 0.001).*

R6/2 mice were monitored constantly and weighed weekly throughout their lives [at 5 weeks: t= -1.889, df= 27, p= 0.035; 6 weeks: t= -1.794, df= 27, p= 0.042; 10 weeks: t= 2.990, df= 27, p= 0.003 and 11 weeks: t= 3.937, df= 27, p< 0.001] (**Fig.9**).

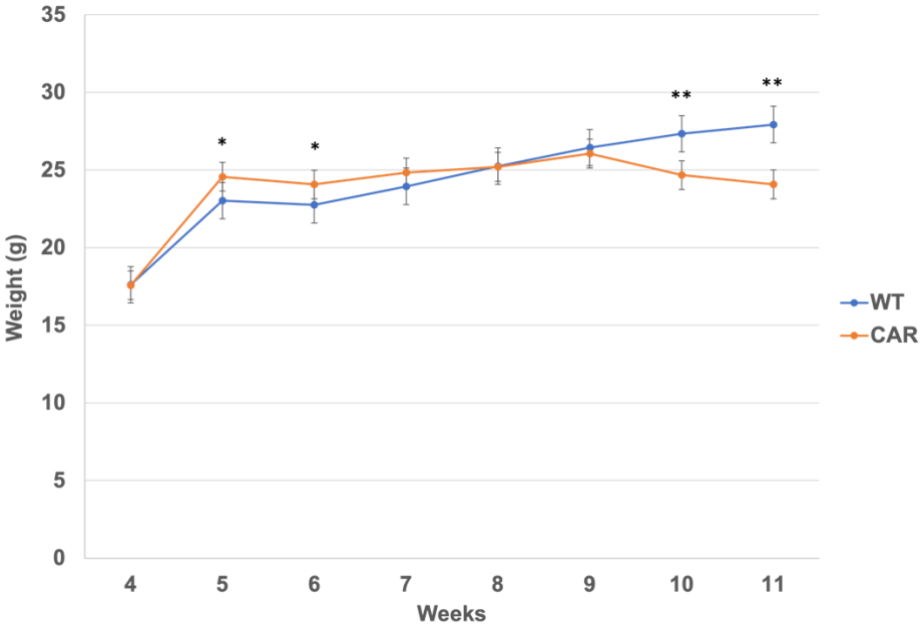

***Figure 9**. Evolution of R6/2 mice body mass at different stages of the disease. A one-tailed independent-sample t-test was conducted to evaluate differences in weight between R6/2 groups (*p< 0.05; **p< 0.005). R6/2 CAR mice weighed heavier at 5 and 6 weeks compared to R6/2 WT but lost considerable weight at 10 and 11 weeks. R6/2 WT n= 11; R6/2 CAR n= 18.*

Effects of AAV5-BDNF-hrGFP in the behavior of R6/2 mouse line

After studying the baseline of the model behavior, the AAV5-BDNF-GFP Vector Biolabs (Malvern, PA, USA) vector was tested as a therapeutic agent. R6/2 CAR mice were injected bilaterally in the PF at 4 weeks of age establishing three separate groups: 1) not

injected R6/2 WT mice, 2) not injected R6/2 CAR mice and 3) AAV5-BDNF-IRES2-hrGFP injected R6/2 carrier mice (R6/2 CAR-BDNF). Clasping, Open Field test and elevated plus maze were performed following the previously established schedule (**Fig.5**).

Clasping test with AAV

Clasping test was performed every week starting at 4 weeks before AAV administration; treated mice were left to recover at week 5 and continued testing at week 6. The clasping test was analyzed by comparing R6/2 CAR vs R6/2 CAR-BDNF mice with an Independent-samples T-test. Results showed a statistically significant reduction in clasping score in R6/2 CAR-BDNF mice at 9 weeks [t= -2.168, df=22, p = 0.041] and 11 weeks [t= -3.100, df=8.393, p = 0.014] (**Fig.10**). As noted in the baseline studies performed before, in R6/2 CAR mice clasping score was increased dramatically at 6 weeks, however, there was a difference in the pattern of the score evolution between R6/2 CAR groups. R6/2 CAR-BDNF mice presented a softer gradual increase in the phenotype apparently reaching a plateau from week 7 to 10 and finally increasing again at 11 weeks. On the other hand, not treated R6/2 CAR mice sharply increased their score at 6 weeks, dropped at 8 weeks and greatly increased from 9 to 11 weeks.

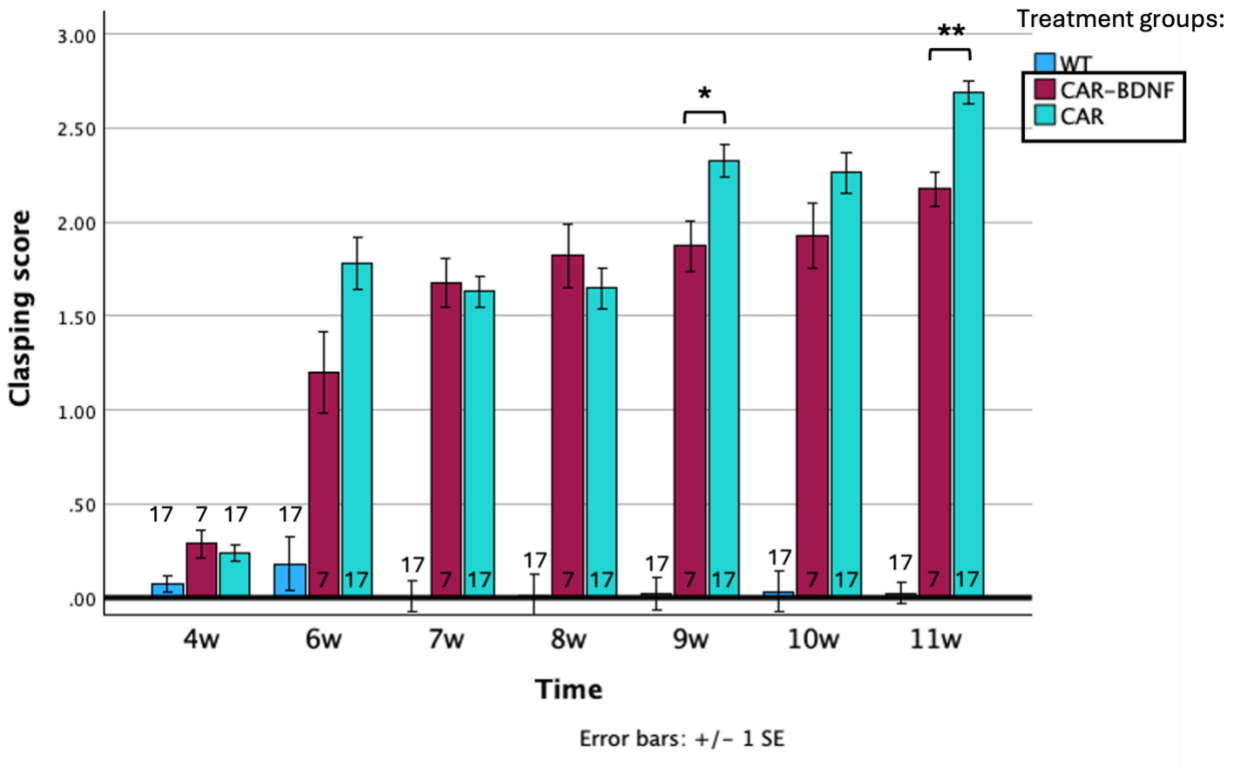

Figure 10. *Clasping test performed with AAV-injected R6/2 mice at different stages of the disease. Independent-sample t-test was used to compare R6/2 CAR vs R6/2 CAR-BDNF. Statistically significant decrease in clasping score at 9 and 11 weeks (*p< 0.05). Error bars: +/- 1 SE. R6/2 WT n= 17; R6/2 CAR-BDNF n= 7; R6/2 CAR n= 17.*

Open field test with AAV

The open field test was analyzed comparing R6/2 WT, R6/2 CAR, and R6/2 CAR-BDNF mice using a Two-way mixed ANOVA (**Fig.11**). Representative recorded traces showed intense activity at high velocity in all directions at 11 weeks in R6/2 WT mice. R6/2 CAR and R6/2 CAR-BDNF mice presented considerably less activity based on the recorded tracks. However, R6/2 CAR-BDNF mice moved at higher velocity (**Fig.11A**). Regarding the total distance moved in the arena, there was no statistically significant interaction

between the three groups and time [F(4.307,49.528) = .688, p = .614, partial η2 = .056, Ɛ=0.718] (**Fig.11B**). However, total distance moved in all groups at 6 and 9 weeks was statistically significantly greater compared to 11 weeks (p< 0.001). The main effect of the groups showed that there was a statistically significant difference in the total distance moved between groups [F(2, 23) = 4.164, p = .029, partial η2 = .266]. Data for all groups had to be converted using a logarithmic transformation from strong positively skewed data to normality. The analysis of mean velocity observed a statistically significant interaction between the groups and time of disease progression [F(6,66) = 2.331, p = 0.042, partial η2 = 0.175] (**Fig.11C**). A significant difference between groups was noted at 6 weeks [R6/2 WT vs. R6/2 CAR, p= 0.020], 9 weeks [R6/2 WT vs. R6/2 CAR-BDNF, p= 0.022; R6/2 WT vs. R6/2 CAR, p= 0.003] and 11 weeks [R6/2 WT vs. R6/2 CAR, p= 0.009]. That is, at different ages R6/2 WT mice moved at a higher velocity, followed by R6/2 CAR-BDNF mice. R6/2 CAR mice moved at the lowest velocity. There was also a significant effect of time on mean velocity in R6/2 WT and R6/2 CAR-BDNF mice. R6/2 WT group moved at a greater velocity at 9 weeks compared to 11 weeks (p= 0.002), whereas R6/2 CAR-BDNF mice showed a reduction in velocity at 11 weeks compared to 4 and 9 weeks (p= 0.011 and p= 0.039, respectively). Data for all groups had to be converted using a square root transformation from moderately positively skewed data to normality.

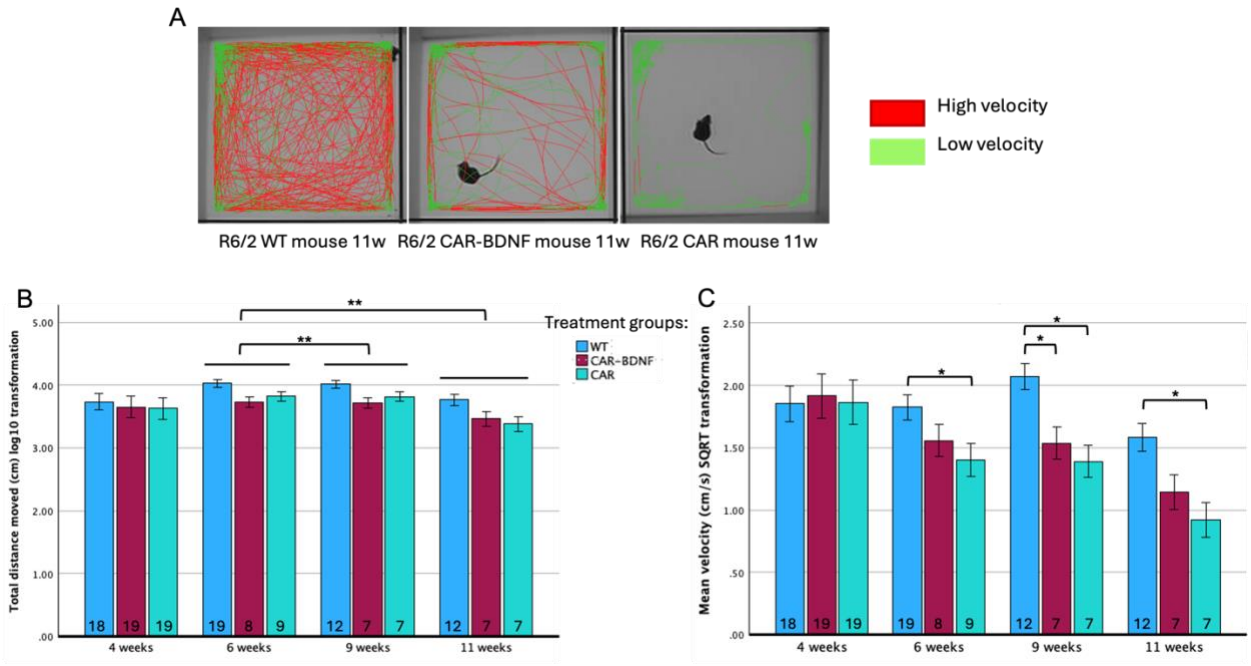

Figure 11. *Open field test performed with AAV-injected R6/2 mice at different stages of the disease; a statistical analysis was performed using a Two-way mixed ANOVA. Error bars: +/- 1 SE. ("n" per group specified at the bottom of each graph bar) A. Representative activity traces recorded from R6/2 groups at 11 weeks of age. B. Total distance traveled in R6/2 CAR-BDNF, and R6/2 CAR mice declined progressively as disease advanced compared to R6/2 WT mice (**p< 0.001). Data converted using a logarithmic transformation. C. Mean velocity in R6/2 CAR-BDNF and R6/2 CAR mice was reduced as the disease progressed compared to R6/2 WT mice (*p< 0.05). Data converted using a square root transformation.*

Elevated plus maze with AAV

Elevated plus maze was analyzed comparing R6/2 WT, R6/2 CAR, and R6/2 CAR-BDNF mice using a Two-way mixed ANOVA (**Fig.12**). Representative recorded traces in R6/2 WT mice at 6 weeks showed intense activity in the closed arms and exploratory walks in the open arms. R6/2 CAR-BDNF traces at 9 weeks presented more activity in the open

arms and R6/2 CAR mice at 11 weeks suggested reduced activity overall (**Fig.12A**). Time spent in open and closed arms was analyzed using the ratio of open arms/closed arms. No statistically significant differences were obtained possibly due to the high variability observed in the data. Multiple unsuccessful transformations were attempted to find a normal distribution (**Fig.12B**). After analyzing the total distance moved in the maze, there was no statistically significant interaction between the groups and the time of disease progression. The main effect of time did not show any significant differences [$F(4.251,2.125)= 1.040$, $p= 0.398$]. The main effect of the groups showed that there was a significant difference in the total distance moved. R6/2 WT was statistically higher than R6/2 CAR-BDNF (**p= 0.004) and higher than R6/2 CAR (*p= 0.022) (**Fig.12C**). The mean velocity analyzed showed no statistically significant interaction between the groups and time of disease progression [$F(3.789,1.894)= 1.069$, $p= 0.381$]. The main effect of time showed significant differences at different ages, mice moved at higher velocity at 4 weeks compared to 9 and 11 weeks (*$p< 0.05$). From the bar graph, R6/2 WT mice seemed to move at a higher velocity, followed by R6/2 CAR-BDNF and R6/2 CAR mice, however, data suggests high variability in the groups possibly hindering potential statistical differences (**Fig.12D**).

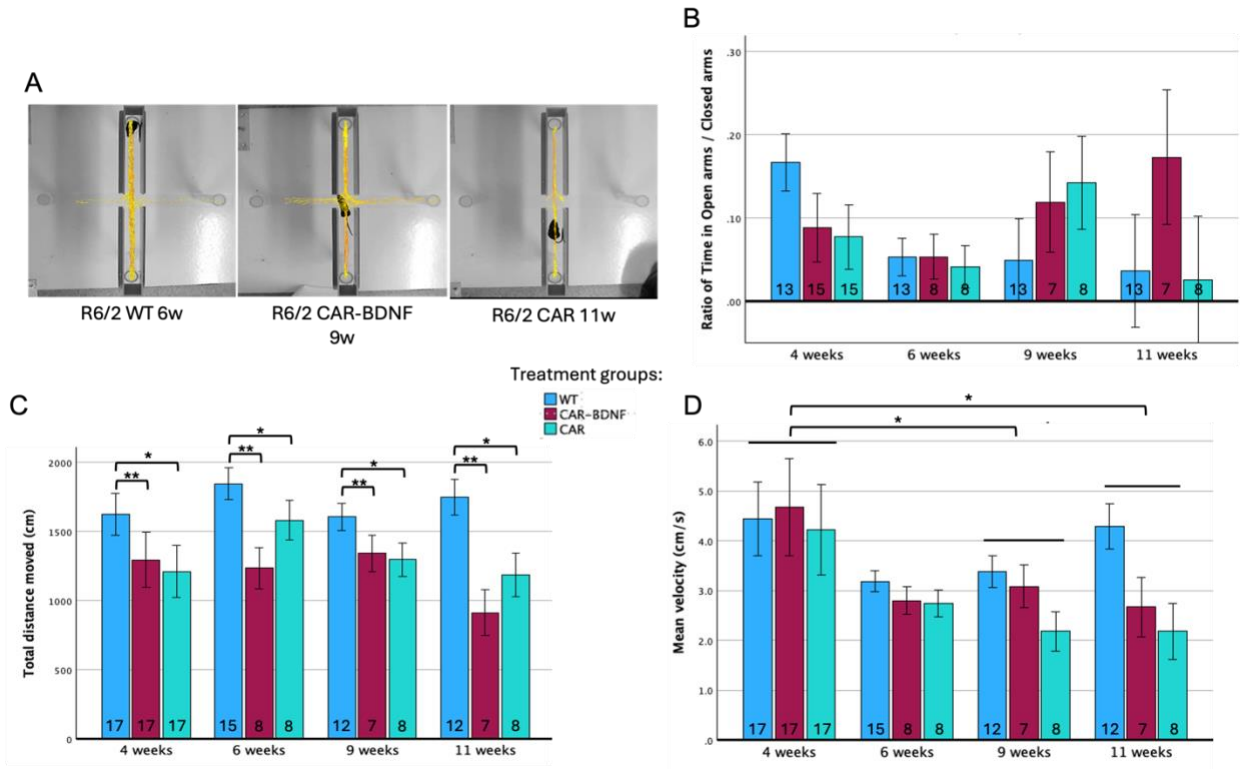

Figure 12*. Elevated plus maze performed with AAV-injected R6/2 mice at different stages of the disease; a Two-way mixed ANOVA statistical analysis was performed. Error bars: +/- 1 SE. ("n" per group specified at the bottom of each graph bar) A. Representative activity traces recorded from R6/2 WT mice at 6 weeks, R6/2 CAR mice at 9 weeks and R6/2 CAR mice at 11 weeks of age. B. Ratio of time spent in open/closed arms in R6/2 mice showed no statistical differences due to high variability in the data. C. Total distance moved was statistically higher in R6/2 WT compared to R6/2 CAR-BDNF (**p= 0.004) and higher than R6/2 CAR (*p= 0.022). D. Mean velocity in R6/2 mice was statistically higher at 4 weeks compared to 9 and 11 weeks (*p< 0.05).*

Morphological changes of AAV-injected brains evaluated by Stereology

To evaluate morphological changes in the striatum of 11.5-week-old R6/2 mice injected bilaterally in the PF with AAV5-BDNF-IRES2-hrGFP, unbiased stereology was carried out

on NeuN^{+} coronal sections. These neuronal counts were done by a summer student in 2019, Chris Valenti (**Fig.13**). Contours of the striatum of the right hemisphere were drawn at a 4x magnification according to defined boundaries using the Paxinos Mouse brain atlas (Franklin & Paxinos, 2008). The number of cells in the striatum was counted and used to determine if there was an increase in the R6/2 CAR-BDNF mice compared to the other groups. A One-way ANOVA was performed followed by a Tukey's post hoc test (*p= 0.02; **p= 0.001). Results reflected that R6/2 WT striata have more neurons than R6/2 CAR-BDNF and R6/2 CAR group. However, R6/2 CAR-BDNF striata have more neurons than the R6/2 CAR group, suggesting that the AAV5-BDNF-IRES2-hrGFP vector in the thalamostriatal system might provide striatal neuroprotection.

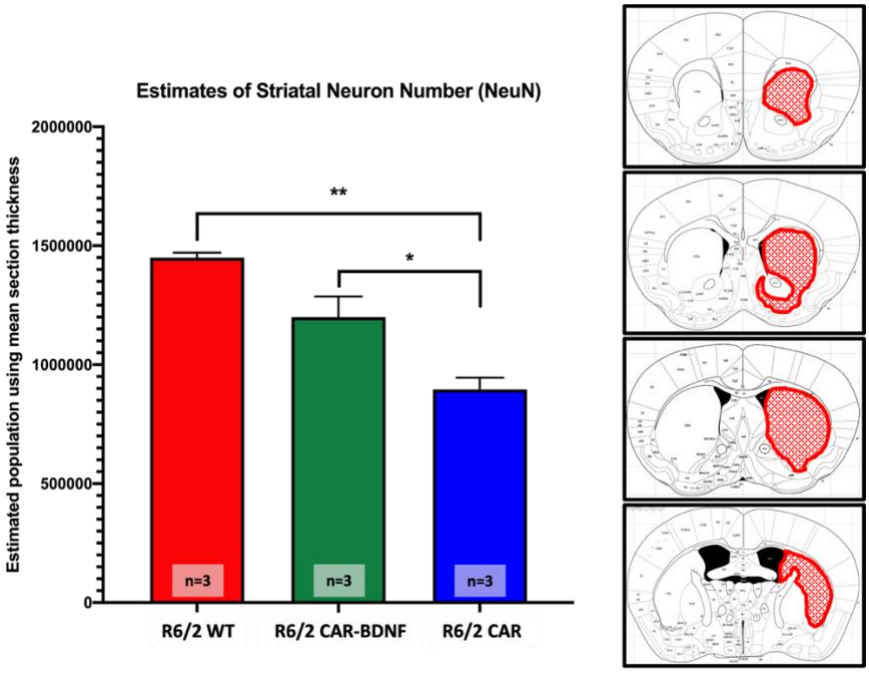

***Figure 13**. Unbiased stereology on striata of AAV-injected R6/2 mice. A One-way ANOVA test was performed followed by a Tukey's post hoc analysis (*p= 0.02; **p= 0.001) to evaluate differences in the number of striatal neurons between groups. R6/2 CAR-BDNF striata showed a statistically significantly higher number of neurons compared to the R6/2 CAR group.*

Verification of accurate AAV5-BDNF-GFP injection

To conduct a proper locomotor and behavioral analysis evaluating the effects of the AAV-BDNF vector, only R6/2 CAR mice that have been accurately injected in the PF should be part of the R6/2 CAR-BDNF group. To validate AAV5-BDNF-GFP injection in the PF, GFP immunohistochemistry was performed in 11.5 weeks old R6/2 CAR brain sections (**Fig.14**). After multiple unsuccessful attempts at visualizing AAV5-BDNF-GFP gene expression with GFP-IR and GFP natural fluorescence, it was concluded that it was not possible to verify AAV5-BDNF-GFP injections in these R6/2 mice. Therefore, we cannot conclude that the locomotor, behavioral and morphological changes seen in R6/2 CAR-BDNF mice were induced by AAV5-BDNF-GFP delivery.

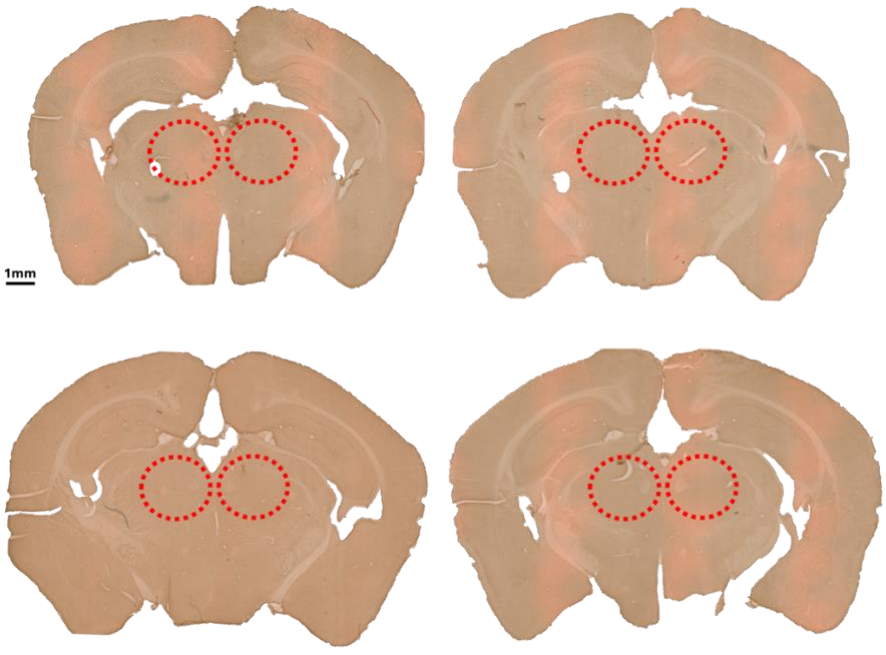

***Figure 14**. Representative coronal sections of AAV-injected R6/2 mice showing unsuccessful verification of AAV injection. Sections were obtained from R6/2 mice injected bilaterally in the PF with the AAV5-BDNF-IRES2-hrGFP vector.*

AAV5-GFP vs AAV5-BDNF-GFP expression in PF and striatum

To understand why it was not possible to visualize AAV5-BDNF-GFP gene expression while observing locomotor and morphology changes in R6/2 CAR-BDNF mice, histological and molecular comparative experiments were conducted in C57BL/6J mice using AAV5-BDNF-GFP and AAV5-GFP as a control vector.

AAV5-BDNF-GFP vector was used to determine if BDNF levels could be increased in the PF and influence its anterograde transport to the striatum of C57BL/6J mice (**Fig.15**). Increased GFP expression in the axons reaching the striatum and TrkB activation in the striatum (pTrkB) were also evaluated.

First, the AAV5-BDNF-GFP vector was injected in the right PF and the AAV5-GFP vector in the left PF and mice were left to survive 3 weeks. Abundant GFP expression was observed in the left PF and along the injection tract but surprisingly, no GFP expression was found in the right PF injected with AAV5-BDNF-GFP (**Fig.15A**). Similarly, AAV5-BDNF-GFP vector was now injected in the right striatum and AAV5-GFP vector in the left striatum. Mice were left to survive 3 weeks post-injection. Intense GFP expression was observed on the left striatum, light staining in the cerebral cortex and along the injection tract whereas no GFP expression was observed in the right hemisphere from the AAV5-BDNF-GFP vector (**Fig.15B**).

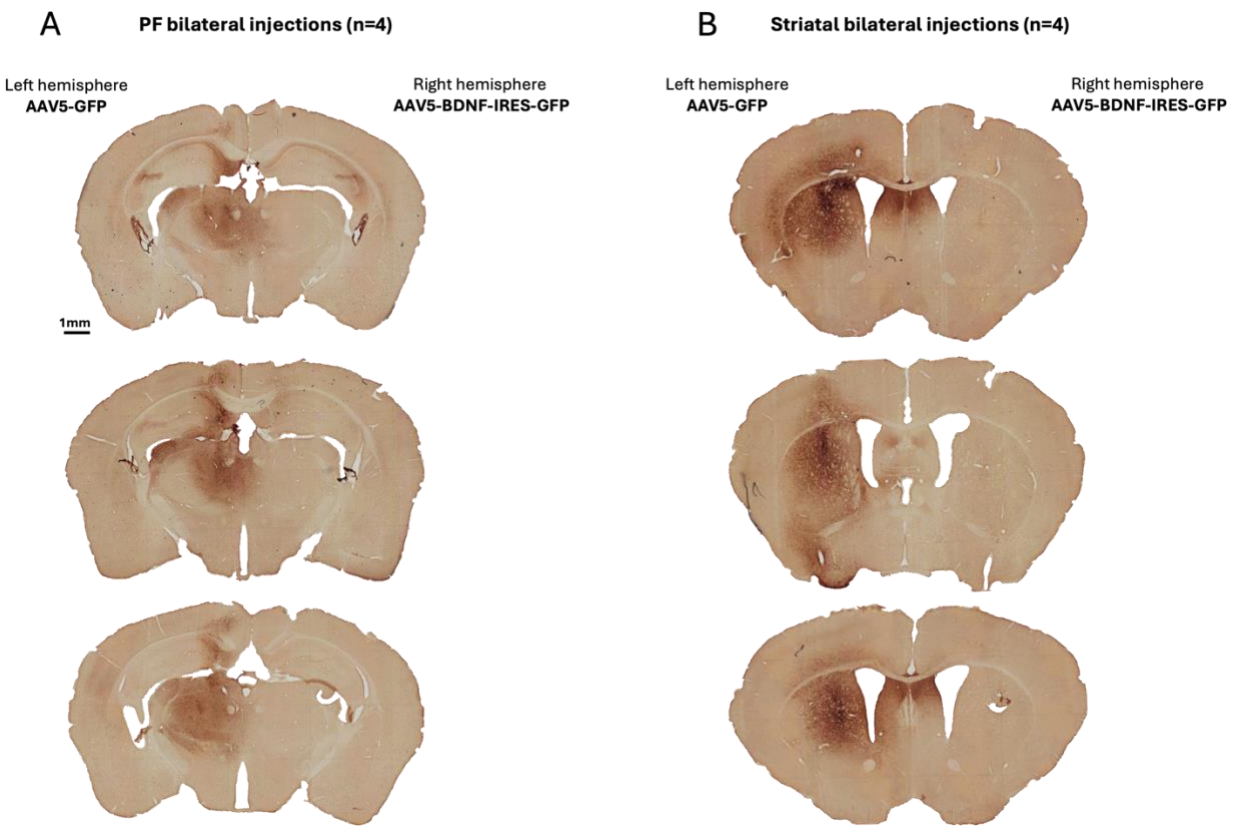

***Figure 15**. Coronal sections of C57BL/6J brains showing GFP expression in brains comparing AAV5-GFP versus AAV5-BDNF-GFP expression, 3 weeks post-injection. In both cases, abundant GFP expression was observed in the left hemisphere and no GFP expression was observed in the right hemisphere. A. Bilateral AAV injection made in the PF, B. Bilateral AAV injection made in the striatum.*

AAV-induced BDNF and pTrkB content at the injection site

To investigate further the gene expression at the injection site from AAV-injected brains, C57BL/6J mice were injected bilaterally in the PF with AAV5-GFP or AAV5-BDNF-GFP. Western blot was used to compare BDNF, GFP and pTrkB expression at the injection site after 5 weeks of injection when AAV transgene expression reached a plateau (**Fig.16**). The striatum was also analyzed to evaluate BDNF and GFP transport from the PF and

striatal TrkB activation as a consequence of potential BDNF increased delivery (**Fig.17**). Independent-samples t-tests were run to determine if there were differences in gene expression between AAV5-GFP injected brains compared to the ones with AAV5-BDNF-GFP in the PF and the striatum. There were no statistical differences in BDNF levels (**Fig.16A, 17A**), nor TrkB activation (**Fig.16C, 17C**) in the PF or the striatum, however, there was a significant increase in GFP expression (**p= 0.001) at the injected site (**Fig.16B**). On the contrary, no differences were observed in GFP in the striatum (**Fig.17B**). Even though GFP expression levels increased in the AAV5-GFP injected PF, there appears to be great variability. The amount of protein loaded per well during electrophoresis is not the reason for this variability because GFP values were normalized against tubulin β-3 levels. It could be due to a lack of accuracy during the AAV injection or the tissue sampling with the cylindrical micro punch in the PF. Another alternative could be inconsistencies in the AAV5-GFP vector transduction capacity.

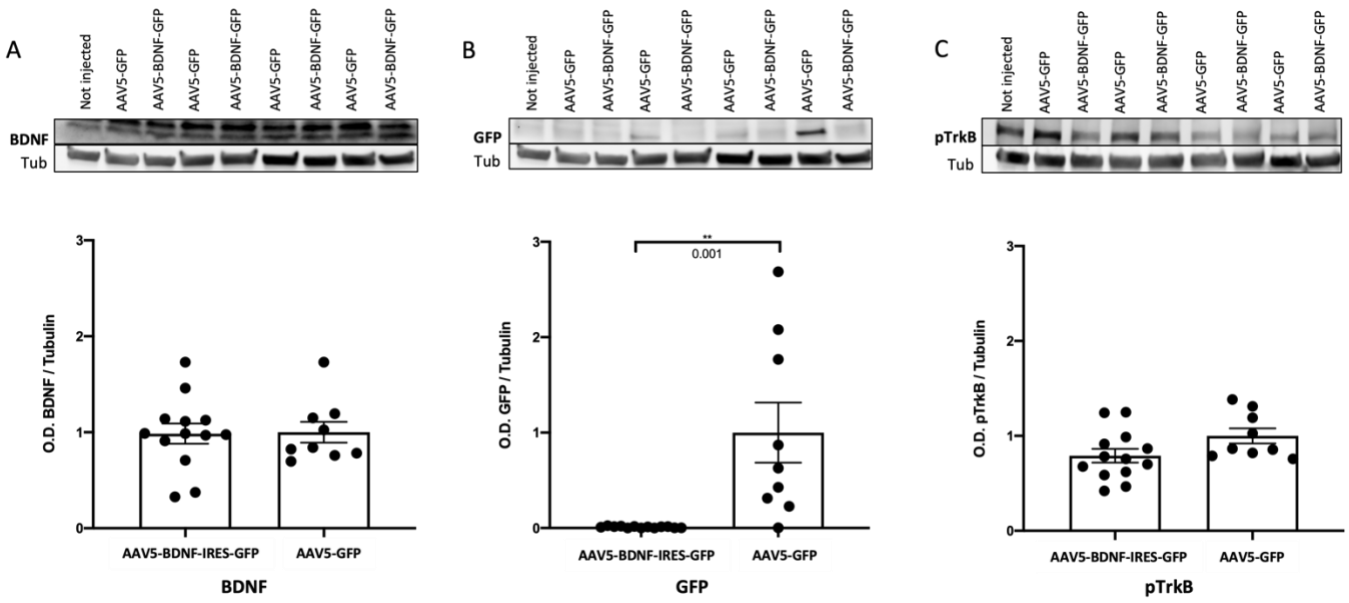

***Figure 16**. BDNF, GFP and pTrkB levels analyzed by Western blotting of protein extracts obtained from PF of AAV-injected C57BL/6J mice injected bilaterally with AAV5-GFP or AAV5-BDNF-GFP, 5 weeks post injection. Not-injected mice were included as a negative control but were not contemplated in the statistical analysis. Independent-samples t-test was performed AAV5-BDNF-GFP vs. AAV5-GFP, **p< 0.001. (AAV5-BDNF-GFP n= 13; AAV5-GFP n= 9)*

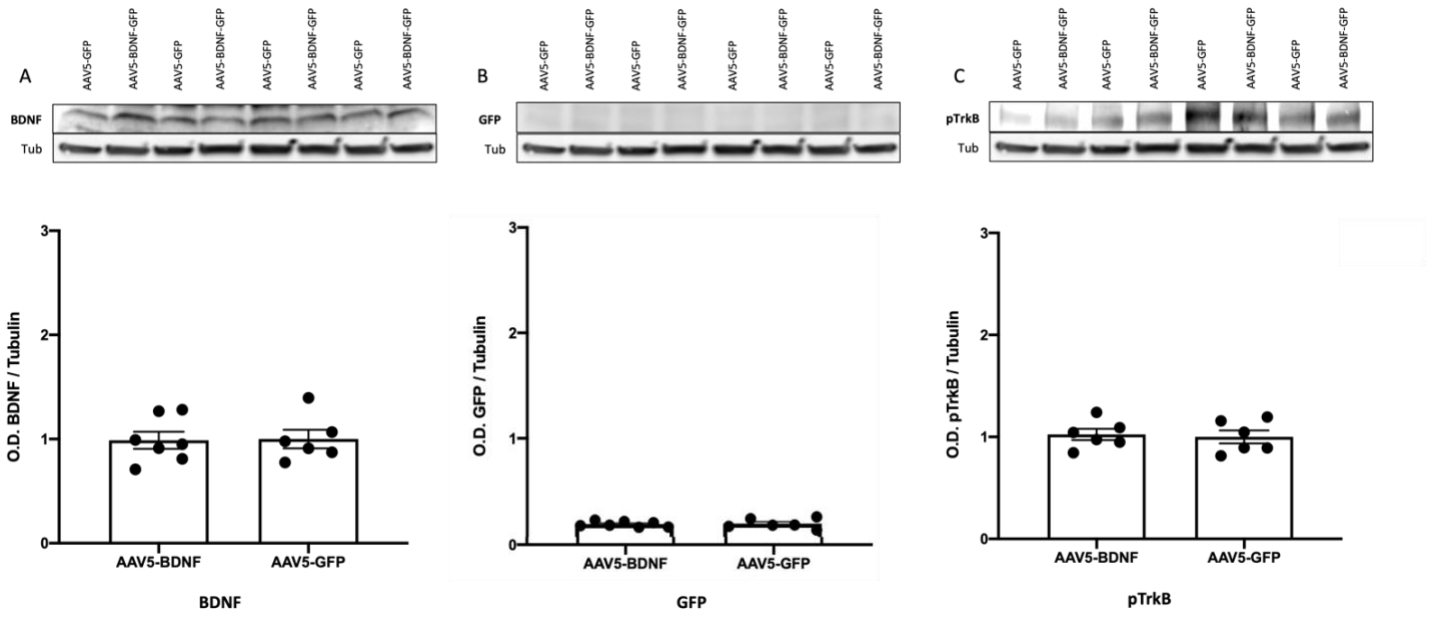

***Figure 17**. BDNF, GFP and pTrkB levels analyzed by Western blotting of protein extracts obtained from the striatum of AAV-injected C57BL/6J mice injected bilaterally in the PF with AAV5-GFP or AAV5-BDNF-GFP, 5 weeks post injection. Independent-samples t-test was performed AAV5-BDNF-GFP vs. AAV5-GFP. (AAV5-BDNF-GFP n= 7; AAV5-GFP n= 6)*

After obtaining the GFP immunohistochemistry and BDNF/GFP/TrkB western blots results from the AAV5-BDNF-GFP vs AAV5-GFP injected brains, no evidence was found that could suggest that AAV5-BDNF-GFP vector transduces the neurons in the injection site, either PF or Striatum; that it induces BDNF or GFP expression or TrkB activation. It

was hypothesized that since BDNF is a highly regulated neurotrophin, injecting an AAV expressing BDNF in the healthy thalamus, an area with high BDNF synthesis or in the healthy striatum, an area with high levels of BDNF delivery by its afferents (Conner et al., 1997), the basal cellular machinery could potentially lower exogenous BDNF expression. Therefore, a brain region that does not synthetize BDNF nor receives BDNF from other projections was selected to test if the AAV5-BDNF-GFP vector could induce the injected neurons to express exogenous BDNF. According to Conner et at., (Conner et al., 1997) the globus pallidus does not show $BDNF^+$ fibers, $BDNF^+$ cell bodies nor BDNF mRNA. To investigate further the vector's capacity to transduce neurons, C57BL/6J mice were injected unilaterally in the globus pallidus with AAV5-BDNF-GFP. Western blot was used to compare BDNF and GFP expression at the injection site after 5 weeks of injection (**Fig.18**); an independent-samples t-test was used to determine if there were statistically significant differences between groups. No differences were measured in BDNF levels (**Fig.18A**) and no GFP expression was observed (**Fig.18B**) in AAV5-BDNF-GFP injected globus pallidus compared to not injected ones, suggesting the vector does not work properly in the PF, striatum nor globus pallidus neurons.

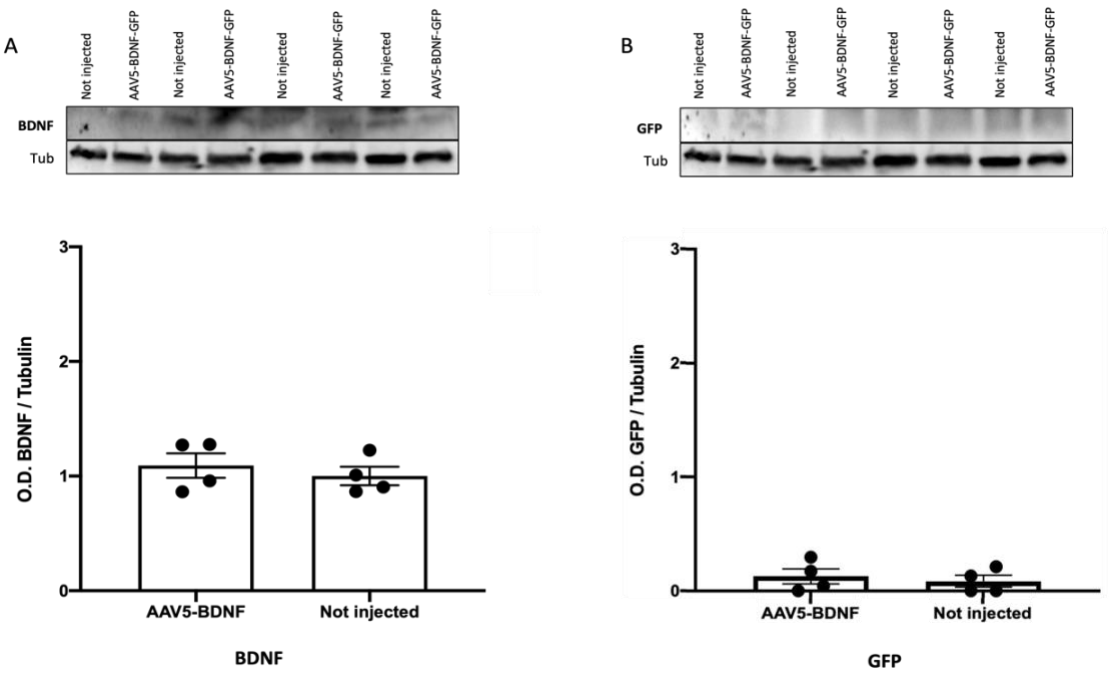

***Figure 18**. BDNF, GFP and pTrkB levels analyzed by Western blotting of protein extracts obtained from globus pallidus of AAV-injected C57BL/6J mice injected unilaterally with AAV5-BDNF-GFP, 5 weeks post injection. Independent-samples t-test was performed AAV5-BDNF-GFP vs. not injected. (AAV5-BDNF-GFP n= 4, not injected n= 4)*

Part 2.

Preclinical evaluation of BDNF-expressing plasmids and AAV vectors

A) *In vitro* plasmid evaluation

pCMV-hBDNF-IRES2-hrGFP sequenced

To understand why the AAV5-BDNF-GFP vector was not inducing BDNF and GFP expression in transduced neurons, a collaboration was established with Dr. Rénald Gilbert's laboratory from the NRC. The plasmid inside the vector (pCMV-hBDNF-IRES2-GFP) was provided separately by Vector Biolabs (Malvern, PA, USA) and was sequenced by Dr. Gilbert's team. They found the CMV promoter followed by a T7 promoter, the human full BDNF sequence, next, the internal ribosome entry site (IRES2) that is used to express two genes from the same promoter and finally the GFP marker (**Fig.19A**). Interestingly, the GFP sequence was that of humanized *renilla* GFP (hrGFP), not the one isolated from the jellyfish *Aequorea victoria* (eGFP). To this point, the fact that it was hrGFP instead of eGFP was not known to us. A comparison of the amino acids alignment of the resulting hrGFP with a regular eGFP was performed (**Fig.19B**) showing an identity score of 27.16% and a similarity score of 45.68%. This possibly could explain why the resulting protein (hrGFP) was not detected by regular GFP antibodies, and its fluorescence was not observed *in vivo* under the fluorescence microscope.

***Figure 19**. Sequencing of the AAV5-BDNF-GFP plasmid and comparison of the amino acids alignment resulted in an Identity score of 27.16% and a Similarity score of 45.68%.*

Evaluation of pCMV-hBDNF-IRES2-GFP compared to pCMV-eGFP

To evaluate pCMV-hBDNF-IRES2-hrGFP *in vitro*, Dr. Gilbert's group transfected HEK293SF cells with pCMV-hBDNF-IRES2-hrGFP and pCMV-eGFP as a positive control. GFP^+ HEK293SF cells were observed under an inverted microscope and FACS assay was performed at 48 and 72 hours post-transfection (**Fig.20**). At 48 hours post-transfection, the percentage of GFP^+ HEK293SF cells transfected with pCMV-hBDNF-

IRES2-hrGFP was lower compared to pCMV-eGFP, with 14.8% and 43.7% respectively. At 72 hours post-transfection, the percentage of GFP$^+$ HEK293SF cells transfected with pCMV-hBDNF-IRES2-hrGFP was still considerably lower compared to pCMV-eGFP, with 21.7% and 58.7% respectively.

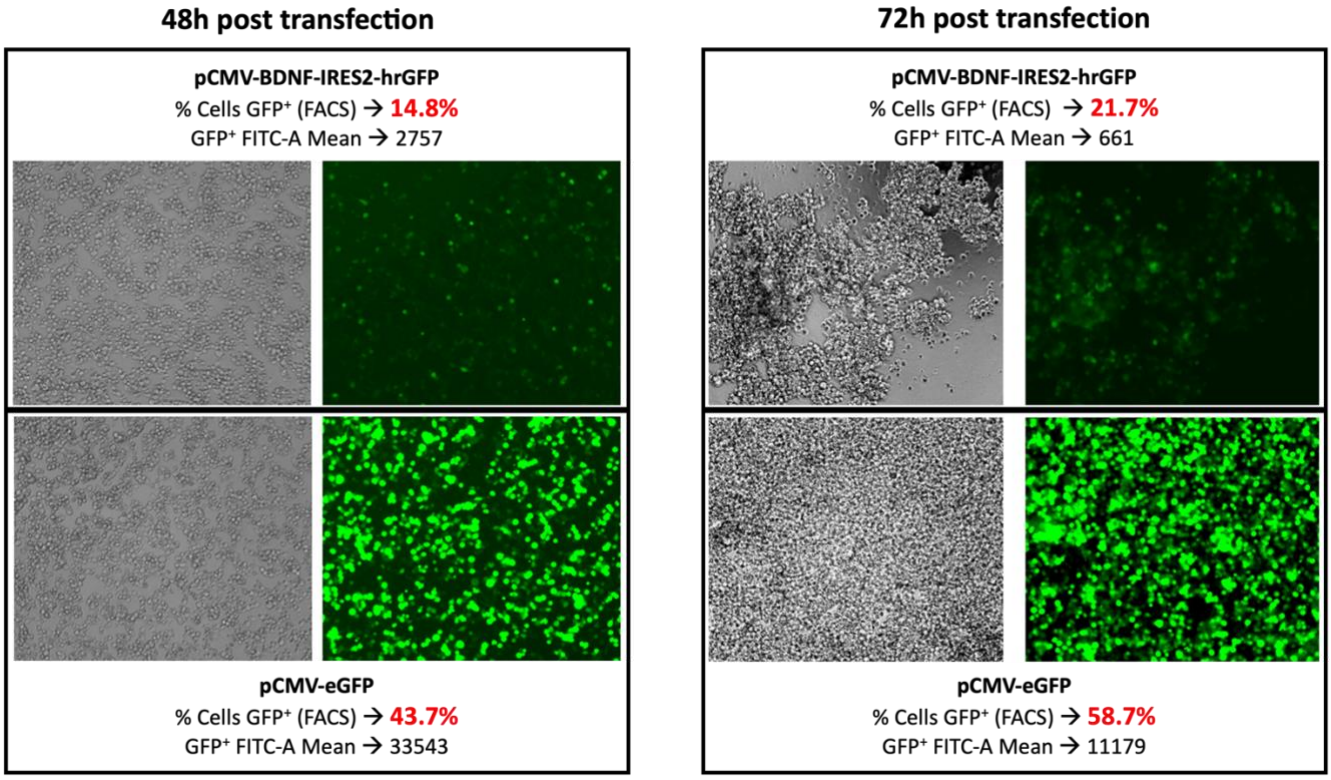

***Figure 20**. Fluorescence intensity of GFP+ HEK293SF cells transfected with pCMV-hBDNF-IRES2-hrGFP and pCMV-GFP at 48- and 72-hours post-transfection.*

Pellets of the transfected HEK293 cells 48 hours post-transfection were processed for western blot to evaluate BDNF and GFP expression levels (**Fig.21**); a One-way ANOVA was used to determine if there were statistically significant differences between cell cultures transfected with different plasmids followed by a Tukey HSD post hoc analysis.

There was a statistically significant increase in BDNF levels (**Fig.21A**) in the cells transfected with pCMV-hBDNF-IRES2-hrGFP compared to cells transfected with pCMV-eGFP and cells not transfected (*p< 0.001). This is the first result that indicates that the full human BDNF sequence used in the plasmid CMV-hBDNF-IRES2-hrGFP is functional given that cells transfected with it effectively increased BDNF synthesis. Recombinant BDNF protein was used as a positive control. GFP expression levels (**Fig.21B**) were statistically significantly greater in cell cultures transfected with pCMV-eGFP compared to cells transfected with pCMV-hBDNF-IRES2-hrGFP and cells not transfected (*p< 0.001). There was no GFP expression in cell cultures transfected with pCMV-hBDNF-IRES2-hrGFP plasmid nor in the not-transfected cultures. These results suggest that eGFP is superior to hrGFP in terms of fluorescence intensity and capability of detection by commercial antibodies *in vivo* and *in vitro*.

Synthesis and in vitro evaluation of pCMV-hBDNF-2A-eGFP compared to pCMV-eGFP

Taking together the CMV sequence from Cell Biolabs, the functional full human BDNF sequence tested above (**Fig.21A**) and the eGFP sequence from the control plasmid (**Fig.21B**), a new plasmid was designed using the linker sequence 2A instead of IRES2. IRES sequence often causes the expression of the downstream gene to be reduced therefore expression of the two genes is not equivalent whereas the viral 2A sequence is approximately 20 amino acids long and can overcome IRES limitations (Lewis et al., 2015). The resulting plasmid was CMV-hBDNF-2A-eGFP. To validate the resulting plasmid, HEK293 cells were transfected with pCMV-hBDNF-2A-eGFP or pCMV-eGFP. Western blots were run with the transfected cell pellets to evaluate GFP expression and

ELISAs were performed with the transfected cell's supernatants to quantify the amount of BDNF protein secreted (**Fig.22**).

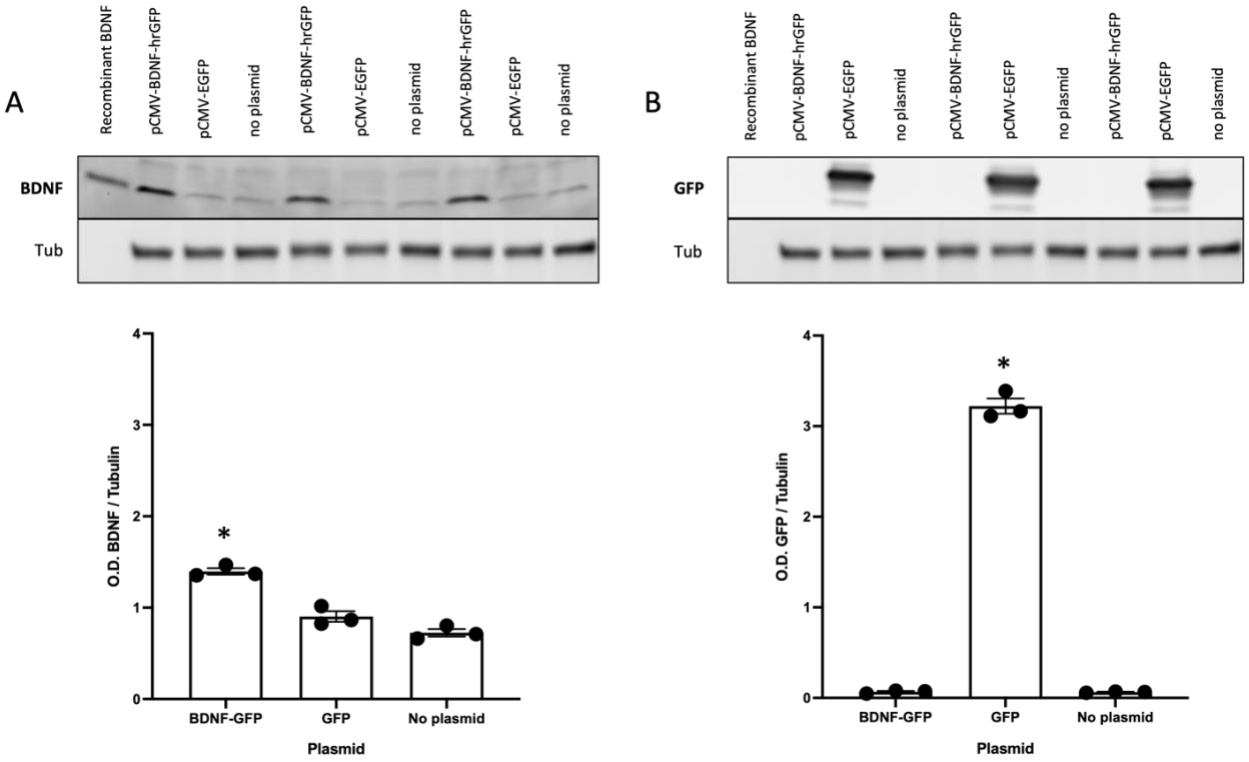

***Figure 21**. BDNF and GFP levels analyzed by Western blotting of protein extracts obtained from transfected HEK293 cell pellets transfected with pCMV-hBDNF-IRES2-hrGFP, pCMV-eGFP or no plasmid, 48 hours post-transfection. A One-way ANOVA was performed with Tukey HSD post hoc analysis (*p< 0.001). Results indicate that the BDNF sequence in CMV-hBDNF-IRES2-hrGFP plasmid is functional and induced BDNF synthesis in vitro. Functional GFP sequence and expression only detected in the cultures transfected with pCMV-eGFP.*

Not transfected cell cultures were used as negative control. GFP expression from cells transfected with pCMV-eGFP was statistically significantly higher than cell cultures transfected with pCMV-hBDNF-2A-eGFP, and the ones not transfected (****p< 0.001). At the same time, GFP expression increase in cells transfected with pCMV-hBDNF-2A-

eGFP was statistically higher than the cell cultures that were not transfected (**p< 0.001) indicating eGFP sequence is functional in both plasmids (**Fig.22A**). BDNF protein levels secreted in supernatants of pCMV-hBDNF-2A-eGFP transfected cells were statistically higher than BDNF protein levels secreted in pCMV-eGFP transfected cell cultures (3812.14 ± 67.04 pg/ml, 43.57 ± 18.85 pg/ml respectively) and the ones not transfected (62.98 ± 1.92 pg/ml) (****p< 0.001). These results show a functional BDNF sequence in CMV-hBDNF-2A-eGFP plasmid because of increased BDNF synthesis but importantly, increased secretion to the media (mean ± standard error of the mean) (**Fig.22B**).

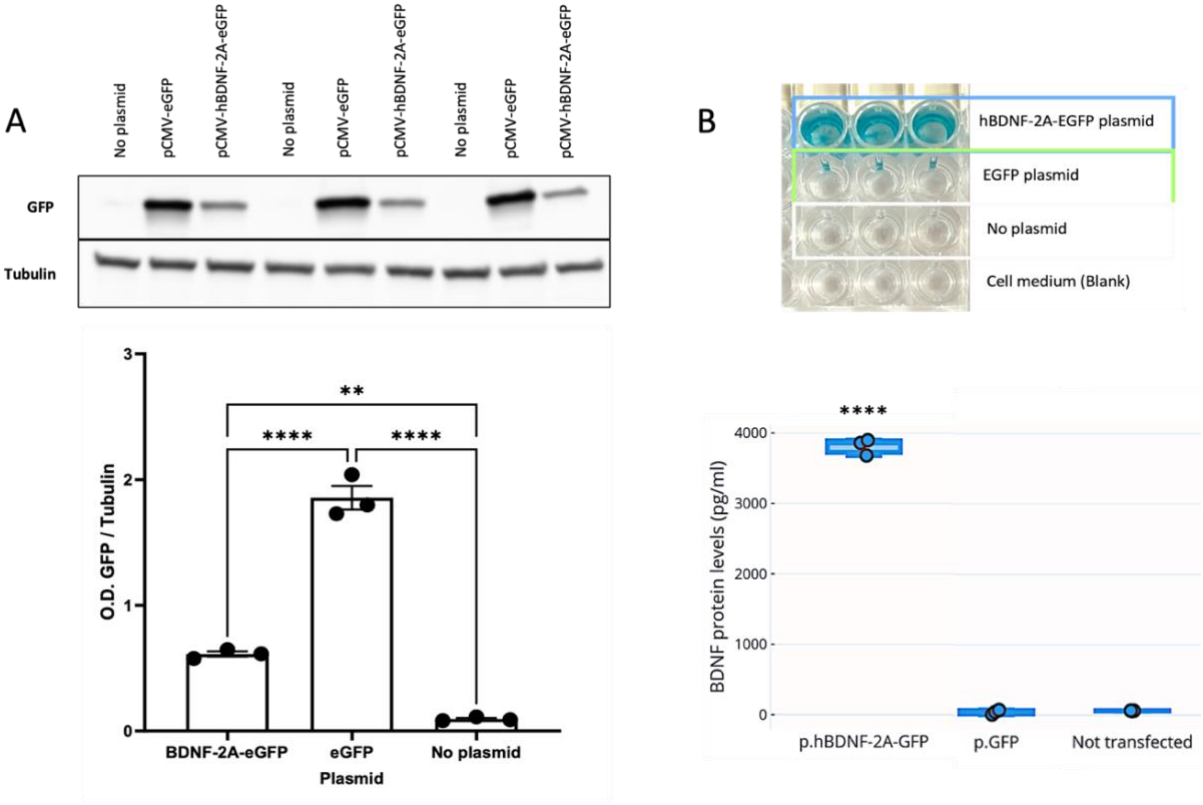

***Figure 22**. Western blot and ELISA assays of protein extracts obtained from transfected HEK293 cells pellets and supernatant, respectively, 48 hours post-transfection. A One-way ANOVA was performed with Tukey HSD post hoc analysis (**p< 0.001, ****p< 0.0001). Results indicate a functional eGFP and BDNF sequence in CMV-hBDNF-2A-eGFP plasmid.*

Synthesis of AAV5 and AAV9 BDNF encoding vectors

Once the CMV-hBDNF-2A-eGFP plasmid was validated, the goal was to achieve overexpression of BDNF *in vivo* using a recombinant AAV. The specific goals were to transduce the cell body of the PF neurons and to have BDNF processed through the cell secretory pathway and transported through the thalamostriatal projections to the striatum. To this effect, Dr. Gilbert's team at the NRC produced the following BDNF expressing vectors: AAV2/5-CMV-hBDNF-2A-eGFP and AAV2/9-CMV-hBDNF-2A-eGFP with their corresponding control vectors: AAV2/5-CMV-eGFP and AAV2/9-CMV-eGFP.

B) AAV viral vector candidate evaluation

The preclinical evaluation of the AAV vector candidate was done by injecting unilaterally the BDNF-expressing vectors and their control vector counterparts in the PF of C57BL/6J mice. Mice were left to survive 3 weeks post-injection and then GFP expression and distribution were analyzed (**Fig.23**). Brains injected with AAV5-eGFP, AAV9-eGFP and AAV9-BDNF-eGFP vector showed strong GFP expression in PF neurons and anterograde transport to the ipsilateral striatum and cortical layers (**Fig.23A, C, D**). Hippocampal regions appear to be GFP^+ too but it could be due to contamination from the needle track. AAV5-BDNF-eGFP injected brains show slight GFP expression around the injection site, however, no GFP^+ fibers were seen in the striatum (**Fig.23B**).

To evaluate if the AAV5-BDNF-eGFP vector required more incubation time to express GFP in the cell bodies of the neurons at the injection site and then transport it to the striatum, another set of C57BL/6J mice were injected unilaterally in the PF with AAV5-BDNF-eGFP or AAV9-BDNF-eGFP; this time mice were left to survive 9 weeks post-

injection. GFP expression and distribution were analyzed (**Fig.24**). After 9 weeks of viral incubation, brains injected with AAV5-BDNF-eGFP showed a stronger GFP stain in the PF area, however, no GFP^+ fibers were observed reaching the striatum (**Fig.24A**).

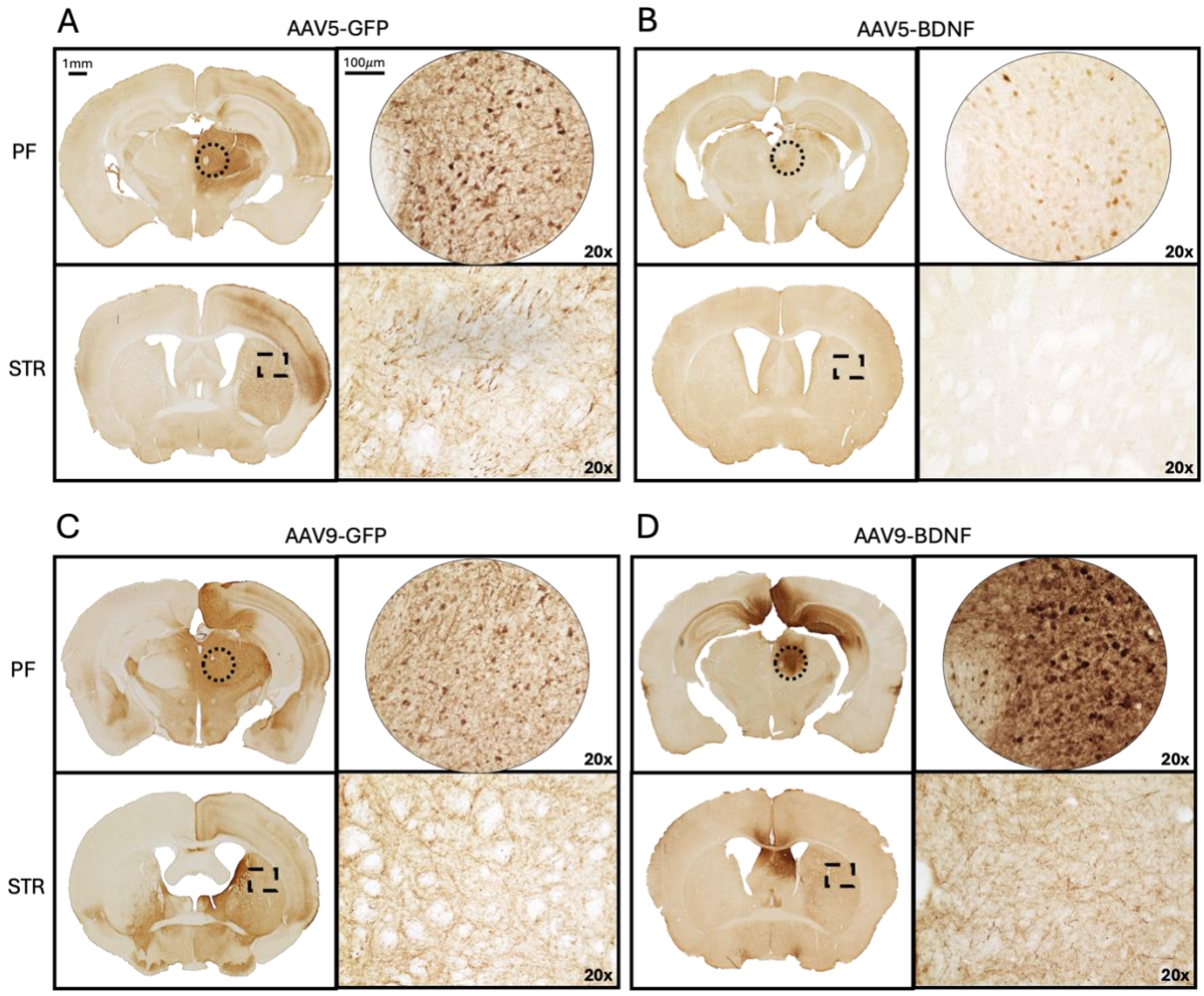

***Figure 23**. Comparative GFP expression in the PF and anterograde transport to the ipsilateral striatum of injected C57BL/6J mice with NRC vectors, 3 weeks post-injection. The following vectors were used: A. AAV5-eGFP, B. AAV5-BDNF-eGFP, C. AAV9-eGFP and D. AAV9-BDNF-eGFP. Results show abundant GFP expression in the PF and GFP^+ fibers in the striatum of mice injected with control vectors and AAV9-BDNF-eGFP. AAV5-BDNF-eGFP injected PF showed slight GFP expression and no GFP^+ fibers were observed in the 20x striatum.*

In contrast, brains injected with AAV9-BDNF-eGFP after 9 weeks of injection showed stable and defined GFP expression in the PF neurons and the GFP⁺ fibers reaching the striatum (**Fig.24B**). Some GFP stain was observed in the hippocampal and cortical regions, possibly from contamination from the needle track.

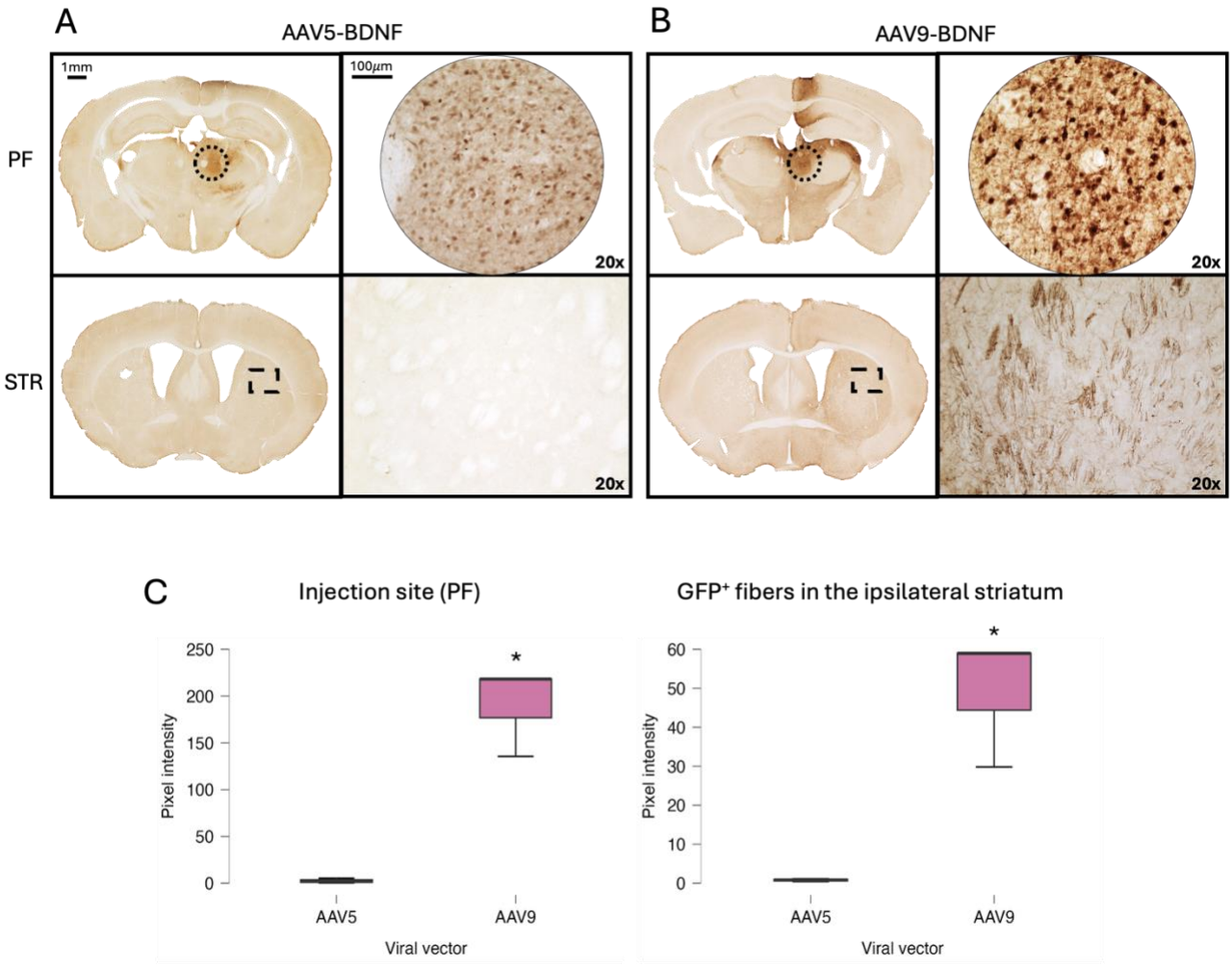

***Figure 24**. Comparative GFP expression in the PF and anterograde transport to the ipsilateral striatum of injected C57BL/6J mice with NRC vectors, 9 weeks post-injection. The following vectors were used: A. AAV5-BDNF-eGFP and B. AAV9-BDNF-eGFP. Results show slight GFP expression in the PF and no GFP⁺ fibers observed in the 20x striatum of mice injected with the AAV5-BDNF-eGFP vector. Defined GFP expression in the PF and GFP⁺ fibers observed reaching the striatum of mice injected with AAV9-*

*BDNF-eGFP. C. Mann-Whitney U test was used to evaluate differences in the pixel intensity values (*p= 0.038). Results show vector AAV9-BDNF-eGFP was superior in terms of GFP expression and anterograde transport at 9 weeks post-injection.*

The GFP-stained coronal sections from brains injected unilaterally in the PF with AAV5-BDNF-eGFP or AAV9-BDNF-eGFP 9 weeks post-injection were analyzed using Image J (**Fig.24C**). GFP expression was measured as pixel intensity at the injected site and the GFP^+ fibers in the ipsilateral striatum from both groups. A Mann-Whitney U test was used to analyze the pixel intensity values because the data obtained failed to meet a normal distribution (p= 0.038). Results show vector AAV9-BDNF-eGFP was superior compared to AAV5-BDNF-eGFP in terms of GFP expression and anterograde transport.

Evidence of stable GFP expression from AAV9-BDNF-eGFP transduced neurons

Figure 25 shows histological evidence in different coronal brain sections of stable GFP expression and anterograde transport from the PF injected with AAV9-BDNF-eGFP to the anterior striatum at 3- and 9-weeks post-injection. Knowing that the injection site was at the specific coordinate of Bregma: -2.27mm, GFP can be measured to have been anterogradely transported ~3.88mm in 3 weeks given that the most anterior portion of the striatum with GFP^+ fibers is at Bregma +1.7mm. After 9 weeks of injection, GFP expression and distribution remains stable in the anterior portion of the striatum.

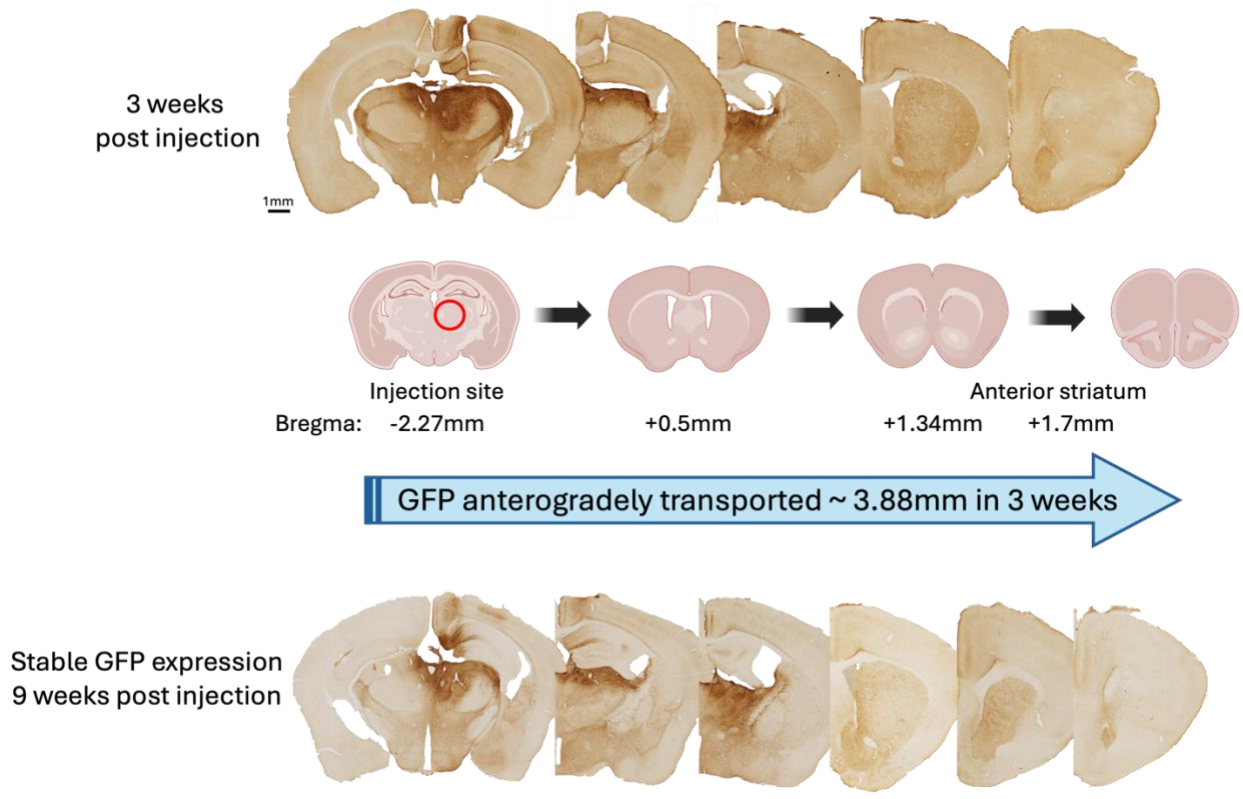

***Figure 25**. Evidence of AAV-induced GFP anterograde transport ~3.88mm from the PF to the striatum of C57BL/6J mice after 3 weeks and its stable expression after 9 weeks of injection. Sketches of coronal sections obtained from Biorender, 2023.*

Gene expression in AAV-injected hemispheres

To evaluate if the AAV9-BDNF-eGFP vector increases BDNF levels and activation of TrkB receptor *in vivo*, C57BL/6J mice were injected in the right PF and left to survive 3 weeks. As controls, the AAV vehicle buffer or AAV9-eGFP vector was injected in the left PF. Brains were obtained and sectioned into two blocks, the anterior block contained the striatum (**Fig.26A**) and the posterior block contained the thalamus.

Verification of accurate AAV injection

GFP expression was visualized using immunohistochemistry in the thalamic block to verify accurate AAV injection in the PF (**Fig.26B**) whereas the striatal block was processed for Western blot and ELISA.

Striatal BDNF, GFP and pTrkB expression

To compare BDNF, GFP and pTrkB levels in mice injected in the right PF with AAV9-BDNF-eGFP and in the left PF with AAV vehicle buffer, striatal extracts were analyzed with western blot (**Fig.26A**). For the statistical analysis a t-test was performed to evaluate differences between hemispheres in BDNF, GFP and pTrkB levels. There was a statistically significant increase in striatal BDNF protein in the AAV9-BDNF-eGFP injected hemisphere compared to the vehicle-injected side (*p≤ 0.05) (**Fig.26C**). A significant increase was also observed in striatal GFP levels in the AAV9-BDNF-eGFP injected hemisphere compared to the vehicle-injected side (*p≤ 0.05) (**Fig.26D**). Even though, there was a slight increase in striatal pTrkB levels in the AAV9-BDNF-eGFP injected side compared to the vehicle side, no statistically significant difference was observed (**Fig.26E**).

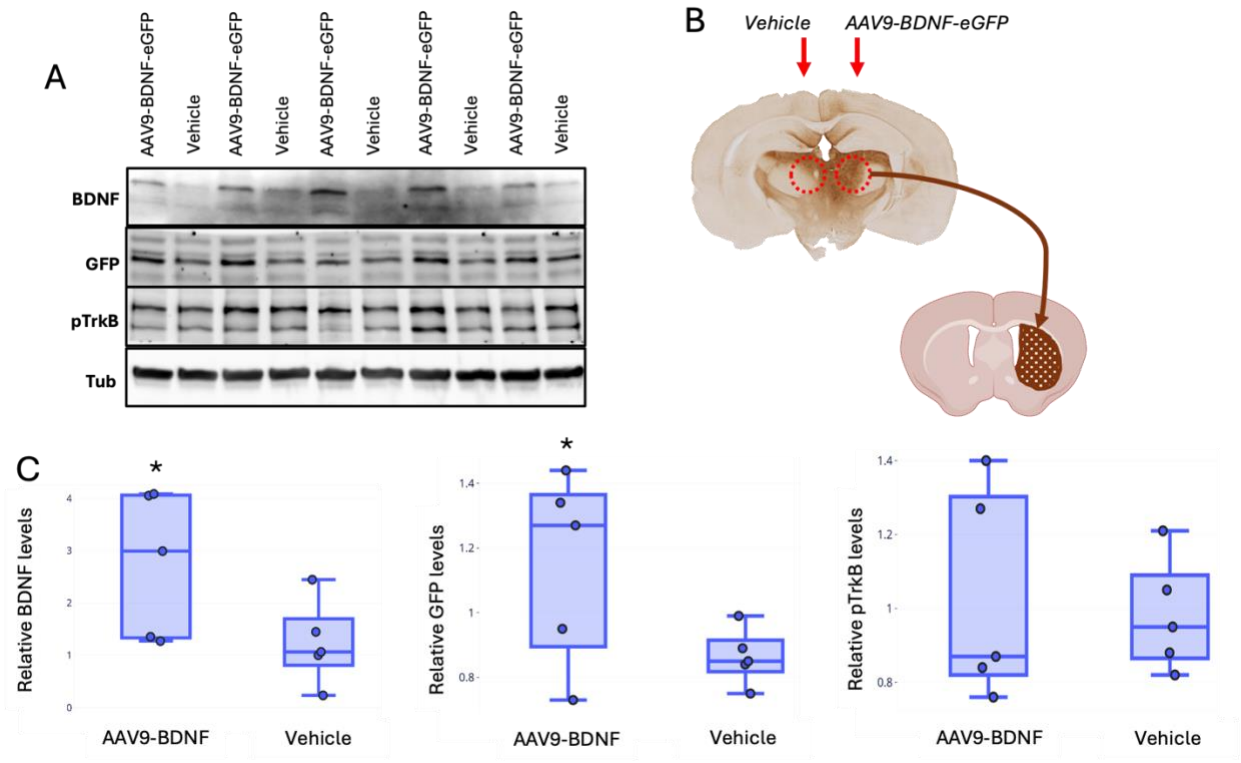

***Figure 26**. BDNF, GFP and pTrkB levels in the striatum of AAV-injected C57BL/6J mice analyzed using Western blot. B. Representative GFP immunohistochemistry confirming the accurate AAV injection site. Striatal extracts were obtained from mice injected in the right PF with AAV9-BDNF-eGFP and the left PF with AAV vehicle buffer and were left to survive 3 weeks post-injection. A t-test was used to evaluate differences between C. BDNF, D. GFP and E. pTrkB levels. Results show a statistically significant increase in BDNF protein and GFP in striata injected with AAV9-BDNF-eGFP compared to the vehicle-injected side (*p ≤ 0.05). Sketches of coronal sections obtained from Biorender, 2023.*

AAV9-BDNF-eGFP induced BDNF protein quantification in striatum

To quantify and compare BDNF protein levels in mice injected in the right PF with AAV9-BDNF-eGFP diluted 1:5 with PBS and in the left PF with AAV9-eGFP, striatal extracts were processed and analyzed with an ELISA kit against BDNF (**Fig.27**). A t-test was

performed to evaluate statistically significant differences between hemispheres. BDNF protein levels increased statistically significantly (*p= 0.036) in the striatal samples from hemispheres injected with AAV9-BDNF-eGFP (1:5) compared to AAV9-eGFP (2492.86 ± 286.73 pg/ml and 1629.37 pg/ml respectively) (mean ± standard error of the mean) (**Fig.27B**).

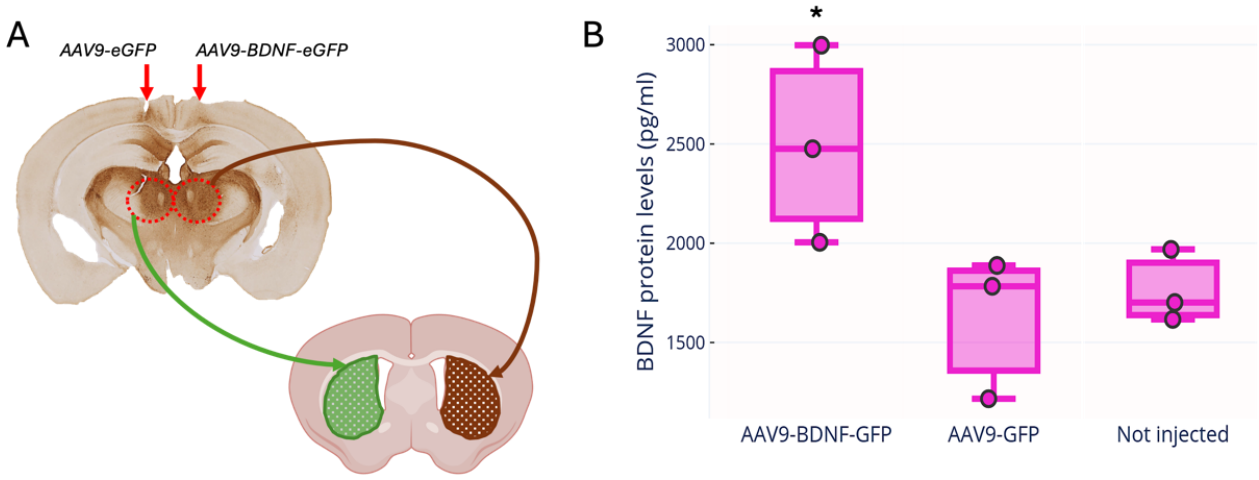

***Figure 27**. Striatal BDNF protein levels quantified and analyzed with an ELISA of AAV-injected C57BL/6J mice. B. There was a statistically significant increase in BDNF protein levels in the striata on the side injected with AAV9-BDNF-eGFP compared to the side injected with AAV9-eGFP (t-test, *p= 0.036). BDNF protein levels between the hemispheres injected with AAV9-eGFP and the brains not-injected showed no difference therefore not-injected mice were not considered in the statistical analysis. Mice survived 3 weeks after the injection. Sketches of coronal sections obtained from Biorender, 2023.*

Part 3.

Effects of AAV9-BDNF-eGFP in behavior of R6/2 mouse line

After validating the efficiency and stability of the NRC-produced AAV9-BDNF-eGFP vector in C57BL/6J mice, it was tested alongside the AAV9-eGFP vector in the PF of R6/2 mice. AAV9 vectors were injected at 4 weeks old and left to incubate 7 weeks post-injection, therefore R6/2 mice were euthanized at 11.5 weeks of age (**Fig.28**). GFP expression in R6/2 WT and CAR brains injected with AAV9-BDNF-eGFP was intense and localized in neurons of the injection site with GFP^+ projections covering the striatum including the anterior portion. Additional GFP^+ projections were observed in the cerebral cortex and contamination from the needle track at the injection site. In the R6/2 CAR mice, GFP expression had a faded appearance in the most lateral portion of the striatum and fewer GFP^+ projections were observed in the cerebral cortex. On the other hand, R6/2 WT and CAR brains injected with the AAV9-eGFP control vector showed intense and wide-spread GFP expression in the subcortical region around the injection site with GFP^+ projections covering the striatum including the most anterior and ventral portion. GFP^+ projections to the cerebral cortex were also observed and contamination from the needle track at the injection site.

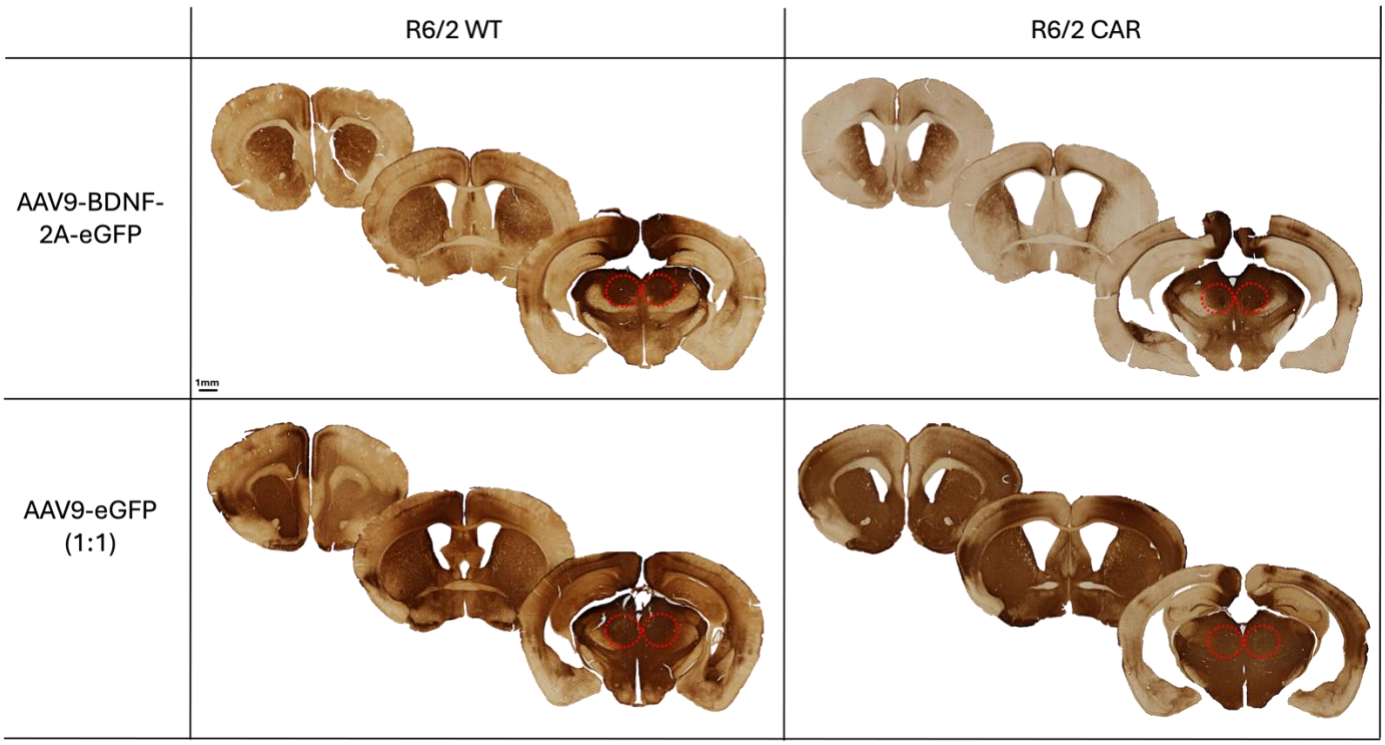

***Figure 28**. Representative coronal sections of R6/2 brains injected with AAV9 vectors processed for GFP immunohistochemistry. Sections were obtained from 11.5-weeks old R6/2 WT and R6/2 CAR mice injected bilaterally in the PF with AAV9-BDNF-eGFP or AAV9-eGFP vector.*

Survival curves of AAV9 injected R6/2 mice

Mice from all groups were monitored throughout their lives and survival curves were built; surprisingly, almost half of the R6/2 CAR mice injected with AAV9-BDNF-eGFP started dying 1 week after the injection and continued dying after 4 weeks of injection. AAV9-BDNF-eGFP vector was diluted to 1:5 and 1:10 with PBS and then injected bilaterally into R6/2 CAR mice PF. The survival distributions of the three different vector dilutions were compared using Kaplan-Meier survival analysis and were found to be statistically different, $\mathcal{X}^2(2) = 9.509$, p= 0.009 (**Fig.29**). A Breslow pairwise comparison was run to

determine which vector dilution had different survival distribution in the injected mice. A Bonferroni correction was made with statistical significance accepted at the p< 0.0167 level. There was a statistically significant difference in survival distributions for the not diluted vector compared to the 1:10 dilution ($\mathcal{X}^2(1) = 6.124$, p= 0.013), and the 1:5 dilution compared to the 1:10 dilution ($\mathcal{X}^2(1) = 10.922$, p< 0.001). However, there was no difference for the not diluted vector compared to the 1:5 dilution ($\mathcal{X}^2(1) = 0.035$, p= 0.851). Results revealed that the median survival time of the vector at 1:10 dilution was 6 weeks post-injection (95% confidence intervals from 4.2 to 7.8 weeks) which was longer than the not diluted vector or 1:5 dilution, which had median times of 4 weeks (95% confidence intervals from 1.6 to 6.4 weeks) and 3 weeks, respectively.

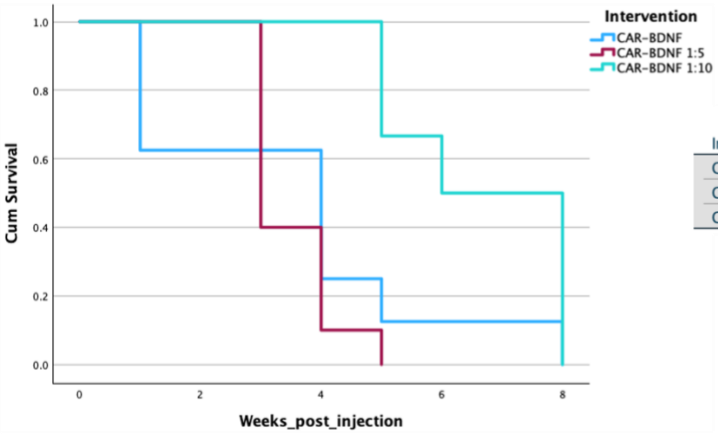

Pairwise comparisons: Breslow test

Intervention	CAR-BDNF		CAR-BDNF 1:5		CAR-BDNF 1:10	
	Chi-Square	Sig.	Chi-Square	Sig.	Chi-Square	Sig.
CAR-BDNF			.035	.851	6.124	.013
CAR-BDNF 1:5	.035	.851			10.922	<.001
CAR-BDNF 1:10	6.124	.013	10.922	<.001		

Intervention	Total N	N of Events	Censored N	Censored Percent
CAR-BDNF	8	8	0	0.0%
CAR-BDNF 1:5	10	10	0	0.0%
CAR-BDNF 1:10	6	6	0	0.0%
Overall	24	24	0	0.0%

Figure 29*. Kaplan-Meier survival analysis comparing survival distributions of R6/2 CAR mice injected with different dilutions of AAV9-BDNF-eGFP vector (not diluted, dilution 1:5 and dilution 1:10). Median survival time of the vector diluted 1:10 was statistically significantly longer than the not diluted vector or the 1:5 dilution.*

The survival distributions of the AAV9-eGFP vector injected into the PF of R6/2-WT and CAR mice were compared using Kaplan-Meier survival analysis and were not found to be statistically different, $\mathcal{X}^2(1) = 1.250$, p= 0.264. The median survival time of the R6/2-WT and CAR mice injected with the AAV9-eGFP vector was 8 weeks post-injection (**Fig.30**).

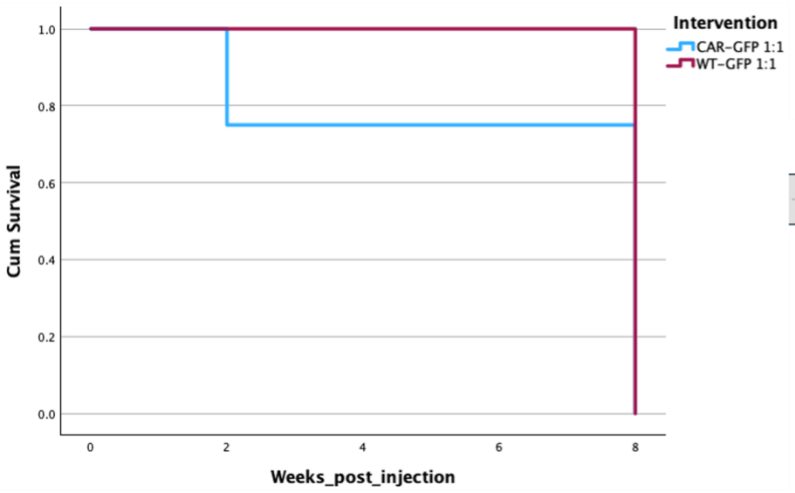

Intervention	CAR-GFP 1:1 Chi-Square	CAR-GFP 1:1 Sig.	WT-GFP 1:1 Chi-Square	WT-GFP 1:1 Sig.
CAR-GFP 1:1			1.250	.264
WT-GFP 1:1	1.250	.264		

Intervention	Total N	N of Events	Censored N	Censored Percent
CAR-GFP 1:1	4	4	0	0.0%
WT-GFP 1:1	5	5	0	0.0%
Overall	9	9	0	0.0%

***Figure 30**. Kaplan-Meier survival analysis comparing survival distributions of R6/2 WT and CAR mice injected with AAV9-eGFP vector. No significant differences were found. The median survival time of both groups of injected mice was 8 weeks post-injection.*

The survival curve of R6/2 WT mice injected bilaterally in the PF with not diluted AAV9-BDNF-eGFP vector showed the mean survival time was 8 weeks post-injection (**Fig.31**).

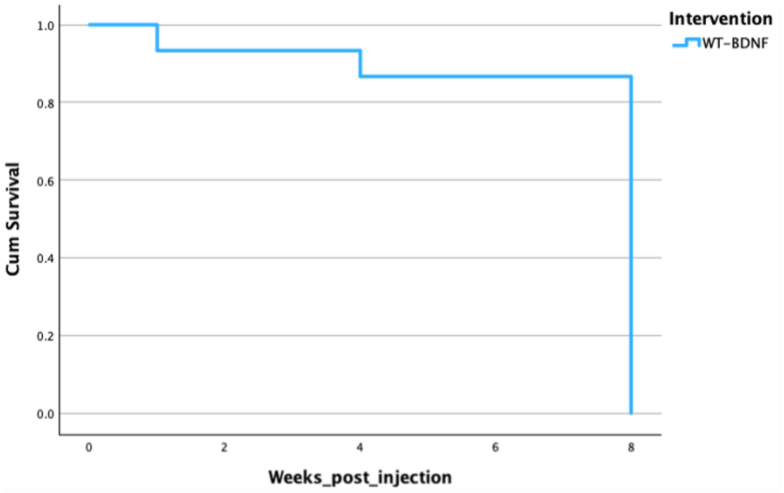

Intervention	Total N	N of Events	Censored N	Censored Percent
WT-BDNF	15	15	0	0.0%
Overall	15	15	0	0.0%

***Figure 31**. Survival distribution of R6/2 WT mice injected with AAV9-BDNF-eGFP vector. Median survival time was 8 weeks post-injection.*

These results strongly indicate that there is a specific vulnerability of R6/2 CAR mice to the AAV9-BDNF-eGFP vector. The survival distribution analysis with the different vector dilutions in **Fig.29** could suggest a dose-response effect, however, more studies must be done to further investigate this statement.

The next step in the overall goal is to administer bilaterally in the PF the adequate dilution of the AAV9-BDNF-eGFP vector as a therapeutic agent to 4-week-old R6/2 mice. Then follow them with the same battery of locomotor and behavioral tests (**Fig. 5**), accompanied by molecular and morphological analysis between R6/2 WT, R6/2 CAR and R6/2 CAR-BDNF groups.

Chapter 5: DISCUSSION

Thalamostriatal pathway as a target for therapeutic overexpressed BDNF

The first hypothesis of this study aimed to determine whether BDNF overexpression in striatal afferents could enhance neuronal survival and maintain phenotype in the striatum of the R6/2 HD mouse model. Previous studies have identified three primary pathways crucial for striatal afferents: the corticostriatal, thalamostriatal and nigrostriatal projections, all of which play essential roles in the anterograde transport of BDNF in the adult striatum (Altar et al., 1997; Conner et al., 1997; Mandelbaum et al., 2019). According to unilateral ablation studies (Altar et al., 1997), the frontoparietal cortex provides 66% of the BDNF protein present in the ipsilateral striatum and 22% in the contralateral striatum, while the SNpc provides 14% of the BDNF protein in the ipsilateral striatum. Thalamic nuclei are rich in cells containing BDNF mRNA and exhibiting immunoreactivity to BDNF protein, as well as fibers presenting immunoreactivity to BDNF; with the PF being one such area (Conner et al., 1997). We selected the PF as the target for BDNF overexpression because axonal mapping revealed it projects extensively to the striatum, and according to Conner et al., the PF plays a pivotal role in the anterograde transport of BDNF to this region (Conner et al., 1997). Lateral PF axons project to the striatal sensorimotor territories, mediodorsal PF axons target the striatal associative territories, and medial PF axons connect to the striatal limbic territories (Gonzalo-Martín et al., 2024; Mandelbaum et al., 2019; Sadikot, Parent, & François, 1992; Sadikot, Parent, Smith, et al., 1992). Although the cerebral cortex provides higher levels of BDNF to the striatum compared to the PF (Altar et al., 1997; Mandelbaum et al., 2019), it is a much larger structure to target, necessitating multiple AAV injections. Therefore, we chose the PF as

a therapeutical target in the R6/2 mouse model to deliver an AAV encoding BDNF (Sadikot & Rymar, 2009).

PF projections visualized using an anterograde BDA tracer in C57bl/6J mice

To evaluate our hypothesis, we first used C57BL/6J mice to determine if the PF could be used to anterogradely deliver overexpressed BDNF to the striatum and which portions of the striatal structure would be affected. We visualized the thalamostriatal system by injecting BDA anterograde tracer into the PF and observed that it was transported 3.87 mm to the ipsilateral striatum within one week, covering the distance from the caudal to the most anterior part (**Fig. 2**). The next step was to administer a specific AAV serotype capable of expressing GFP at the injection site and along the thalamostriatal projections to the striatal terminals in C57BL/6J mice.

AAV5-GFP expression peak at 3 weeks post-injection

We utilized AAV5 with GFP as a transgene to evaluate expression at different time points post-injection, assessing how soon GFP would be expressed in the PF and how long it would take to reach the striatum. We found that GFP^+ neurons in the PF appeared after one week, but it took three weeks for expression to reach the striatum (**Fig. 3**). After GFP expression peaked at three weeks, it remained stable until the last evaluation at eleven weeks post-injection (**Fig. 3 and 4**). These findings align with previous reports indicating that rAAVs typically reach peak expression around three weeks, followed by a plateau (Aschauer et al., 2013).

AAV transgene anterograde transport in relation to Huntington's disease progression in R6/2 mice

Establishing the timeline for GFP expression was crucial for comparing this specific AAV5 expression timeline to disease progression in R6/2 CAR mice (**Fig. 5**). According to studies conducted in our laboratory, Samadi et al. (Samadi et al., 2013) reported that clasping scores increased starting at four weeks of age, with the substantia nigra and prelimbic and cingulate cortices showing decreased BDNF mRNA content. In the early stages of HD, beginning around six to eight weeks of age, significant declines in locomotor activity and rotarod performance are evident, accompanied by reduced neostriatum volume and BDNF mRNA levels in the motor cortex (M1 and M2) and the PF. In the later stages of the disease, around eleven weeks of age, there is a marked decline in locomotor activity, rotarod performance, and grip strength, along with increased clasping scores, significant weight loss, and substantial reductions in neostriatum volume and striatal neuronal loss, accompanied by a drastic decrease in BDNF mRNA content in M1, M2 and PF (Bates et al., 1998; Carter et al., 1999; Mangiarini et al., 1996; Samadi et al., 2013). R6/2 CAR mice typically live for around thirteen to fifteen weeks, exhibiting advanced stage of HD (Samadi et al., 2013); however, we established the humane endpoint at eleven and a half weeks of age.

AAV5-BDNF delivery in the early stages of HD

Considering the progression of disease in R6/2 CAR mice and the need to slow down early cell degeneration, we decided to administer an AAV5 vector encoding BDNF in the PF at four weeks of age, prior to the onset of the symptoms (Shilpa Ramaswamy &

Kordower, 2012). AAV transgene expression at the injection site begins one week post-injection, just before the anticipated reduction of BDNF mRNA in the PF. Consequently, we expect peak AAV expression to coincide with the early symptomatic stage, delivering BDNF protein to the striatum from the caudal to the most anterior regions. While there have been reports of early alterations in thalamostriatal transmission to MSN, compensatory mechanisms ensuring glutamate release have also been documented in YAC128 and R6/2 mice (Holley et al., 2022; Kolodziejczyk & Raymond, 2016; Parievsky et al., 2017; Reiner & Deng, 2018). Furthermore, it has been suggested that the thalamostriatal pathway remains relatively viable until the later stages of the disease (Heinsen et al., 1996; Reiner & Deng, 2018).

Possible PF retrograde transport from AAV5

At this point, we know the PF is a striatal afferent capable of delivering AAV transgenes to the striatum, with projections abundant enough to cover the entire structure (Gonzalo-Martín et al., 2024; Mandelbaum et al., 2019; Sadikot, Parent, & François, 1992) (**Fig. 4**). One important consideration is that the PF is also connected to other brain regions through PF afferents that could potentially uptake the AAV via their axon terminals in the PF and transport it retrogradely to their cell bodies. Retrograde tracers used to map projections have shown that the predominant PF afferent is the cerebral cortex, which contributes over > 75%, primarily from the sensorimotor cortical areas (M2, M1, S1) followed by the insular, frontal association and cingulate cortices (Cornwall & Phillipson, 1988; Gonzalo-Martín et al., 2024; Paré et al., 1988). Approximately 22% of PF input comes from subcortical regions, such as the entopeduncular nucleus (known as internal Globus pallidus in primates), SNpr, superior colliculus, the thalamic reticular nucleus,

pedunculopontine nucleus, pontine reticular formation, contralateral deep cerebellar lateral nuclei, raphe, locus coeruleus, parabrachial nuclei and periaqueductal gray (Cornwall & Phillipson, 1988; Gonzalo-Martín et al., 2024). In our results from C57bl/6J mice, we observed a few GFP^+ cell bodies in the superior colliculus, red nucleus, raphe, reticular nucleus, and other thalamic nuclei, indicating that AAV5-GFP was taken by afferent axons and transported retrogradely to their cell bodies (**Fig. 4)**. Notably, no tissue damage was observed in the areas where few cell bodies were transduced by AAV-BDNF vector. In HD, BDNF synthesis is reduced in various brain regions. Therefore, BDNF delivery could be beneficial, as it plays a crucial role in cell long-term survival, differentiation and maintenance, and aids in the regulation of synaptic transmission and activity-dependent plasticity (Hempstead, 2015; Miranda, Morici, Zanoni, & Bekinschtein, 2019).

Lack of BDNF expression in AAV5-BDNF-GFP injected brains of C57bl/6J mice

After evaluating the dynamics of AAV5-GFP expression, we proceeded with bilateral delivery of AAV5-BDNF-GFP into the PF of C57BL/6J mice to increase BDNF protein levels in the PF and facilitate physiological transport to the striatum. Surprisingly, we found no GFP immunoreactivity (GFP-IR) in the brains injected with the AAV5-BDNF-GFP vector after three weeks. To evaluate potential sources of error, we injected additional C57BL/6J mice bilaterally, administering AAV5-BDNF-GFP in the right hemisphere and AAV5-GFP in the left hemisphere. Results confirmed that after three weeks, there was no GFP-IR in the hemisphere injected with AAV5-BDNF-GFP, whereas AAV5-GFP exhibited a strong GFP^+ signal in the injected PF and the ipsilateral striatum

(**Fig. 15A**). We hypothesized that the AAV5-BDNF-GFP vector might perform better if injected directly into the striatum, considering the different AAV capsid properties that could influence neuron compatibility. Therefore, we injected AAV5-BDNF-GFP in the right striatum and AAV5-GFP in the left. The results were similar: after three weeks, no GFP-IR was detected in the striatum injected with AAV5-BDNF-GFP, while AAV5-GFP showed an intense GFP^+ signal (**Fig. 15B**). Due to the fluorescent nature of the GFP, we attempted to visualize the non-processed injected brain sections directly under the fluorescence microscope; however, no fluorescence was detected (data not shown). Notably, Western blot analysis of BDNF, GFP and pTrkB proteins in PF samples, comparing AAV5-BDNF-GFP and AAV5-GFP after five weeks of injection, revealed no change in BDNF or pTrkB content, and no presence of GFP in the PF injected with the BDNF vector (**Fig. 16**). We considered the possibility that BDNF levels might have increased in the ipsilateral striatum of the injected PF, potentially activating striatal pTrkB. However, analyses of the striata of the same PF-injected brains confirmed our previous results, showing no change in pTrkB (**Fig. 17**). Given that BDNF is a highly regulated neurotrophin with significant impacts on neuronal differentiation, maintenance, and survival, as well as being a synaptic modulator (Colucci-D'Amato, Speranza, & Volpicelli, 2020), it is possible that the thalamostriatal system downregulates the AAV-induced BDNF. To investigate this further, we performed unilateral injections of an AAV5-BDNF-GFP vector into a brain region devoid of $BDNF^+$ fibers, $BDNF^+$ cell bodies or BDNF mRNA -the globus pallidus (Conner et al., 1997). Western blot results from this experiment also showed no changes in BDNF or GFP content (**Fig. 18**).

AAV5 serotype interaction with specific brain regions based on cell receptors

Characterization of AAV serotypes has revealed that each serotype exhibits distinct patterns of transduction, tropism and transgene distribution across various tissues, largely dependent on the specific cell surface receptors required for cell entry (Burger et al., 2004; Davidson et al., 2000; Issa et al., 2023; Watakabe et al., 2015; Zincarelli et al., 2008). The AAV5 serotype, in particular, necessitates the presence of α-2,3-N-linked sialic acid for efficient binding and utilizes the Platelet-derived growth factor receptor (PDGFR) for cell entry (Pasquale et al., 2003). PDGFR mRNA has been detected via *in situ* hybridization in neurons, astrocytes and microglia across multiple brain regions, including the olfactory bulb, cerebral cortex, thalamus, striatum, hippocampus, substantia nigra, cerebellum and retina, amongst others (Oumesmar, Vignais, & Baron-Van Evercooren, 1997; Sil, Periyasamy, Thangaraj, Chivero, & Buch, 2018). It is concerning that the AAV5-BDNF-GFP vector appears unable to transduce neurons in both the PF and the striatum, particularly since the AAV5 capsid of the GFP vector is capable of transduction (**Fig. 3, 4, 15, 16**). Given that PDGFR mRNA is present in neurons, astrocytes, and microglia (Oumesmar et al., 1997; Sil et al., 2018), it is possible that the AAV5 vector does transduce those cellular types. However, we are confident that PF neurons were effectively transduced by the control vector, as evidenced by the PF GFP^+ projections extending into the striatum and some collaterals reaching the cerebral cortex (**Fig. 3, 4**). More studies are necessary to evaluate the presence of AAV capsid proteins in the neurons at the injection site over various time points to determine if the neurons internalized the viral particles. If transduction occurred, the issue may lie in the AAV´s ability to deliver the genome into the target neuron's nucleus or in the synthesis and post-translational modification of the transgenes. Conversely, if the

neurons were not transduced, the problem may relate to the interaction -or lack thereof- between the AAV capsid with the cell surface receptors needed for internalization.

Findings from pCMV-hBDNF-IRES2-GFP sequencing

To further explore why the AAV5-BDNF-GFP vector was unable to transduce cells in the injected areas, we initiated a collaboration with Dr. Rénald Gilbert's laboratory at the NRC. Dr. Gilbert's group sequenced the genetic component of the AAV5-BDNF-GFP vector: the plasmid CMV-hBDNF-IRES2-GFP. They found that the GFP sequence corresponded to hrGFP, not the one isolated from the jellyfish *Aequorea victoria* (eGFP). These two proteins share an identity score of 27.16% and a similarity score of 45.68% (**Fig. 19**). The identity score reflects the percentage of identical amino acids between aligned sequences over the aligned length, while the similarity score indicates the percentage of aligned residues that share similar characteristics between the compared sequences. This may explain the absence of hrGFP expression from the AAV5-BDNF-GFP vector *in vivo* as evidenced by immunohistochemistry and western blot analysis using antibodies directed toward eGFP.

***in vitro* evaluation of pCMV-hBDNF-IRES2-hrGFP compared to *in vivo* evaluation of AAV5-BDNF-GFP**

In contrast to *in vivo* studies, HEK293 cells were successfully transfected with pCMV-hBDNF-IRES2-hrGFP using the PEIpro DNA transfection reagent, suggesting that the plasmid is stable and functional upon entry into cells. The lack of fluorescence from AAV5-BDNF-GFP *in vivo* in the injected PF, striatum and globus pallidus was mirrored *in vitro,* where cell cultures transfected with pCMV-hBDNF-IRES2-hrGFP showed low percentages of GFP^+ cells and minimal fluorescent intensity compared to cultures transfected with a

control plasmid, pCMV-eGFP (**Fig. 20**). The presence of GFP^+ cells in the transfected cultures indicates that plasmid DNA sequences are recognizable by cellular machinery, resulting in the transcription of mRNA and subsequent translation into the protein of interest. The issue with the AAV5-BDNF-GFP vector may reside in the viral capsid's ability to recognize, bind and ultimately gain entry into cells.

Selection of plasmid elements to build a new BDNF encoding plasmid

Cell pellets from the transfected cultures were analyzed via western blot for BDNF and GFP expression. Surprisingly, we observed an increase in BDNF content in cultures transfected with pCMV-hBDNF-IRES2-hrGFP, demonstrating that the full human BDNF sequence is functional (**Fig. 21A**). Conversely, the anti-eGFP antibody was unable to detect any hrGFP from the pCMV-hBDNF-IRES2-hrGFP, while intense eGFP bands from the control plasmid were evident (**Fig. 21B**). This result suggests that although faint fluorescence was observed under the microscope in the pCMV-hBDNF-IRES2-hrGFP transfected cultures, hrGFP levels were insufficient for detection by the anti-eGFP antibody in western blot assays; alternatively, the anti-eGFP antibodies may not recognize hrGFP due to the low identity and similarity scores with eGFP (**Fig. 19**). We conclude BDNF sequence is functional, while eGFP demonstrates superior fluorescence intensity and detectability compared to hrGFP.

IRES element vs 2A family peptides

Another important consideration is the IRES element. Utilizing the IRES element provides advantages such as ensuring co-expression of genes positioned upstream and downstream of the IRES, as well as enabling the insertion in the downstream gene of subcellular localization sequences, which in this case is GFP, a cytosolic protein. However, the

translation efficiency of the gene downstream of an IRES is significantly lower than that of the upstream gene, typically around 10-20% (Ho et al., 2013; Kim et al., 2011; Lewis et al., 2015). The observed low hrGFP fluorescence *in vitro* may be attributed to the limited quantities of protein synthesized from the IRES-containing plasmid. In contrast, the lack of hrGFP fluorescence and immunoreactivity observed *in vivo,* combined with the unchanged BDNF content, may reflect the inability of the AAV5-BDNF-hrGFP capsid to enter cells. To address the limitations of the linker sequence, “self-cleaving” 2A family peptides can be employed. These 2A elements are short peptides, averaging 18-22 amino acids, that facilitate the production of multiple proteins from a single transcript, and they provide the stoichiometric expression of adjacent proteins at a ratio of 1:1 (Ho et al., 2013; Kim et al., 2011; Lewis et al., 2015).

Taking these considerations into account, we synthesized a new plasmid using the CMV promoter to drive the full human BDNF sequence linked to the eGFP sequence from the control plasmid via a 2A peptide element: pCMV-hBDNF-2A-eGFP.

in vitro evaluation of pCMV-hBDNF-2A-eGFP shows BDNF protein secreted to the medium

Analysis of cell cultures transfected with pCMV-hBDNF-2A-eGFP and the plasmid control pCMV-eGFP revealed a functional eGFP band in the western blot results (**Fig. 22A**). As anticipated, the relative intensity of the eGFP band from the control plasmid was higher compared to that from the BDNF plasmid, since expression of the control eGFP is directly driven by the CMV promoter, while eGFP expression from the BDNF plasmid is indirectly influenced by the same promoter, with the full effect primarily benefiting the BDNF sequence.

ELISA experiments using supernatants from transfected cell cultures demonstrated a significant increase in BDNF synthesis and release into the medium from cultures transfected with the BDNF plasmid (**Fig. 22B**). Notably, these transfected cells synthesized higher levels of BDNF protein, successfully processed it post-translationally, and incorporated the resulting BDNF into the cell's secretory pathway for release into the culture medium. Extrapolating these findings to an *in vivo* model, PF neurons transduced with AAV-BDNF would likely be capable of synthesizing higher levels of BDNF protein, transporting it anterogradely, and releasing it to striatal neurons. We conclude that both BDNF and eGFP sequences are functional in the newly synthesized plasmid.

Evaluation of AAV5 and AAV9 vectors encoding BDNF

After validating the BDNF plasmid, Dr. Gilbert's team at the NRC introduced the control and BDNF constructs into new AAV5 and AAV9 vectors. Following three weeks of injection into the PF of C57BL/6J mice, control vectors (AAV5-eGFP and AAV9-eGFP) exhibited strong GFP signals and diffusion at the injection site, as well as projections to the ipsilateral striatum and cortical layers (**Fig.23**). In contrast, BDNF vectors (AAV5-BDNF-eGFP and AAV9-BDNF-eGFP) displayed a different expression pattern. AAV5-BDNF-eGFP produced faint GFP expression in the PF, occupying only a small portion, with no observable projections reaching the ipsilateral striatum or cortical layers. This suggests that the quantity of viral vector internalized by PF neurons was low, resulting in insufficient GFP production for transport to PF efferent targets.

Conversely, GFP expression from the AAV9-BDNF-eGFP vector was more intense, exhibiting discrete diffusion in the PF and projections to the ipsilateral striatum (**Fig.23)**. To allow for more extended AAV incubation, we evaluated GFP expression after nine weeks of

injection. Similar to the results at three weeks, brains injected with AAV5-BDNF-eGFP displayed faint GFP expression at the injection site, with few GFP^+ cell bodies and no transport to the ipsilateral striatum or cerebral cortex. In contrast, after nine weeks, AAV9-BDNF-eGFP induced robust GFP expression in PF neurons and anterograde transport to the ipsilateral striatum (**Fig.24**). Given that these vectors incorporate the 2A peptide construct, the low GFP expression induced by AAV5-BDNF-eGFP likely indicates similarly low BDNF expression, due to the characteristic stoichiometric expression of proteins flanking the 2A peptide sequence (Kim et al., 2011).

To select an appropriate AAV candidate, evaluations must share the same delivery route and consider kinetics, expression levels, persistence, and anatomical localization of the delivered transgenes (Zincarelli et al., 2008). Based on our findings, we conclude that AAV9-BDNF-eGFP is superior to AAV5-BDNF-eGFP regarding stable GFP expression, potential BDNF expression, and anterograde transport (**Fig.24**).

Comparison between AAV5-BDNF vectors

It is insightful to analyze the similarities and differences in transduction patterns between the AAV5 vector provided from Vector Biolabs (Malvern, PA, USA) and the AAV5 vector produced by the NRC team. Although the GFP sequence of the BDNF vector from Vector Biolabs is hrGFP, the GFP sequence in their control vector is derived from *Aequorea victoria* (eGFP). Both control vectors utilize a CMV promoter to drive eGFP expression, enabling them to transduce neurons in the PF and produce sufficient GFP for anterograde transport to PF efferents. In contrast, the Vector Biolabs BDNF vector employs an IRES element

linking the BDNF sequence to the hrGFP sequence, whereas the NRC vector incorporates the 2A peptide as a linker sequence between BDNF and eGFP.

Despite both vectors being of the AAV5 serotype, one might expect similar transduction patterns. However, the NRC-produced AAV5-BDNF-eGFP vector demonstrated low levels of GFP fluorescence in the PF (data not shown) and low-intensity GFP immunoreactivity, while the AAV5-BDNF-GFP from Vector Biolabs exhibited no fluorescence or GFP-IR detectable by commercial anti-eGFP antibodies.

Since the vectors were produced in different facilities, the AAV5 capsids from Vector Biolabs and NRC may have slight variations that could affect particle dissemination due to capsid stability, subsequently influencing cell surface receptor binding and intercellular trafficking (L. Samaranch et al., 2017). As previously mentioned, the low translation efficiency with the IRES element in the Vector Biolabs vector may hinder protein expression in the limited number of transduced neurons (Ho et al., 2013; Kim et al., 2011; Lewis et al., 2015). Overall, the combined effects of the capsid characteristics, the CMV promoter, the two transgenes, and the linker sequences likely weakened the overall AAV infection efficiency in both cases.

Validation of stable GFP expression from AAV9 vector encoding BDNF-eGFP

In contrast to AAV5, the AAV9 vector encoding BDNF successfully transduced neurons in the PF and facilitated anterograde transport of GFP to the striatum. AAV9 is known for its superior cell transduction efficiency, rapid onset, and higher protein levels compared to other AAVs (Issa et al., 2023). Independent of the promoter used, AAV9 injections produce widespread transduction patterns (Watakabe et al., 2015). The observed differences in transduction efficiency or tropism between AAV5 and AAV9 control vectors

are likely attributable to variations in viral capsid proteins, their receptor interaction, and intracellular trafficking after cell entry (Burger et al., 2004).

GFP, a cytosolic protein synthesized near the cell bodies of transduced PF neurons, is passively transported along neuronal projections to the terminals in an anterograde manner, without being released at the PF axon terminals. Immunohistological analysis of GFP expression in AAV9-BDNF-eGFP injected brains (**Fig.23, 24, 26**), revealed that most transduced cell bodies were located in the PF, with a few neurons in PF afferents that retrogradely acquired the viral vector. The remaining GFP-IR corresponded to fibers extending from the PF to the striatum (**Fig.25**).

In a study by Burger et al., (Burger et al., 2004), injections of 2μl of AAV1, AAV2 and AAV5 vectors expressing eGFP into the striatum of rats demonstrated average GFP^+ neuron distributions of approximately 1.7mm, 0.9mm and 2.0mm, respectively, after four weeks. AAV1 and AAV5 exhibited more widespread distribution of GFP^+ neurons compared to AAV2, though it did not sufficiently cover the striatal structure. Notably, our results showed that, after three weeks of injecting 1μl of AAV9-BDNF-eGFP into the PF, the average caudal to rostral distribution of GFP^+ thalamostriatal fibers covering the striatum extended to ~3.88mm. This distribution pattern remained stable after nine weeks (**Fig.25**).

Striatal BDNF increase in AAV9-BDNF-eGFP injected hemispheres

To assess BDNF expression in C57bl/6J mice, we verified accurate AAV9-BDNF-eGFP injection in the PF through GFP immunohistochemistry, ensuring any changes in the analyzed striata came from the PF injection. Western blotting of striatal extracts indicated elevated levels of BDNF and GFP in the ipsilateral striata of AAV-injected PF compared

to those injected with vehicle buffer (**Fig.26**). Striatal pTrkB levels were also evaluated, showing a slight increase, though not statistically significant. The increases in BDNF and GFP levels are localized to PF projections reaching the striatum. As established in our *in vitro* results (**Fig.22**), BDNF synthesized in transduced PF neurons follows the cell secretory pathway and is transported anterogradely to be released from axon terminals contacting striatal neurons. Binding of released BDNF to TrkB receptors on the surface of striatal neurons activates intracellular phosphorylation of tyrosine residues, leading to the internalization of the BDNF-pTrkB complex and initiation of neurotrophin-induced signaling cascades.

Previous studies by Ho and Kim et al. (Ho et al., 2013; Kim et al., 2011) described how the 2A element “self-cleaves”, producing different band patterns from a single 2A construct flanked by two proteins. The cleaving mechanism of 2A results in a proline residue being attached to the signal peptide of the downstream protein, producing a weight similar to the standard molecular weight. Meanwhile, the remaining 2A amino acids attach to the C-terminus of the upstream protein, resulting in a protein slightly larger than the standard molecular weight. Consequently, a higher molecular weight band may correspond to a fusion protein linking the two expressed proteins via the 2A peptide, or a combination of the three (Ho et al., 2013; Lewis et al., 2015). The latter indicates possibly that the 2A sequence was not entirely cleaved, which could potentially be a concern in some therapeutic applications (Kim et al., 2011). In our analysis (**Fig.26**) we focused on the expected molecular weights of mature BDNF and GFP, so we cannot definitely assess the presence of a fusion protein.

However, previous studies have successfully overexpressed BDNF as a fusion protein with a marker while maintaining its functionality as a neurotrophin.

For instance, Ziemlinska et al., (Ziemlińska et al., 2014), demonstrated that AAV-induced overexpression of BDNF fused with cMyc was able to enhance the excitability of the lumbar spinal network, leading to locomotor recovery in completely spinalized rats. The fused BDNF protein was detected and analyzed through ELISA and western blotting. Although cMyc has a molecular weight of only 1kDa -much smaller than GFP at 27kDa- Wang et al. (J. Wang et al., 2016) reported that overexpression of BDNF fused with eGFP in AAV vectors effectively activated specific signaling cascades mediated by TrkB in the VTA in a drug abuse-related behavior model in rats. Similarly, Han et al., (Han et al., 2019) demonstrated that overexpressing BDNF and eGFP with a 2A linker sequence using an AAV vector in diabetic mice decreased neuroinflammation in the hippocampus via modulation of the HMGB1/RAGE/NF-kB pathway. These results collectively suggest that AAV-induced overexpression of BDNF, whether as a single or fused protein, retains functional properties.

Striatal BDNF quantification in AAV9-BDNF-eGFP injected hemispheres

In a comparative study of different AAV serotypes utilizing a CMV promoter, Watakabe et al., (Watakabe et al., 2015) found that AAV5 and AAV9 transduced neurons and glial cells expressing high levels of modified hrGFP (hrGFP II). In the transduced neurons of marmosets, macaques, and mouse cerebral cortex, a reduction in NeuN marker was observed, possibly due to general toxicity from high levels of AAV infection or hrGFP II expression mediated by the CMV promoter. They suggested that lower expression levels might be more advantageous for long-term experiments. Similarly, Eslamboli and Kells

(Eslamboli et al., 2005; Kells et al., 2008) noted that excessive overexpression of neurotrophins can have deleterious effects, potentially hindering therapeutic outcomes, and recommended diluting AAV vectors for studies.

Following this guidance, we diluted the AAV9-BDNF-eGFP vector to 1:5 and 1:10 with PBS. After verifying an accurate AAV9-BDNF-eGFP (1:5) injection into the PF of C57bl/6J mice, we observed a significant increase in striatal BDNF protein levels via ELISA (**Fig.27**).

Notably, the overexpressed BDNF protein levels *in vivo* (2492.86 ± 286.73 pg/ml) were lower than those measured *in vitro* (3812.14 ± 67.04 pg/ml) from p.CMV-hBDNF-2A-eGFP transfected HEK293 cells (**Fig.22B**). Direct comparisons are complicated since the cell cultures were directly transfected with 2.5 μg of DNA plasmid and the PF were injected with 1μl of AAV9/2-CMV-hBDNF-2A-eGFP diluted 1:5 (original titer was 2.99E+13 vg/ml). Furthermore, the transfected cultures consisted of human embryonic kidney cells (HEK cells), whereas the PF injections targeted neurons projecting to the striatum. However, variance in quantified BDNF protein levels can be compared by evaluating the standard error of the mean, which indicates that BDNF levels *in vitro* exhibit considerably less variation than *in vivo* striatal values. This effect could be due to the technical difficulties of achieving an accurate injection (Watakabe et al., 2015), and the challenges AAV vectors encounter being recognized, attached, and internalized by cell surface receptors, escaping ubiquitination and degradation, delivering their genetic material into the nucleus, overcoming the limiting factor of synthesizing the double strand of DNA to be transcribed and translated by cellular machinery -culminating in the transport of synthesized proteins from the PF to the striatum (Berry & Asokan, 2016).

Having established evidence of increased BDNF levels induced by the AAV9-BDNF vector, we aimed to explore its potential as a therapeutic agent in the R6/2 mouse line, a model for HD.

Bilateral BDNF overexpression in R6/2 mouse line

The second hypothesis in this study aimed to determine whether bilateral overexpression of BDNF in the PF could potentially improve the behavioral and spontaneous locomotor alterations observed in the R6/2 mouse model of HD. Before analyzing the effects of overexpressed BDNF, a baseline of the animal's behavior and locomotor activity was established (**Fig.6, 7, 8**). Clasping tests, the open field test, and the elevated plus maze were performed at different time points (**Fig.5**). Subsequently, R6/2 CAR mice were injected bilaterally with the AAV5-BDNF-GFP vector (provided by Vector Biolabs) in the PF at four weeks of age. Their behavior and spontaneous locomotor activity were assessed alongside R6/2 WT and non-injected R6/2 CAR littermates, following the same battery of tests and timeline as the baseline evaluation (**Fig.10, 11, 12**). We established a criterion that only R6/2 CAR-BDNF mice accurately injected in the PF, as validated by GFP immunohistochemistry, would be included in the R6/2 CAR-BDNF group. Unfortunately, we were unable to validate any of the Vector Biolabs AAV5-BDNF-GFP injections due to the lack of detectable hrGFP expression (**Fig.14**). Following further testing, the genetic material of the vector (p.CMV-BDNF-IRES2-hrGFP) was sequenced and analyzed *in vitro* (**Fig.19, 20, 21**). Although these results cannot be considered conclusive, the observed changes will be discussed.

AAV5-BDNF-GFP vector (Vector Biolabs; Malvern, PA, USA)

Clasping score

Clasping is a dystonic movement characterized by the abnormal retraction of limbs toward the body (Bissonnette et al., 2013). Consequently, the clasping test has been extensively used in previous studies as a marker of neurodegenerative disease progression, indicated by the severity and duration of involuntary movements (Guyenet et al., 2010; Pietropaolo, Delage, Cayzac, Crusio, & Cho, 2011; Samadi et al., 2013). It is favoured for being easy to interpret, quick, and cheap to perform (J. Y. Li, Popovic, & Brundin, 2005). R6/2 WT mice displayed very little or no limb-clasping behavior while spreading their four limbs in an attempt to grasp something (J. Y. Li et al., 2005). In fact, during the experiment, WT mice exhibited sufficient strength to climb their tail and fingers of the tester, in stark contrast to R6/2 CAR mice, which clasped their limbs tightly against their thorax and abdomen. A low clasping score was observed in R6/2 CAR mice at the initial evaluation time point of four weeks, prior to the early stages of HD (Samadi et al., 2013). The clasping behavior noted in R6/2 CAR mice at four weeks of age indicates detrimental changes already occurring in the pre-symptomatic HD stage, possibly linked to the reduced BDNF mRNA content in striatal afferents, combined with an early reduction in neostriatum volume (Carter et al., 1999; Samadi et al., 2013). The clasping score sharply increased at six weeks and continued to rise more slowly until eleven weeks (**Fig.6**). In contrast, other reports indicate that motor coordination in R6/2 mice begins to markedly deteriorate around eight weeks of age, with involuntary movements, changes in gait patterns, balance issues, dyskinesia, resting tremor, and muscle atrophy (Carter et al., 1999; J. Y. Li et al., 2005). R6/2 CAR-BDNF mice showed increased clasping at six

weeks, similar to their non-injected counterparts; however, the subsequent increase in score was less pronounced in the R6/2 CAR-BDNF group. Similar scores were noted in R6/2 CAR-BDNF mice from weeks eight to ten, with a slight increase at eleven weeks. Clasping scores for R6/2 CAR and R6/2 CAR-BDNF mice were significantly different at nine and eleven weeks. Overall, it appears that the pattern of clasping score increase is more gradual and subdued in the AAV5-BDNF-treated CAR group (**Fig.10**).

Open field test

We utilized total distance traveled and mean velocity as metrics to evaluate spontaneous locomotor activity in the Open field test. At four weeks old, R6/2 WT and R6/2 CAR mice exhibited higher values of distance traveled and mean velocity compared to other evaluated time points within their groups. At this age, the mice are still young (Brooks & Faulkner, 1988) and are entering into the Open field arena for the first time. Mice, being naturally curious, tend to explore their surroundings while remaining near the walls to feel safe. This behavior is evident in the activity traces recorded by the overhead video camera and analyzed using Ethovision software. At this time point, differences between WT and CAR mice were not visible in the activity traces. At both four and six weeks, but not in the following weeks, R6/2 CAR mice displayed a trend of higher values in total distance and mean velocity compared to R6/2 WT; CAR mice tend to be more hyperactive, moving and jumping more when young (J. Y. Li et al., 2005), in addition to possibly experiencing anxiety and fear of being handled during testing.

This observation aligns with reports stating that R6/2 CAR mice begin to show initial signs of motor alterations around three weeks of age, marked by spontaneous locomotor

hyperactivity, which stabilizes but gradually leads to hypoactive by eight weeks of age, with a significant drop at ten weeks (Dunnett et al., 1998; J. Y. Li et al., 2005; Lüesse et al., 2001). Hyperactivity has also been documented in HD mouse models with the full-length human mhtt gene (Reddy et al., 1998) and in mice with mild focal striatal lesions (Borlongan et al., 1995), although more sustained striatal lesions typically cause hypoactivity. This pattern may reflect a gradual striatal dysfunction as early as three weeks of age, likely due to progressive changes in the relationship between receptor and neurotransmitter expression in the cortico-striatal circuit (Lüesse et al., 2001), in combination with a significant reduction in BDNF mRNA in striatal afferents (Samadi et al., 2013) and the presence of intranuclear inclusions of mutant huntingtin in striatal neurons (J. Y. Li et al., 2005); leading to neuronal dysfunction despite the absence of neuronal cell death in the striatum (Carter et al., 1999).

From week four to week nine, R6/2 WT mice exhibited a slight decrease in total distance and mean velocity. This decline may result from the mice becoming accustomed to the Open field arena, leading to calmer behavior and less exploration. To mitigate this effect, we placed the mice in different quadrants of the arena each time they were tested. As expected, R6/2 CAR mice displayed decreased total distance traveled and mean velocity at six weeks, with a sharper decline noted at nine and eleven weeks (**Fig.7**). These locomotor deficits align with findings from Samadi's studies (Samadi et al., 2013), where rotarod performance and grip strength are also significantly impaired, coinciding with a marked decrease in BDNF synthesis as the disease progresses. R6/2 CAR mice injected with AAV5-BDNF showed considerable variation in distance traveled and mean velocity; thus, data were transformed for statistical analysis. Overall, the variation in total distance

traveled values from the R6/2 CAR-BDNF group hindered the identification of differences between groups; however, differences were noted across evaluation time points, regardless of the groups. Total distance traveled at six weeks was higher than at nine and eleven weeks, likely influenced by the significantly low values from both R6/2 CAR-BDNF and R6/2 CAR mice at nine and eleven weeks.

Regarding mean velocity, R6/2 WT mice consistently moved at higher velocities than R6/2 CAR-BDNF mice, while R6/2 CAR mice had the lowest velocities. Notably, there was a statistically significant reduction in mean velocity in the R6/2 CAR-BDNF group at eleven weeks compared to other evaluated weeks in the same group. The mean velocity of R6/2 CAR mice showed high variation across evaluated weeks, complicating the identification of statistical differences. Activity traces indicate that, despite extremely reduced mobility in the final weeks, R6/2 CAR-BDNF mice moved at higher velocities compared to the R6/2 CAR group (**Fig.11**). In a study where five-week-old R6/2 mice received an AAV vector to overexpress pre-enkephalin (pENK) in the striatum, significant beneficial effects were reported in behavioral and locomotor tests. Interestingly, there were no differences in total distance traveled between AAV-treated and untreated R6/2 CAR mice; however, AAV-treated mice exhibited increased movement velocity, which was recognized as a beneficial locomotor effect (Bissonnette et al., 2013). The authors concluded that movement velocity appears to be a more sensitive measure of improvement or decline in locomotor activity compared to distance traveled alone. Thus, we conclude that R6/2 CAR-BDNF mice demonstrated improvements in locomotor activity by increasing movement velocity compared to not injected R6/2 CAR mice.

Elevated plus maze

The elevated plus maze evaluates anxiety-like behavior by forcing the mouse to confront its innate curiosity to explore new environments against the fear it experiences in the open and elevated arms (Baldo & Petersén, 2015; File, Mahal, Mangiarini, & Bates, 1998; Komada et al., 2008). We assessed total distance traveled, mean velocity, and anxiety-like behavior by calculating the ratio of time spent in the open arms relative to the time spent in the closed arms. Similar to the Open field test, values for total distance traveled and mean velocity in the elevated plus maze indicated that R6/2 WT mice moved more and faster compared to R6/2 CAR-BDNF and R6/2 CAR mice, particularly as the disease progressed. Additionally, as observed in the Open field test, R6/2 CAR-BDNF mice exhibited higher velocity despite covering less distance than R6/2 CAR mice, highlighting the beneficial locomotor effect of speed in this test as well (Bissonnette et al., 2013).

Regarding the ratio of time spent in open/closed arms, a higher ratio of time spent in the open versus closed arms indicated reduced anxiety-like behavior, as observed in R6/2 WT mice at four weeks. The urge to explore the open arms outweighed their fear and anxiety of the open and elevated spaces. However, as the mice aged, anxiety levels increased, with a tendency to spend more time walking along the closed arms. It is also possible that they recognized the maze, leading to decreased curiosity and heightened fear of the open and elevated spaces (**Fig.8**).

Interestingly, the first R6/2 litters used for baseline behavior data exhibited different behaviors compared to the subsequent litters used in the AAV experiment. In the first experiment, R6/2 CAR mice demonstrated significantly less anxiety than R6/2 WT mice

at nine and eleven weeks, spending more time in the open arms. This pattern was corroborated by recorded activity traces: R6/2 WT mice engaged in abundant exploratory behavior along the closed arms, while R6/2 CAR mice showed considerably less activity but more movement into the open arms (**Fig.8**). In contrast, during the second experiment, R6/2 CAR mice displayed less anxiety than R6/2 WT mice at nine weeks, but at eleven weeks, their anxiety levels surged beyond those of the R6/2 WT group. R6/2 CAR-BDNF mice exhibited a similar pattern to the first R6/2 CAR group, showing less anxiety as they aged. Additionally, the second experiment involved mice with greater overall variability, making for a considerably more challenging analysis and hindering the detection of potential statistical differences (**Fig.12**). The rapid rise in anxiety in the R6/2 CAR group at eleven weeks during the second experiment cannot be attributed to a lack of mobility in the closed arms, as there was no drastic reduction in total distance traveled or velocity values between nine and eleven weeks. This supports the notion that the mice were indeed moving along the closed arms.

The literature on anxiety-like behavior in HD animal models presents inconsistencies; however, the drastic change observed at eleven weeks compared to nine weeks may be attributed to environmental factors rather than disease progression (**Fig.12B**). If disease progression were the cause, a more gradual change would be expected, likely accompanied by significant alterations in locomotion. Environmental factors that could influence behavior include changes in temperature, humidity, ventilation, noise intensity and light intensity (Hockly et al., 2003).

Mood disorders in HD mouse models

Perturbations in the prefrontal and cingulate cortices, striatum, amygdala, and thalamus within the context of HD can contribute to the development of mood disorders, such as anxiety and depression-related behaviors (Patrick Pla et al., 2014). Thalamic degeneration, particularly in thalamic nuclei projecting to prefrontal areas and the striatum, plays a critical role in the impairment of executive function in early HD patients. Magnetic resonance imaging (MRI) data have revealed structural double lesions within the basal ganglia-thalamo-cortical circuitry at both striatal and thalamic levels (Kassubek, Juengling, Ecker, & Landwehrmeyer, 2005).

Patterns of anxiety-like behavior in HD mouse models are inconsistent in the literature. Consistent with our results, several studies have reported that R6/2 CAR mice show lower levels of anxiety from six weeks onward compared to R6/2 WT littermates (Bissonnette et al., 2013; File et al., 1998). To evaluate the function of the GABA-benzodiazepine receptor complex -important in anxiety-related behaviors- eight-week-old R6/2 female mice were treated with flumazenil, a benzodiazepine receptor antagonist. Flumazenil had anxiolytic effects in R6/2 WT mice but appeared anxiogenic in R6/2 CAR mice, suggesting that some of the observed reduction in anxiety could be due to an endogenous anxiolytic ligand (File et al., 1998).

The genetic background of various HD mouse models is significant, as different strains perform differently in behavioral tests (Hockly et al., 2003). For instance, WT mice from C57 and CBA strains tested in the elevated plus maze demonstrated that CBA mice are significantly less anxious, accompanied by increased exploration. However, given that Flumazenil's effects were similar to those in R6/2 WT mice, researchers concluded that

the primary changes in anxiety levels are attributed to the HD transgene (File et al., 1998). Anxiety-like behavior was slightly elevated in R6/2 CAR mice treated with overexpressed striatal pENK (Bissonnette et al., 2013).

Contrary to our results, multiple reports indicate that HD mice display high levels of anxiety-related behavior. It is important to recognize that variations amongst HD mouse models may influence behavior, including the length of the htt transprotein, the number of polyglutamine repeats, the origin of the mhtt, strain, and levels of htt expression (Kuhn et al., 2007). HD mouse models can be categorized based on their type of mhtt expression: transgenic models expressing truncated htt, those expressing full-length htt, and knock-in models. Chemically induced HD animal models do not necessarily reproduce progressive behavioral changes (Carter et al., 1999).

BACHD transgenic mice -expressing full-length human mhtt- showed increased anxiety at all ages in the zero-maze test (Abada, Schreiber, & Ellenbroek, 2013), as well as in the open field and light/dark box tests, compared to WT mice (L. Menalled et al., 2009). The light/dark box test assesses anxiety-like behavior based on mice's aversion to light. In R6/1 mice – similar to R6/2 mice but develop symptoms on a slower timescale - anxiety progressively increased, peaking at twenty-four weeks. YAC128 mice -expressing full-length human mhtt- demonstrated a gradual increase in anxiety as they aged, measured in the zero-maze test (Chiu, Liu, Leeds, & Chuang, 2011). In a separate laboratory, both female and male R6/2 CAR mice exhibited a progressive increase in anxiety behavior (L. Menalled et al., 2009).

Knowing the number of CAG repeats would be useful for comparing and interpreting results, as CAG repeat numbers can slightly vary from one generation to the next due to

germline instability (File et al., 1998). Other differences may arise from dietary factors and/or housing conditions (J. Y. Li et al., 2005). Additionally, HD mutant females are more susceptible to depressive-like behavior, while mutant males tend to exhibit anxiety-like behaviors (Patrick Pla et al., 2014).

A comparative study utilizing consistent, well-validated protocols with quantitative measures for different HD mouse models, same-sex comparisons, and age within the same laboratory would help reach definitive conclusions.

It is also important to consider that when using the open field test, elevated plus maze, or other maze types to evaluate psychiatric symptoms in an animal model that develops locomotor impairment as the disease progresses, it can become challenging to distinguish whether observed behaviors are due to psychiatric changes like anxiety or depression, or if they stem from severe locomotor impairment preventing the animals' movement, regardless of whether they feel curious, scared, or anxious (Chiu et al., 2011; Lüesse et al., 2001; Patrick Pla et al., 2014). Therefore, assessments of depression and anxiety-related behaviors should be conducted before the animals experience locomotor impairment, to avoid confusion in interpretation.

Mood disorders and BDNF

BDNF/TrkB signaling has been linked to the regulation of mood disorders through its role in hippocampal neurogenesis. In adult CaMKCreER^{T2} Htt $^{flox/flox}$ mice, downregulation of htt expression specifically in mature cortical and hippocampal neurons led to decreased anterograde velocity of BDNF vesicular trafficking and reduced BDNF secretion in hippocampal neurons. These mice showed increased anxiety in the open field test and

elevated plus maze; however, clasping behavior was not observed, and an increase in body weight was noted (P. Pla et al., 2013). In mutated mice expressing the htt protein with non-phosphorylatable serines at positions 1181 and 1201, axonal transport of BDNF mediated by microtubules was enhanced, resulting in anxiolytic behavior and increased dendritic arborization along with the survival of newborn neurons in the dentate gyrus (Ben M'Barek et al., 2013).

Furthermore, knock-in mice expressing the mutated BDNF variant V66M demonstrated impaired BDNF secretion and exhibited high levels of anxiety-related behavior in both the open field and elevated plus maze (Chen et al., 2006). These experiments suggest that decreased BDNF levels translates into increased anxiety. In contrast, female conditional mutant mice with BDNF gene deleted from broad forebrain areas showed decreased anxiety. However, in an inducible BDNF mutant model, female mice exhibited heightened susceptibility to anxiety following stress (Autry & Monteggia, 2012). Cyclotraxin-B, a TrkB inhibitor, displayed anxiolytic properties in Swiss mice, comparable to diazepam, with anxiety-like behaviors observed in the open field test and elevated plus maze (Cazorla et al., 2010). Now, according to this set of experiments, decreased BDNF translates into reduced anxiety. Together, these findings indicate that BDNF expression, transport, and secretion -along with TrkB signaling- play roles in anxiety-related behavior, although the underlying neural circuitry remains to be elucidated.

Analysis of various HD mouse models has revealed a link between mhtt, the development of anxious-depressive behaviors, and defects in hippocampal neurogenesis (P. Pla et al.,

2013). Additionally, BDNF/TrkB signaling influences the function of serotonergic neurons, and dysregulation of the serotonergic system is implicated in the development of mood disorders. BDNF +/- mice exhibit altered serotonergic innervation in the cerebral cortex, hypothalamus, and hippocampus (Lyons et al., 1999). A proper level of neurogenesis - neither too low nor too high- that maintains physiological anxiety states can be improved by exercise and environmental enrichment, which could be linked to BDNF/TrkB signaling.

Morphological changes of AAV5-BDNF injected brains evaluated by Stereology

Unbiased stereology confirmed, in line with previous reports, striatal neuronal loss in R6/2 CAR mice at eleven and a half weeks of age (Bissonnette et al., 2013; Samadi et al., 2013). Notably, R6/2 CAR-BDNF mice exhibited more neurons in the striatum compared to the R6/2 CAR group, suggesting that the AAV5-BDNF-GFP vector from Vector Biolabs (Malvern, PA, USA) may provide striatal neuroprotection within the thalamostriatal system. Samadi et al. (Samadi et al., 2013) reported a decline in the striatal volume in R6/2 CAR mice, as well as a reduction in neuronal area starting as early as weeks six and nine respectively, in parallel to BDNF reduction. It would be interesting to evaluate whether AAV-BDNF delivery induces any changes in these variables.

BDNF delivery via mini pumps increased IR in enkephalinergic neurons in R6/1 mice, promoting long-term survival and maintenance of striatal cells (J. Y. Li et al., 2005). A study overexpressing pENK in the striatum of R6/2 mice found no rescue of striatal volume decline, but a slight improvement in striatal neuronal number was observed five weeks post-AAV2-GFP-pENK delivery (Bissonnette et al., 2013). In this approach, the

AAV vector was administered at five weeks of age when endogenous pENK mRNA had already decreased, yet beneficial effects on the HD phenotype were still achieved.

Future studies are needed to evaluate whether AAV-BDNF delivery to the PF at later time points -when endogenous BDNF mRNA in the PF is decreased- can be beneficial and whether it can mitigate potential damaging effects induced by excessive BDNF.

AAV9-BDNF-eGFP vector effects (provided by NRC)

As previously mentioned, we were unable to successfully verify the AAV5-BDNF-GFP injections from Vector Biolabs in the R6/2 CAR mice during our past experiment (**Fig.14**). The next step involved obtaining AAV vectors from our collaboration with the NRC. After validating these vectors in C57BL/6J mice, we selected the AAV9-BDNF-eGFP vector as the therapeutic vector for further use (**Fig.24**). R6/2 mice were injected bilaterally with either AAV9-BDNF-eGFP or control AAV9-eGFP vector in the PF at four weeks of age (**Fig.28**). The gene expression of the AAV9 vectors was successfully detected using GFP immunohistochemistry, demonstrating robust GFP expression in both R6/2 WT and CAR mice.

Even though the AAV9-eGFP vector was diluted 1:1, it exhibited a wider diffusion at the injection site, covering the thalamic region and subthalamic structures. The PF anterograde projections covered the entire striatal structure and specific regions of the cerebral cortex. In contrast, AAV9-BDNF-eGFP showed less diffusion, maintaining localized GFP expression at the injection site. While anterograde projections also covered the striatum, R6/2 CAR mice exhibited a faded appearance of GFP expression in the lateral portion of the striatum, with fewer GFP^+ projections in the cerebral cortex. Given the 1:1 stoichiometric expression of proteins adjacent to the 2A peptide in this vector (Kim

et al., 2011), we can infer that BDNF protein is overexpressed in the same brain regions as GFP. We confirmed successful BDNF synthesis in the AAV9-BDNF-eGFP injected PF, along with anterograde transport, and secretion in the striatal area (**Fig.25, 27, 28**).

Shockingly, one week post-injection, most R6/2 CAR mice receiving the AAV9-BDNF-eGFP vector began displaying severe adverse effects, including drastic locomotor impairment, significant weight loss, and intense seizures, which often resulted in death (**Fig.29**). The remaining mice died within a couple of weeks, displaying similar effects. Consequently, we could not conduct behavioral and locomotor assays. In contrast, R6/2 CAR mice injected with AAV9-eGFP (**Fig.30**), and R6/2 WT mice receiving either vector did not exhibit these detrimental effects (**Fig.31**).

Previous studies have suggested that lower concentrations of AAV vectors using a CMV promoter might be more advantageous for long-term experiments, potentially avoiding toxic effects induced by high levels of AAV infection or high transgene levels driven by the CMV promoter (Eslamboli et al., 2005; Kells et al., 2008; Watakabe et al., 2015). Accordingly, we diluted the AAV9-BDNF-eGFP vector to 1:5 and then to 1:10. We tested both dilutions in C57bl/6J mice prior to administration in R6/2 mice (data not shown). The 1:5 dilution achieved complete coverage of the striatal structure in C57bl/6J mice after three weeks. Surprisingly, no transgene expression was detected with the 1:10 dilution, likely due to the BDNF vector being too diluted to transduce neurons effectively. Consequently, we first tested the 1:5 dilution in R6/2 CAR mice, but most exhibited negative effects and died suddenly with intense seizure activity. Subsequently, we opted to test the 1:10 dilution in R6/2 CAR mice, even though it had proven unsuccessful in

C57bl/6J mice. Remarkably, this dilution resulted in complete coverage of the striatal structure after three weeks, indicating a strain-specific effect of the AAV9-BDNF-GFP vector in R6/2 mice. Kaplan-Meier survival curves analysis (**Fig.29**) showed statistically significant differences between R6/2 mice injected with the undiluted vector and those receiving the 1:5 dilution compared to the 1:10 dilution ($p= 0.013$ and $p< 0.001$ respectively). The lowest concentration tested (1:10) resulted in a median survival time of six weeks post-injection for R6/2 CAR mice, while those injected with control AAV9-eGFP had a median survival time of eight weeks. The latter corresponds with our group's humane endpoint for R6/2 CAR mice, typically set at twelve weeks.

We observed a clear dose-dependent vulnerability of R6/2 CAR mice to the AAV9-CMV-BDNF-2A-eGFP vector, unlike to AAV5-CMV-BDNF-IRES-hrGFP. This discrepancy may stem from the superior cell transduction efficiency and higher protein levels associated with the AAV9 vector compared to other serotypes (Burger et al., 2004; Issa et al., 2023; Watakabe et al., 2015). Alternatively, it is possible that R6/2 CAR mice reacted adversely to an ingredient in the AAV9-BDNF-eGFP vehicle buffer, or there may have been impurities present. Diluting with PBS buffer likely helped reduce toxic effects (Watakabe et al., 2015). We confirmed that the PBS buffer used for dilution was not the source of toxicity, as the undiluted vector was also highly toxic. Moreover, the control vector AAV9-eGFP, which was also diluted 1:1 with PBS, did not exhibit toxic effects.

Technical difficulties related to injection accuracy were ruled out through GFP immunohistochemistry. Studies using identical injection volumes with varying vector concentrations demonstrated a positive correlation between high AAV titers and

extensive protein expression distribution patterns (L. Samaranch et al., 2017). However, widespread patterns can complicate the control of the overexpressed transgene's effects in non-targeted areas, potentially leading to negative outcomes. It is possible that contamination of the AAV9-BDNF-eGFP vector along the needle track resulted in deposition in areas susceptible to AAV infection, leading to BDNF and GFP overexpression in regions such as the cerebral cortex and hippocampus.

Synaptic dysregulation in HD

Another critical aspect to consider is the significant synaptic dysregulation within the corticostriatal and thalamostriatal pathways, which induces progressive electrophysiological alterations in MSN beginning at the pre-symptomatic stage of the disease (Cepeda et al., 2003). Overactivity of corticostriatal glutamate transmission is an early feature of HD; evidence suggests that mhtt in presynaptic terminals may increase glutamate release (Bissonnette et al., 2013). Biphasic age-dependent changes in neurotransmission have been observed: prior to the emergence of behavioral symptoms and during early symptomatic stages, synaptic currents and glutamate release increase, accompanied by elevated intracellular Ca^{2+} flux. However, during later symptomatic stages, evoked synaptic currents decrease, and glutamate release gradually declines (Cepeda et al., 2003; Estrada-Sánchez, Levine, & Cepeda, 2017; P. R. Joshi et al., 2009). In early symptomatic stages, heightened synchronized cortical activity results in transient, large-amplitude synaptic events in the striatum, primarily reflecting spontaneous excitatory neurotransmitter release effects (Cepeda et al., 2003). Unsurprisingly, early symptomatic R6/2 mice, around five to seven weeks old, exhibit epileptic seizures that often worsen and may lead to death (Cano et al., 2021; Carter et al., 1999; Estrada-

Sánchez et al., 2017; J. Y. Li et al., 2005; Lüesse et al., 2001). In juvenile human HD form, R6/2 and R6/1 mouse models, generalized tonic-clonic and myoclonic seizures are prevalent (Estrada-Sánchez et al., 2017). In R6/2 mice, A2a adenosine receptors and metabotropic glutamate receptor mRNA levels decrease at the pre-symptomatic stage of four weeks, while dopamine receptor reduction occurs during the symptomatic stage (eight weeks), diminishing modulation of the presynaptic terminal (Cha et al., 1999; P. R. Joshi et al., 2009). The loss of inhibitory interneurons in the striatum and various regions of the cerebral cortex contributes to hyperexcitability and increased seizure susceptibility in HD.

Intense dysregulation of glutamate release occurs, further increasing epileptogenicity (Estrada-Sánchez et al., 2017). Importantly, BDNF has been associated with seizure activity; acute BDNF delivery enhances glutamatergic responses and elevates cytoplasmatic Ca^{2+} flux (Y. X. Li, Zhang, Lester, Schuman, & Davidson, 1998), while concurrently modulating $GABA_A$ receptors to reduce GABAergic responses (Tanaka, Saito, & Matsuki, 1997), thereby increasing interstitial glutamate levels and promoting epileptic activity. These findings suggest that AAV9-mediated overexpression of BDNF and GFP exacerbated the severe synaptic dysregulation already present in the cortico-striatal-thalamic circuit. In R6/2 mice, BDNF mRNA levels in the PF, M1 and M2 regions begin to decline at six weeks (Samadi et al., 2013). It is possible that the overexpressed BDNF exceeded the system's capacity, becoming neurotoxic before endogenous BDNF levels began to decline due to HD progression. Additionally, contamination of the AAV vector along the needle track at the injection site may have led to BDNF overexpression in the cerebral cortex and hippocampus, areas involved in epileptic activity (Estrada-

Sánchez et al., 2017). This could explain why R6/2 CAR mice injected with AAV9-BDNF-GFP experienced intense seizures and subsequent death within one to three weeks post-injection, coinciding with the time it takes for AAV vector expression to peak.

AAV-CMV caveats

As more experiments are conducted using various AAV vectors across different animal models, we are uncovering important details about the effects of AAV delivery. This is particular true for potent vectors like AAV9 in combination with strong ubiquitous promoters such as CMV. AAV9, AAV5 and AAV1 vectors effectively transduce neurons, astrocytes, and APC like microglia (Ciesielska et al., 2013; Hadaczek et al., 2009; Issa et al., 2023; Lluis Samaranch et al., 2014). Previous studies by Samaranch and colleagues (Lluis Samaranch et al., 2014) in rats and NHP demonstrated that delivering an AAV9-CMV vector encoding a foreign protein -such as GFP- elicited a neurotoxic immune response. They proposed that the transduced APC expressed GFP peptides conjugated with MHC II, thereby activating a classic adaptive immune response in the injected and connected areas. In contrast, the AAV9 vector expressing GFP driven by the CAG promoter and the AAV2 vector did not provoke the same immune reaction, possibly due to AAV2's limited ability to transduce only neurons (Ciesielska et al., 2013; Lluis Samaranch et al., 2014). Furthermore, the injection of AAV1-hrGFP into monkey brains triggered both humoral and cell-mediated immune responses, evidenced by the presence of anti-AAV1 and anti-hrGFP antibodies, $CD4^+$ lymphocyte infiltration, and increase of MHC II expression (Ciesielska et al., 2013; Hadaczek et al., 2009). Similarly, human AADC encoded in an AAV9 vector and injected into rat brains resulted in significant inflammation, along with MHC II upregulation in glial cells and infiltration by CD8+

lymphocytes (Ciesielska et al., 2013). Notably, even when the protein encoded by the AAV is 97% homologous to the host, it can still induce mild gliosis (Forsayeth & Bankiewicz, 2015).

In our case, we did not observe infiltrating lymphocytes, inflammatory conditions, or tissue damage surrounding the injected site following AAV9-BNDF-GFP delivery. However, we cannot dismiss the possibility of subtle immune responses occurring in the background alongside HD progression. It is essential to remain aware of potential complications, as observed in the previous cited studies, due to the complex interplay between engineered AAV capsids and host factors, which can vary between species and strains. For instance, the AAV-PHP.B vector was developed as an AAV9 variant capable of crossing the BBB to transduce the CNS in C57bl/6 mice. However, follow-up studies indicated that the properties of the PHP.B capsid did not translate to other mouse strains, such as BALB/cJ or NHPs (Hordeaux et al., 2018).

Incorporating a cell-specific promoter as a primary strategy for targeted expression could enhance outcomes. One study utilized a scAAV9 vector with an endogenous human survival motor neuron 1 (SMN1) promoter to drive SMN1 expression specifically in neurons, resulting in a remarkable safety profile and improved therapeutic efficacy in SMNdelta7 mice with spinal muscular atrophy (SMA) (Q. Xie et al., 2022). Another strategy to mitigate transgene immunity involves incorporating APC-specific miRNA binding sites into the rAAV cassette, inhibiting expression in cells that express the complementary miRNA, thereby preventing transgene expression from APCs (Muhuri et al., 2021; Xiao et al., 2019).

Successful studies have employed the AAV approach in chemically induced HD animal models. However, it is crucial to highlight that these models do not accurately replicate the disease; they lack the htt mutation and do not mimic HD symptom progression (Borlongan et al., 1995; Strand et al., 2007). No effective therapy in animal models of HD has translated successfully to clinical trials in HD patients. Some animal models also yield inconsistent results, likely due to model-specific-features, varying doses, delivery routes, and assessment protocols. Additionally, the stage of the disease at the time of intervention is a critical factor (J. Y. Li et al., 2005). In developing gene therapy treatments for various diseases, it is vital to consider the specific cell type targeted, as well as the level and range of therapeutic protein required to positively impact symptoms (Hadaczek et al., 2009).

R6/2 mouse model as a therapeutic model

No animal model perfectly corresponds to human disease, and it is expected that different models will exhibit various strengths and weaknesses that will influence their performance in trials (Hockly et al., 2003). However, the R6/2 mouse model closely mimics features of human HD, particularly regarding the sequence of symptom onset and progression of motor coordination deterioration, visuospatial learning, and spontaneous locomotion (Lüesse et al., 2001). The quantifiable progression of these motor deficits makes the R6/2 mouse model particularly suitable for evaluating the effectiveness of potential therapeutic agents aimed at treating motor symptoms of HD (Carter et al., 1999). Transcriptional studies indicate that striatal mRNA expression in R6/2 mice is comparable to that of full-length knock-in HD models (Kuhn et al., 2007). This suggests that the truncated first exon of the human mhtt present in R6/2 does not represent a disadvantage compared to the

full-length mhtt gene. This is important in terms of the reliability of the HD model, as the striatum exhibits the most extensive neuropathology and drastic mRNA changes (Kuhn et al., 2007), reassuring us that R6/2 replicates the neurodegenerative changes.

The rapid progression of symptoms in this animal model may occasionally hinder the ability to detect subtle improvements in cognitive and mood phenotypes due to treatment, especially if the treatment requires time to take effect (Hockly et al., 2003). For example, if mice are injected with the AAV vector at four weeks of age, it takes approximately three weeks for gene expression to peak and for the protein to be transported to the striatum. In our study, R6/2 CAR mice are injected at this age because it represents the pre-motor symptomatic stage of HD, and after the three-week AAV incubation, gene expression would be expected to peak during the symptomatic stage at around seven to eight weeks of age. However, in terms of the R6/2 mice's lifespan, three weeks represents a quarter of their lives. This leaves only a very limited window for therapeutic intervention to demonstrate benefits on pre-motor cognitive abilities and psychiatric symptoms of these HD models. Models that express full-length mhtt generally develop motor deficits later than those expressing truncated mhtt, allowing more time to study anxio-depressive behaviors (Patrick Pla et al., 2014).

Future studies evaluating AAV-mediated gene therapy targeting non-motor aspects of HD might benefit from using models with longer lifespans or later disease onset, enabling the detection of subtle changes caused by therapy before the early motor symptomatic stage. Designing treatments for HD must consider the timing of the gradual degenerative changes.

Overall, using animal models entails the risk of variability concerning symptom onset, severity, and longevity. If this variability is not controlled, it may obscure treatment effects. Some of this variability can arise from genetic and environmental factors. In the context of HD, CAG repeats are inherently unstable, and their number can vary due to environmental factors, litter size, maternal care, age at weaning, cage size, nutrition, and enrichment strategies. Therefore, standardizing as many aspects of the protocols for animal testing as possible is crucial.

Chapter 6: FINAL CONCLUSION AND SUMMARY

In this study, a strategy was proposed for delivering BDNF to the striatum via a recombinant AAV vector to the PF of R6/2 mice, a model of HD. The PF proved to be an important target due to the functional viability of PF neurons and their projections early in HD progression, as well as their topographical organization covering the entire striatum. Targeting this nucleus proved useful in addressing motor, cognitive and psychiatric symptoms of HD by influencing the somatosensory, associative, and limbic circuits converging in the PF.

BDNF synthesis was successfully increased in the PF mediated by an AAV-BDNF vector, BDNF was transported anterogradely, and we were able to quantify functional release at the striatum of C57bl/6J mice, potentially covering a larger area than direct striatal delivery would allow and minimizing the viral vector usage. Additionally, we obtained

evidence of successful AAV-BDNF transduction of the neurons in the PF of R6/2 mice and measured the distance covered by its projections reaching the striatum.

It was not possible to verify AAV injection accurately in the PF of R6/2 mice grouped for behavioral testing using GFP immunodetection. However, improvement in limb-clasping behavior at later stages of the disease was observed, as increased speed in movement at every evaluated time point in the open field test and elevated plus maze and increased striatal neuronal number compared to the not treated R6/2 CAR group. More homogenization between behavioral studies is needed to be able to conclude the influence of BDNF in mood disorders related to HD, especially in HD mouse models like R6/2 mice.

R6/2 CAR mice showed a specific susceptibility for seizure activity induced by AAV9-BDNF but not by AAV5-BDNF vector. AAV9-BDNF vector dilutions were tolerated in a dose-response manner.

The next steps towards the overall goal include the delivery of the AAV9-BDNF-eGFP vector as a therapeutic agent to R6/2 mice, followed by the same battery of locomotor and behavioral tests (**Fig. 5**) and molecular and morphological analysis between treated and untreated R6/2 groups.

BIBLIOGRAPHY

Abada, Y.-s. K., Schreiber, R., & Ellenbroek, B. (2013). Motor, emotional and cognitive deficits in adult BACHD mice: A model for Huntington's disease. *Behavioural Brain Research, 238*, 243-251. doi:https://doi.org/10.1016/j.bbr.2012.10.039

Agbandje-McKenna, M., & Kleinschmidt, J. (2011). AAV capsid structure and cell interactions. *Methods Mol Biol, 807*, 47-92. doi:10.1007/978-1-61779-370-7_3

Akache, B., Grimm, D., Pandey, K., Yant, S. R., Xu, H., & Kay, M. A. (2006). The 37/67-kilodalton laminin receptor is a receptor for adeno-associated virus serotypes 8, 2, 3, and 9. *J Virol, 80*(19), 9831-9836. doi:10.1128/jvi.00878-06

Alberch, J., Pérez-Navarro, E., & Canals, J. M. (2004). Neurotrophic factors in Huntington's disease. *Prog Brain Res, 146*, 195-229. doi:10.1016/s0079-6123(03)46014-7

Altar, C. A., Cai, N., Bliven, T., Juhasz, M., Conner, J. M., Acheson, A. L., . . . Wiegand, S. J. (1997). Anterograde transport of brain-derived neurotrophic factor and its role in the brain. *Nature, 389*(6653), 856-860. doi:10.1038/39885

Aschauer, D. F., Kreuz, S., & Rumpel, S. (2013). Analysis of transduction efficiency, tropism and axonal transport of AAV serotypes 1, 2, 5, 6, 8 and 9 in the mouse brain. *PloS one, 8*(9), e76310. doi:10.1371/journal.pone.0076310

Atchison, R. W., Casto, B. C., & Hammon, W. M. (1965). ADENOVIRUS-ASSOCIATED DEFECTIVE VIRUS PARTICLES. *Science, 149*(3685), 754-756. doi:10.1126/science.149.3685.754

Autry, A. E., & Monteggia, L. M. (2012). Brain-derived neurotrophic factor and neuropsychiatric disorders. *Pharmacol Rev, 64*(2), 238-258. doi:10.1124/pr.111.005108

Baldo, B., & Petersén, Å. (2015). Analysis of Nonmotor Features in Murine Models of Huntington Disease. In (pp. 583-602).

Barbacid, M. (1994). The Trk family of neurotrophin receptors. *Journal of Neurobiology, 25*(11), 1386-1403. doi:10.1002/neu.480251107

Barde, Y. A., Edgar, D., & Thoenen, H. (1982). Purification of a new neurotrophic factor from mammalian brain. *Embo j, 1*(5), 549-553.

Bates, G. P. (2005). History of genetic disease: the molecular genetics of Huntington disease - a history. *Nat Rev Genet, 6*(10), 766-773. doi:10.1038/nrg1686

Bates, G. P., Mangiarini, L., & Davies, S. W. (1998). Transgenic mice in the study of polyglutamine repeat expansion diseases. *Brain Pathol, 8*(4), 699-714. doi:10.1111/j.1750-3639.1998.tb00196.x

Bell, C. L., Gurda, B. L., Van Vliet, K., Agbandje-McKenna, M., & Wilson, J. M. (2012). Identification of the galactose binding domain of the adeno-associated virus serotype 9 capsid. *J Virol, 86*(13), 7326-7333. doi:10.1128/jvi.00448-12

Ben M'Barek, K., Pla, P., Orvoen, S., Benstaali, C., Godin, J. D., Gardier, A. M., . . . Humbert, S. (2013). Huntingtin mediates anxiety/depression-related behaviors and hippocampal neurogenesis. *J Neurosci, 33*(20), 8608-8620. doi:10.1523/jneurosci.5110-12.2013

Benraiss, A., & Goldman, S. A. (2011). Cellular therapy and induced neuronal replacement for Huntington's disease. *Neurotherapeutics, 8*(4), 577-590. doi:10.1007/s13311-011-0075-8

Berkemeier, L. R., Winslow, J. W., Kaplan, D. R., Nikolics, K., Goeddel, D. V., & Rosenthal, A. (1991). Neurotrophin-5: A novel neurotrophic factor that activates trk and trkB. *Neuron, 7*(5), 857-866. doi:https://doi.org/10.1016/0896-6273(91)90287-A

Berry, G. E., & Asokan, A. (2016). Cellular transduction mechanisms of adeno-associated viral vectors. *Curr Opin Virol, 21*, 54-60. doi:10.1016/j.coviro.2016.08.001

Bissonnette, S., Vaillancourt, M., Hébert, S. S., Drolet, G., & Samadi, P. (2013). Striatal pre-enkephalin overexpression improves Huntington's disease symptoms in the R6/2 mouse model of Huntington's disease. *PloS one, 8*(9), e75099. doi:10.1371/journal.pone.0075099

Borlongan, C. V., Koutouzis, T. K., Freeman, T. B., Cahill, D. W., & Sanberg, P. R. (1995). Behavioral pathology induced by repeated systemic injections of 3-nitropropionic acid mimics the motoric symptoms of Huntington's disease. *Brain Res, 697*(1), 254-257. doi:https://doi.org/10.1016/0006-8993(95)00901-2

Brooks, S. V., & Faulkner, J. A. (1988). Contractile properties of skeletal muscles from young, adult and aged mice. *J Physiol, 404*, 71-82. doi:10.1113/jphysiol.1988.sp017279

Brunet, A., Bonni, A., Zigmond, M. J., Lin, M. Z., Juo, P., Hu, L. S., . . . Greenberg, M. E. (1999). Akt Promotes Cell Survival by Phosphorylating and Inhibiting a Forkhead Transcription Factor. *Cell, 96*(6), 857-868. doi:10.1016/s0092-8674(00)80595-4

Burger, C., Gorbatyuk, O. S., Velardo, M. J., Peden, C. S., Williams, P., Zolotukhin, S., . . . Muzyczka, N. (2004). Recombinant AAV viral vectors pseudotyped with viral capsids from serotypes 1, 2, and 5 display differential efficiency and cell tropism after delivery to different regions of the central nervous system. *Mol Ther, 10*(2), 302-317. doi:10.1016/j.ymthe.2004.05.024

Cano, A., Fonseca, E., Ettcheto, M., Sánchez-López, E., de Rojas, I., Alonso-Lana, S., . . . Ruíz, A. (2021). Epilepsy in Neurodegenerative Diseases: Related Drugs and Molecular Pathways. *Pharmaceuticals (Basel), 14*(10). doi:10.3390/ph14101057

Carter, R. J., Lione, L. A., Humby, T., Mangiarini, L., Mahal, A., Bates, G. P., . . . Morton, A. J. (1999). Characterization of progressive motor deficits in mice transgenic for the human Huntington's disease mutation. *J Neurosci, 19*(8), 3248-3257. doi:10.1523/jneurosci.19-08-03248.1999

Cazorla, M., Jouvenceau, A., Rose, C., Guilloux, J. P., Pilon, C., Dranovsky, A., & Prémont, J. (2010). Cyclotraxin-B, the first highly potent and selective TrkB inhibitor, has anxiolytic properties in mice. *PloS one, 5*(3), e9777. doi:10.1371/journal.pone.0009777

Cearley, C. N., & Wolfe, J. H. (2006). Transduction characteristics of adeno-associated virus vectors expressing cap serotypes 7, 8, 9, and Rh10 in the mouse brain. *Mol Ther, 13*(3), 528-537. doi:10.1016/j.ymthe.2005.11.015

Cearley, C. N., & Wolfe, J. H. (2007). A single injection of an adeno-associated virus vector into nuclei with divergent connections results in widespread vector distribution in the brain and global correction of a neurogenetic disease. *J Neurosci, 27*(37), 9928-9940. doi:10.1523/jneurosci.2185-07.2007

Cecyn, M. N., & Abrahao, K. P. (2023). Where do you measure the Bregma for rodent stereotaxic surgery? *IBRO Neurosci Rep, 15*, 143-148. doi:10.1016/j.ibneur.2023.07.003

Ceni, C., Kommaddi, R. P., Thomas, R., Vereker, E., Liu, X., McPherson, P. S., . . . Barker, P. A. (2010). The p75NTR intracellular domain generated by neurotrophin-induced receptor cleavage potentiates Trk signaling. *J Cell Sci, 123*(Pt 13), 2299-2307. doi:10.1242/jcs.062612

Ceni, C., Unsain, N., Zeinieh, M. P., & Barker, P. A. (2014). Neurotrophins in the Regulation of Cellular Survival and Death. In (pp. 193-221): Springer Berlin Heidelberg.

Cepeda, C., Hurst, R. S., Calvert, C. R., Hernández-Echeagaray, E., Nguyen, O. K., Jocoy, E., . . . Levine, M. S. (2003). Transient and progressive electrophysiological alterations in the

corticostriatal pathway in a mouse model of Huntington's disease. *Journal of Neuroscience, 23*(3), 961-969. doi:10.1523/jneurosci.23-03-00961.2003

Cha, J. H., Frey, A. S., Alsdorf, S. A., Kerner, J. A., Kosinski, C. M., Mangiarini, L., . . . Young, A. B. (1999). Altered neurotransmitter receptor expression in transgenic mouse models of Huntington's disease. *Philos Trans R Soc Lond B Biol Sci, 354*(1386), 981-989. doi:10.1098/rstb.1999.0449

Chen, Z. Y., Jing, D., Bath, K. G., Ieraci, A., Khan, T., Siao, C. J., . . . Lee, F. S. (2006). Genetic variant BDNF (Val66Met) polymorphism alters anxiety-related behavior. *Science, 314*(5796), 140-143. doi:10.1126/science.1129663

Chiu, C. T., Liu, G., Leeds, P., & Chuang, D. M. (2011). Combined treatment with the mood stabilizers lithium and valproate produces multiple beneficial effects in transgenic mouse models of Huntington's disease. *Neuropsychopharmacology, 36*(12), 2406-2421. doi:10.1038/npp.2011.128

Ciesielska, A., Hadaczek, P., Mittermeyer, G., Zhou, S., Wright, J. F., Bankiewicz, K. S., & Forsayeth, J. (2013). Cerebral infusion of AAV9 vector-encoding non-self proteins can elicit cell-mediated immune responses. *Mol Ther, 21*(1), 158-166. doi:10.1038/mt.2012.167

Clark, K. R., Sferra, T. J., Lo, W., Qu, G., Chen, R., & Johnson, P. R. (1999). Gene transfer into the CNS using recombinant adeno-associated virus: analysis of vector DNA forms resulting in sustained expression. *J Drug Target, 7*(4), 269-283. doi:10.3109/10611869909085510

Cohen, S. (1960). PURIFICATION OF A NERVE-GROWTH PROMOTING PROTEIN FROM THE MOUSE SALIVARY GLAND AND ITS NEURO-CYTOTOXIC ANTISERUM. *Proc Natl Acad Sci U S A, 46*(3), 302-311. doi:10.1073/pnas.46.3.302

Colucci-D'Amato, L., Speranza, L., & Volpicelli, F. (2020). Neurotrophic Factor BDNF, Physiological Functions and Therapeutic Potential in Depression, Neurodegeneration and Brain Cancer. *Int J Mol Sci, 21*(20). doi:10.3390/ijms21207777

Conner, J. M., Lauterborn, J. C., & Gall, C. M. (1998). Anterograde transport of neurotrophin proteins in the CNS--a reassessment of the neurotrophic hypothesis. *Rev Neurosci, 9*(2), 91-103. doi:10.1515/revneuro.1998.9.2.91

Conner, J. M., Lauterborn, J. C., Yan, Q., Gall, C. M., & Varon, S. (1997). Distribution of brain-derived neurotrophic factor (BDNF) protein and mRNA in the normal adult rat CNS: evidence for anterograde axonal transport. *J Neurosci, 17*(7), 2295-2313.

Connor, B., Sun, Y., von Hieber, D., Tang, S. K., Jones, K. S., & Maucksch, C. (2016). AAV1/2-mediated BDNF gene therapy in a transgenic rat model of Huntington's disease. *Gene Ther, 23*(3), 283-295. doi:10.1038/gt.2015.113

Cornwall, J., & Phillipson, O. T. (1988). Afferent projections to the parafascicular thalamic nucleus of the rat, as shown by the retrograde transport of wheat germ agglutinin. *Brain Research Bulletin, 20*(2), 139-150. doi:https://doi.org/10.1016/0361-9230(88)90171-2

Costa, R. O., Perestrelo, T., & Almeida, R. D. (2018). PROneurotrophins and CONSequences. *Molecular Neurobiology, 55*(4), 2934-2951. doi:10.1007/s12035-017-0505-7

Crevier-Sorbo, G., Rymar, V. V., Crevier-Sorbo, R., & Sadikot, A. F. (2020). Thalamostriatal degeneration contributes to dystonia and cholinergic interneuron dysfunction in a mouse model of Huntington's disease. *Acta Neuropathol Commun, 8*(1), 14. doi:10.1186/s40478-020-0878-0

Datta, S. R., Dudek, H., Tao, X., Masters, S., Fu, H., Gotoh, Y., & Greenberg, M. E. (1997). Akt Phosphorylation of BAD Couples Survival Signals to the Cell-Intrinsic Death Machinery. *Cell, 91*(2), 231-241. doi:10.1016/s0092-8674(00)80405-5

Davidson, B. L., Stein, C. S., Heth, J. A., Martins, I., Kotin, R. M., Derksen, T. A., . . . Chiorini, J. A. (2000). Recombinant adeno-associated virus type 2, 4, and 5 vectors: transduction of variant cell types and regions in the mammalian central nervous system. *Proc Natl Acad Sci U S A, 97*(7), 3428-3432. doi:10.1073/pnas.97.7.3428

Daya, S., & Berns, K. I. (2008). Gene therapy using adeno-associated virus vectors. *Clin Microbiol Rev, 21*(4), 583-593. doi:10.1128/cmr.00008-08

De Souza, R. A., & Leavitt, B. R. (2015). Neurobiology of Huntington's Disease. *Curr Top Behav Neurosci, 22*, 81-100. doi:10.1007/7854_2014_353

DiFiglia, M. (2002). Huntingtin Fragments that Aggregate Go Their Separate Ways. *Molecular Cell, 10*(2), 224-225. doi:https://doi.org/10.1016/S1097-2765(02)00609-3

DiFiglia, M., Sapp, E., Chase, K., Schwarz, C., Meloni, A., Young, C., . . . Aronin, N. (1995). Huntingtin is a cytoplasmic protein associated with vesicles in human and rat brain neurons. *Neuron, 14*(5), 1075-1081. doi:https://doi.org/10.1016/0896-6273(95)90346-1

Douar, A. M., Poulard, K., Stockholm, D., & Danos, O. (2001). Intracellular trafficking of adeno-associated virus vectors: routing to the late endosomal compartment and proteasome degradation. *J Virol, 75*(4), 1824-1833. doi:10.1128/jvi.75.4.1824-1833.2001

Dudek, A. M., Zabaleta, N., Zinn, E., Pillay, S., Zengel, J., Porter, C., . . . Vandenberghe, L. H. (2020). GPR108 Is a Highly Conserved AAV Entry Factor. *Mol Ther, 28*(2), 367-381. doi:10.1016/j.ymthe.2019.11.005

Dunnett, S. B., Carter, R. J., Watts, C., Torres, E. M., Mahal, A., Mangiarini, L., . . . Morton, A. J. (1998). Striatal Transplantation in a Transgenic Mouse Model of Huntington's Disease. *Experimental Neurology, 154*(1), 31-40. doi:https://doi.org/10.1006/exnr.1998.6926

Emborg, M. E., Hurley, S. A., Joers, V., Tromp do, P. M., Swanson, C. R., Ohshima-Hosoyama, S., . . . Alexander, A. L. (2014). Titer and product affect the distribution of gene expression after intraputaminal convection-enhanced delivery. *Stereotact Funct Neurosurg, 92*(3), 182-194. doi:10.1159/000360584

Eslamboli, A., Georgievska, B., Ridley, R. M., Baker, H. F., Muzyczka, N., Burger, C., . . . Kirik, D. (2005). Continuous low-level glial cell line-derived neurotrophic factor delivery using recombinant adeno-associated viral vectors provides neuroprotection and induces behavioral recovery in a primate model of Parkinson's disease. *J Neurosci, 25*(4), 769-777. doi:10.1523/jneurosci.4421-04.2005

Estrada-Sánchez, A. M., Levine, M. S., & Cepeda, C. (2017). Chapter 71 - Epilepsy in Other Neurodegenerative Disorders: Huntington's and Parkinson's Diseases. In A. Pitkänen, P. S. Buckmaster, A. S. Galanopoulou, & S. L. Moshé (Eds.), *Models of Seizures and Epilepsy (Second Edition)* (pp. 1043-1058): Academic Press.

Fawcett, J. P., Alonso-Vanegas, M. A., Morris, S. J., Miller, F. D., Sadikot, A. F., & Murphy, R. A. (2000). Evidence that brain-derived neurotrophic factor from presynaptic nerve terminals regulates the phenotype of calbindin-containing neurons in the lateral septum. *J Neurosci, 20*(1), 274-282.

Ferrer, I., Goutan, E., Marin, C., Rey, M. J., & Ribalta, T. (2000). Brain-derived neurotrophic factor in Huntington disease. *Brain Res, 866*(1-2), 257-261.

Ferry, B., Gervasoni, D., & Vogt, C. (2014). Stereotaxic Approach of a Target Structure. In *Stereotaxic Neurosurgery in Laboratory Rodent: Handbook on Best Practices* (pp. 69-86). Paris: Springer Paris.

File, S. E., Mahal, A., Mangiarini, L., & Bates, G. P. (1998). Striking changes in anxiety in Huntington's disease transgenic mice. *Brain Res, 805*(1), 234-240. doi:https://doi.org/10.1016/S0006-8993(98)00736-7

Fisher, E. R., & Hayden, M. R. (2014). Multisource ascertainment of Huntington disease in Canada: prevalence and population at risk. *Mov Disord, 29*(1), 105-114. doi:10.1002/mds.25717

Fisher, K. J., Gao, G. P., Weitzman, M. D., DeMatteo, R., Burda, J. F., & Wilson, J. M. (1996). Transduction with recombinant adeno-associated virus for gene therapy is limited by leading-strand synthesis. *J Virol, 70*(1), 520-532. doi:10.1128/jvi.70.1.520-532.1996

Forsayeth, J., & Bankiewicz, K. S. (2015). Transduction of antigen-presenting cells in the brain by AAV9 warrants caution in preclinical studies. *Molecular Therapy, 23*(4), 612. doi:10.1038/mt.2015.35

Franich, N. R., Hickey, M. A., Zhu, C., Osborne, G. F., Ali, N., Chu, T., . . . Chesselet, M. F. (2019). Phenotype onset in Huntington's disease knock-in mice is correlated with the incomplete splicing of the mutant huntingtin gene. *J Neurosci Res, 97*(12), 1590-1605. doi:10.1002/jnr.24493

Franklin, K. B., & Paxinos, G. (2008). *The mouse brain in stereotaxic coordinates* (Vol. 3): Academic press New York:.

Fusco, F. R., Zuccato, C., Tartari, M., Martorana, A., De March, Z., Giampà, C., . . . Bernardi, G. (2003). Co-localization of brain-derived neurotrophic factor (BDNF) and wild-type huntingtin in normal and quinolinic acid-lesioned rat brain. *Eur J Neurosci, 18*(5), 1093-1102. doi:10.1046/j.1460-9568.2003.02844.x

Gauthier, L. R., Charrin, B. C., Borrell-Pages, M., Dompierre, J. P., Rangone, H., Cordelieres, F. P., . . . Saudou, F. (2004). Huntingtin controls neurotrophic support and survival of neurons by enhancing BDNF vesicular transport along microtubules. *Cell, 118*(1), 127-138. doi:10.1016/j.cell.2004.06.018

Gervais, F. G., Singaraja, R., Xanthoudakis, S., Gutekunst, C. A., Leavitt, B. R., Metzler, M., . . . Nicholson, D. W. (2002). Recruitment and activation of caspase-8 by the Huntingtin-interacting protein Hip-1 and a novel partner Hippi. *Nature Cell Biology, 4*(2), 95-105. doi:10.1038/ncb735

Ghosh, R., & Tabrizi, S. J. (2015). Clinical Aspects of Huntington's Disease. *Curr Top Behav Neurosci, 22*, 3-31. doi:10.1007/7854_2013_238

Gibon, J., & Barker, P. A. (2017). Neurotrophins and Proneurotrophins: Focus on Synaptic Activity and Plasticity in the Brain. *Neuroscientist, 23*(6), 587-604. doi:10.1177/1073858417697037

Gil, J. M., & Rego, A. C. (2009). The R6 lines of transgenic mice: a model for screening new therapies for Huntington's disease. *Brain Res Rev, 59*(2), 410-431. doi:10.1016/j.brainresrev.2008.12.001

Gonzalo-Martín, E., Alonso-Martínez, C., Sepúlveda, L. P., & Clasca, F. (2024). Micropopulation mapping of the mouse parafascicular nucleus connections reveals diverse input–output motifs. *Frontiers in Neuroanatomy, 17*. doi:10.3389/fnana.2023.1305500

Gould, T. D., Dao, D. T., & Kovacsics, C. E. (2009). The Open Field Test. In T. D. Gould (Ed.), *Mood and Anxiety Related Phenotypes in Mice: Characterization Using Behavioral Tests* (pp. 1-20). Totowa, NJ: Humana Press.

Gray, M., Shirasaki, D. I., Cepeda, C., André, V. M., Wilburn, B., Lu, X. H., . . . Yang, X. W. (2008). Full-length human mutant huntingtin with a stable polyglutamine repeat can elicit progressive and selective neuropathogenesis in BACHD mice. *J Neurosci, 28*(24), 6182-6195. doi:10.1523/jneurosci.0857-08.2008

Grimes, M. L., Beattie, E., & Mobley, W. C. (1997). A signaling organelle containing the nerve growth factor-activated receptor tyrosine kinase, TrkA. *Proceedings of the National Academy of Sciences, 94*(18), 9909-9914. doi:10.1073/pnas.94.18.9909

Guyenet, S. J., Furrer, S. A., Damian, V. M., Baughan, T. D., La Spada, A. R., & Garden, G. A. (2010). A simple composite phenotype scoring system for evaluating mouse models of cerebellar ataxia. *J Vis Exp*(39). doi:10.3791/1787

Hadaczek, P., Forsayeth, J., Mirek, H., Munson, K., Bringas, J., Pivirotto, P., . . . Bankiewicz, K. S. (2009). Transduction of nonhuman primate brain with adeno-associated virus serotype 1: vector trafficking and immune response. *Hum Gene Ther, 20*(3), 225-237. doi:10.1089/hum.2008.151

Hallbook, F., Ibanez, C. F., & Persson, H. (1991). Evolutionary studies of the nerve growth factor family reveal a novel member abundantly expressed in Xenopus ovary. *Neuron, 6*(5), 845-858. doi:10.1016/0896-6273(91)90180-8

Han, R., Liu, Z., Sun, N., Liu, S., Li, L., Shen, Y., . . . Xu, Q. (2019). BDNF Alleviates Neuroinflammation in the Hippocampus of Type 1 Diabetic Mice via Blocking the Aberrant HMGB1/RAGE/NF-κB Pathway. *Aging Dis, 10*(3), 611-625. doi:10.14336/ad.2018.0707

Heinsen, H., Rüb, U., Gangnus, D., Jungkunz, G., Bauer, M., Ulmar, G., . . . Strik, M. (1996). Nerve cell loss in the thalamic centromedian-parafascicular complex in patients with Huntington's disease. *Acta Neuropathol, 91*(2), 161-168. doi:10.1007/s004010050408

Hempstead, B. L. (2015). Brain-Derived Neurotrophic Factor: Three Ligands, Many Actions. *Transactions of the American Clinical and Climatological Association, 126*, 9-19.

Ho, S. C. L., Bardor, M., Li, B., Lee, J. J., Song, Z., Tong, Y. W., . . . Yang, Y. (2013). Comparison of Internal Ribosome Entry Site (IRES) and Furin-2A (F2A) for Monoclonal Antibody Expression Level and Quality in CHO Cells. *PloS one, 8*(5), e63247. doi:10.1371/journal.pone.0063247

Hockly, E., Woodman, B., Mahal, A., Lewis, C. M., & Bates, G. (2003). Standardization and statistical approaches to therapeutic trials in the R6/2 mouse. *Brain Research Bulletin, 61*(5), 469-479. doi:10.1016/s0361-9230(03)00185-0

Hohn, A., Leibrock, J., Bailey, K., & Barde, Y. A. (1990). Identification and characterization of a novel member of the nerve growth factor/brain-derived neurotrophic factor family. *Nature, 344*(6264), 339-341. doi:10.1038/344339a0

Holley, S. M., Oikonomou, K. D., Swift, C. M., Mohan, L., Matthews, B., Vega, O., . . . Levine, M. S. (2022). Thalamocortical Projections Are Significantly Impaired in the R6/2 Mouse Model of Huntington's Disease. *eneuro, 9*(3). doi:10.1523/eneuro.0103-22.2022

Hordeaux, J., Wang, Q., Katz, N., Buza, E. L., Bell, P., & Wilson, J. M. (2018). The Neurotropic Properties of AAV-PHP.B Are Limited to C57BL/6J Mice. *Mol Ther, 26*(3), 664-668. doi:10.1016/j.ymthe.2018.01.018

Howe, C. L., Valletta, J. S., Rusnak, A. S., & Mobley, W. C. (2001). NGF Signaling from Clathrin-Coated Vesicles. *Neuron, 32*(5), 801-814. doi:10.1016/s0896-6273(01)00526-8

Huang, L., Wan, J., Wu, Y., Tian, Y., Yao, Y., Yao, S., . . . Xu, H. (2021). Challenges in adeno-associated virus-based treatment of central nervous system diseases through systemic injection. *Life Sciences, 270*, 119142. doi:https://doi.org/10.1016/j.lfs.2021.119142

Hudry, E., & Vandenberghe, L. H. (2019). Therapeutic AAV Gene Transfer to the Nervous System: A Clinical Reality. *Neuron, 101*(5), 839-862. doi:10.1016/j.neuron.2019.02.017

Illarioshkin, S. N., Klyushnikov, S. A., Vigont, V. A., Seliverstov, Y. A., & Kaznacheyeva, E. V. (2018). Molecular Pathogenesis in Huntington's Disease. *Biochemistry (Mosc), 83*(9), 1030-1039. doi:10.1134/s0006297918090043

Ip, N. Y., Ibanez, C. F., Nye, S. H., McClain, J., Jones, P. F., Gies, D. R., . . . et al. (1992). Mammalian neurotrophin-4: structure, chromosomal localization, tissue distribution, and receptor specificity. *Proc Natl Acad Sci U S A, 89*(7), 3060-3064. doi:10.1073/pnas.89.7.3060

Ip, N. Y., Stitt, T. N., Tapley, P., Klein, R., Glass, D. J., Fandl, J., . . . Yancopoulos, G. D. (1993). Similarities and differences in the way neurotrophins interact with the Trk receptors in neuronal and nonneuronal cells. *Neuron, 10*(2), 137-149. doi:10.1016/0896-6273(93)90306-c

Issa, S. S., Shaimardanova, A. A., Solovyeva, V. V., & Rizvanov, A. A. (2023). Various AAV Serotypes and Their Applications in Gene Therapy: An Overview. *Cells, 12*(5). doi:10.3390/cells12050785

Jalšić, L., Lytvyn, V., Elahi, S. M., Hrapovic, S., Nassoury, N., Chahal, P. S., . . . Gilbert, R. (2023). Inducible HEK293 AAV packaging cell lines expressing Rep proteins. *Mol Ther Methods Clin Dev, 30*, 259-275. doi:10.1016/j.omtm.2023.07.002

Johnson, D., Lanahan, A., Buck, C. R., Sehgal, A., Morgan, C., Mercer, E., . . . Chao, M. (1986). Expression and structure of the human NGF receptor. *Cell, 47*(4), 545-554. doi:https://doi.org/10.1016/0092-8674(86)90619-7

Jones, K. R., & Reichardt, L. F. (1990). Molecular cloning of a human gene that is a member of the nerve growth factor family. *Proc Natl Acad Sci U S A, 87*(20), 8060-8064. doi:10.1073/pnas.87.20.8060

Joshi, C. R., Labhasetwar, V., & Ghorpade, A. (2017). Destination Brain: the Past, Present, and Future of Therapeutic Gene Delivery. *J Neuroimmune Pharmacol, 12*(1), 51-83. doi:10.1007/s11481-016-9724-3

Joshi, P. R., Wu, N. P., André, V. M., Cummings, D. M., Cepeda, C., Joyce, J. A., . . . Bamford, N. S. (2009). Age-dependent alterations of corticostriatal activity in the YAC128 mouse model of huntington disease. *Journal of Neuroscience, 29*(8), 2414-2427. doi:10.1523/JNEUROSCI.5687-08.2009

Kaplan, D. R., Hempstead, B. L., Martin-Zanca, D., Chao, M. V., & Parada, L. F. (1991). The trk proto-oncogene product: a signal transducing receptor for nerve growth factor. *Science, 252*(5005), 554-558. doi:10.1126/science.1850549

Kaplan, D. R., Martin-Zanca, D., & Parada, L. F. (1991). Tyrosine phosphorylation and tyrosine kinase activity of the trk proto-oncogene product induced by NGF. *Nature, 350*(6314), 158-160. doi:10.1038/350158a0

Kassubek, J., Juengling, F. D., Ecker, D., & Landwehrmeyer, G. B. (2005). Thalamic atrophy in Huntington's disease co-varies with cognitive performance: a morphometric MRI analysis. *Cereb Cortex, 15*(6), 846-853. doi:10.1093/cercor/bhh185

Kells, A. P., Fong, D. M., Dragunow, M., During, M. J., Young, D., & Connor, B. (2004). AAV-mediated gene delivery of BDNF or GDNF is neuroprotective in a model of Huntington disease. *Mol Ther, 9*(5), 682-688. doi:10.1016/j.ymthe.2004.02.016

Kells, A. P., Forsayeth, J., & Bankiewicz, K. S. (2012). Glial-derived neurotrophic factor gene transfer for Parkinson's disease: anterograde distribution of AAV2 vectors in the primate brain. *Neurobiol Dis, 48*(2), 228-235. doi:10.1016/j.nbd.2011.10.004

Kells, A. P., Hadaczek, P., Yin, D., Bringas, J., Varenika, V., Forsayeth, J., & Bankiewicz, K. S. (2009). Efficient gene therapy-based method for the delivery of therapeutics to primate cortex. *Proc Natl Acad Sci U S A, 106*(7), 2407-2411. doi:10.1073/pnas.0810682106

Kells, A. P., Henry, R. A., & Connor, B. (2008). AAV-BDNF mediated attenuation of quinolinic acid-induced neuropathology and motor function impairment. *Gene Ther, 15*(13), 966-977. doi:10.1038/gt.2008.23

Khursigara, G., Bertin, J., Yano, H., Moffett, H., Distefano, P. S., & Chao, M. V. (2001). A Prosurvival Function for the p75 Receptor Death Domain Mediated via the Caspase Recruitment Domain Receptor-Interacting Protein 2. *The Journal of Neuroscience, 21*(16), 5854-5863. doi:10.1523/jneurosci.21-16-05854.2001

Kim, J. H., Lee, S.-R., Li, L.-H., Park, H.-J., Park, J.-H., Lee, K. Y., . . . Choi, S.-Y. (2011). High Cleavage Efficiency of a 2A Peptide Derived from Porcine Teschovirus-1 in Human Cell Lines, Zebrafish and Mice. *PloS one, 6*(4), e18556. doi:10.1371/journal.pone.0018556

Kirschenbaum, B., & Goldman, S. A. (1995). Brain-derived neurotrophic factor promotes the survival of neurons arising from the adult rat forebrain subependymal zone. *Proc Natl Acad Sci U S A, 92*(1), 210-214.

Klein, R., Conway, D., Parada, L. F., & Barbacid, M. (1990). The trkB tyrosine protein kinase gene codes for a second neurogenic receptor that lacks the catalytic kinase domain. *Cell, 61*(4), 647-656. doi:10.1016/0092-8674(90)90476-u

Klein, R., Parada, L. F., Coulier, F., & Barbacid, M. (1989). trkB, a novel tyrosine protein kinase receptor expressed during mouse neural development. *Embo j, 8*(12), 3701-3709.

Kolodziejczyk, K., & Raymond, L. A. (2016). Differential changes in thalamic and cortical excitatory synapses onto striatal spiny projection neurons in a Huntington disease mouse model. *Neurobiol Dis, 86*, 62-74. doi:10.1016/j.nbd.2015.11.020

Komada, M., Takao, K., & Miyakawa, T. (2008). Elevated plus maze for mice. *J Vis Exp*(22). doi:10.3791/1088

Kuhn, A., Goldstein, D. R., Hodges, A., Strand, A. D., Sengstag, T., Kooperberg, C., . . . Luthi-Carter, R. (2007). Mutant huntingtin's effects on striatal gene expression in mice recapitulate changes observed in human Huntington's disease brain and do not differ with mutant huntingtin length or wild-type huntingtin dosage. *Hum Mol Genet, 16*(15), 1845-1861. doi:10.1093/hmg/ddm133

Kumar, V., Bhat, Z. A., & Kumar, D. (2013). Animal models of anxiety: a comprehensive review. *J Pharmacol Toxicol Methods, 68*(2), 175-183. doi:10.1016/j.vascn.2013.05.003

Lamballe, F., Klein, R., & Barbacid, M. (1991). trkC, a new member of the trk family of tyrosine protein kinases, is a receptor for neurotrophin-3. *Cell, 66*(5), 967-979. doi:10.1016/0092-8674(91)90442-2

Landles, C., & Bates, G. P. (2004). Huntingtin and the molecular pathogenesis of Huntington's disease. Fourth in molecular medicine review series. *EMBO Rep, 5*(10), 958-963. doi:10.1038/sj.embor.7400250

Lee, E. J., Guenther, C. M., & Suh, J. (2018). Adeno-Associated Virus (AAV) Vectors: Rational Design Strategies for Capsid Engineering. *Curr Opin Biomed Eng, 7*, 58-63. doi:10.1016/j.cobme.2018.09.004

Levi-Montalcini, R., & Hamburger, V. (1951). Selective growth stimulating effects of mouse sarcoma on the sensory and sympathetic nervous system of the chick embryo. *J Exp Zool, 116*(2), 321-361. doi:10.1002/jez.1401160206

Lewis, J. E., Brameld, J. M., Hill, P., Barrett, P., Ebling, F. J. P., & Jethwa, P. H. (2015). The use of a viral 2A sequence for the simultaneous over-expression of both the vgf gene and enhanced green fluorescent protein (eGFP) in vitro and in vivo. *J Neurosci Methods, 256*, 22-29. doi:https://doi.org/10.1016/j.jneumeth.2015.08.013

Li, J. Y., Popovic, N., & Brundin, P. (2005). The use of the R6 transgenic mouse models of Huntington's disease in attempts to develop novel therapeutic strategies. *NeuroRx, 2*(3), 447-464. doi:10.1602/neurorx.2.3.447

Li, S. F., Wang, R. Z., Meng, Q. H., Li, G. L., Hu, G. J., Dou, W. C., . . . Zhang, Z. X. (2006). Intra-ventricular infusion of rAAV1-EGFP resulted in transduction in multiple regions of adult rat brain: a comparative study with rAAV2 and rAAV5 vectors. *Brain Res, 1122*(1), 1-9. doi:10.1016/j.brainres.2006.09.042

Li, Y. X., Zhang, Y., Lester, H. A., Schuman, E. M., & Davidson, N. (1998). Enhancement of neurotransmitter release induced by brain-derived neurotrophic factor in cultured hippocampal neurons. *J Neurosci, 18*(24), 10231-10240. doi:10.1523/jneurosci.18-24-10231.1998

Lin, Z., Tann, J. Y., Goh, E. T., Kelly, C., Lim, K. B., Gao, J. F., & Ibanez, C. F. (2015). Structural basis of death domain signaling in the p75 neurotrophin receptor. *eLife, 4*, e11692. doi:10.7554/eLife.11692

Liot, G., Zala, D., Pla, P., Mottet, G., Piel, M., & Saudou, F. (2013). Mutant Huntingtin alters retrograde transport of TrkB receptors in striatal dendrites. *J Neurosci, 33*(15), 6298-6309. doi:10.1523/jneurosci.2033-12.2013

Lloret, A., Dragileva, E., Teed, A., Espinola, J., Fossale, E., Gillis, T., . . . Wheeler, V. C. (2006). Genetic background modifies nuclear mutant huntingtin accumulation and HD CAG repeat instability in Huntington's disease knock-in mice. *Hum Mol Genet, 15*(12), 2015-2024. doi:10.1093/hmg/ddl125

Lowery, R. L., & Majewska, A. K. (2010). Intracranial injection of adeno-associated viral vectors. *J Vis Exp*(45). doi:10.3791/2140

Lüesse, H.-G., Schiefer, J., Spruenken, A., Puls, C., Block, F., & Kosinski, C. M. (2001). Evaluation of R6/2 HD transgenic mice for therapeutic studies in Huntington's disease: behavioral testing and impact of diabetes mellitus. *Behavioural Brain Research, 126*(1), 185-195. doi:https://doi.org/10.1016/S0166-4328(01)00261-3

Luthi-Carter, R., Strand, A., Peters, N. L., Solano, S. M., Hollingsworth, Z. R., Menon, A. S., . . . Olson, J. M. (2000). Decreased expression of striatal signaling genes in a mouse model of Huntington's disease. *Hum Mol Genet, 9*(9), 1259-1271. doi:10.1093/hmg/9.9.1259

Lyons, W. E., Mamounas, L. A., Ricaurte, G. A., Coppola, V., Reid, S. W., Bora, S. H., . . . Tessarollo, L. (1999). Brain-derived neurotrophic factor-deficient mice develop aggressiveness and hyperphagia in conjunction with brain serotonergic abnormalities. *Proc Natl Acad Sci U S A, 96*(26), 15239-15244. doi:10.1073/pnas.96.26.15239

Mahadeo, D., Kaplan, L., Chao, M. V., & Hempstead, B. L. (1994). High affinity nerve growth factor binding displays a faster rate of association than p140trk binding. Implications for multi-subunit polypeptide receptors. *J Biol Chem, 269*(9), 6884-6891.

Mandelbaum, G., Taranda, J., Haynes, T. M., Hochbaum, D. R., Huang, K. W., Hyun, M., . . . Sabatini, B. L. (2019). Distinct Cortical-Thalamic-Striatal Circuits through the Parafascicular Nucleus. *Neuron, 102*(3), 636-652.e637. doi:10.1016/j.neuron.2019.02.035

Mangiarini, L., Sathasivam, K., Seller, M., Cozens, B., Harper, A., Hetherington, C., . . . Bates, G. P. (1996). Exon 1 of the HD gene with an expanded CAG repeat is sufficient to cause a progressive neurological phenotype in transgenic mice. *Cell, 87*(3), 493-506.

Martin-Zanca, D., Hughes, S. H., & Barbacid, M. (1986). A human oncogene formed by the fusion of truncated tropomyosin and protein tyrosine kinase sequences. *Nature, 319*(6056), 743-748. doi:10.1038/319743a0

Matusica, D., Skeldal, S., Sykes, A. M., Palstra, N., Sharma, A., & Coulson, E. J. (2013). An Intracellular Domain Fragment of the p75 Neurotrophin Receptor (p75NTR) Enhances Tropomyosin Receptor Kinase A (TrkA) Receptor Function. *Journal of Biological Chemistry, 288*(16), 11144-11154. doi:10.1074/jbc.m112.436469

McBride, J. L., During, M. J., Wuu, J., Chen, E. Y., Leurgans, S. E., & Kordower, J. H. (2003). Structural and functional neuroprotection in a rat model of Huntington's disease by viral gene transfer of GDNF. *Exp Neurol, 181*(2), 213-223. doi:10.1016/s0014-4886(03)00044-x

McLaughlin, S. K., Collis, P., Hermonat, P. L., & Muzyczka, N. (1988). Adeno-associated virus general transduction vectors: analysis of proviral structures. *J Virol, 62*(6), 1963-1973. doi:10.1128/jvi.62.6.1963-1973.1988

Meakin, S. O., Macdonald, J. I. S., Gryz, E. A., Kubu, C. J., & Verdi, J. M. (1999). The Signaling Adapter FRS-2 Competes with Shc for Binding to the Nerve Growth Factor Receptor TrkA. *Journal of Biological Chemistry, 274*(14), 9861-9870. doi:10.1074/jbc.274.14.9861

Meldolesi, J. (2017). Neurotrophin Receptors in the Pathogenesis, Diagnosis and Therapy of Neurodegenerative Diseases. *Pharmacological Research*. doi:10.1016/j.phrs.2017.04.024

Menalled, L., El-Khodor, B. F., Patry, M., Suárez-Fariñas, M., Orenstein, S. J., Zahasky, B., . . . Brunner, D. (2009). Systematic behavioral evaluation of Huntington's disease transgenic and knock-in mouse models. *Neurobiology of Disease, 35*(3), 319-336. doi:10.1016/j.nbd.2009.05.007

Menalled, L. B., & Chesselet, M.-F. (2002). Mouse models of Huntington's disease. *Trends in Pharmacological Sciences, 23*(1), 32-39. doi:https://doi.org/10.1016/S0165-6147(00)01884-8

Metzler, M., Legendre-Guillemin, V., Gan, L., Chopra, V., Kwok, A., McPherson, P. S., & Hayden, M. R. (2001). HIP1 Functions in Clathrin-mediated Endocytosis through Binding to Clathrin and Adaptor Protein 2*. *Journal of Biological Chemistry, 276*(42), 39271-39276. doi:https://doi.org/10.1074/jbc.C100401200

Michaël, H., Laura, G., Mickael, A., Samantha, P., & Nathalie, C. (2016). Adeno-Associated Virus-Based Gene Therapy for CNS Diseases. *27*(7), 478-496. doi:10.1089/hum.2016.087

Milnerwood, A. J., Gladding, C. M., Pouladi, M. A., Kaufman, A. M., Hines, R. M., Boyd, J. D., . . . Raymond, L. A. (2010). Early Increase in Extrasynaptic NMDA Receptor Signaling and Expression Contributes to Phenotype Onset in Huntington's Disease Mice. *Neuron, 65*(2), 178-190. doi:https://doi.org/10.1016/j.neuron.2010.01.008

Miranda, M., Morici, J. F., Zanoni, M. B., & Bekinschtein, P. (2019). Brain-Derived Neurotrophic Factor: A Key Molecule for Memory in the Healthy and the Pathological Brain. *Front Cell Neurosci, 13*. doi:10.3389/fncel.2019.00363

Muhuri, M., Zhan, W., Maeda, Y., Li, J., Lotun, A., Chen, J., . . . Gao, G. (2021). Novel Combinatorial MicroRNA-Binding Sites in AAV Vectors Synergistically Diminish Antigen Presentation and Transgene Immunity for Efficient and Stable Transduction. *Front Immunol, 12*, 674242. doi:10.3389/fimmu.2021.674242

Nasir, J., Floresco, S. B., O'Kusky, J. R., Diewert, V. M., Richman, J. M., Zeisler, J., . . . Hayden, M. R. (1995). Targeted disruption of the Huntington's disease gene results in embryonic lethality and behavioral and morphological changes in heterozygotes. *Cell, 81*(5), 811-823.

Nguyen, K. Q., Rymar, V. V., & Sadikot, A. F. (2016). Impaired TrkB Signaling Underlies Reduced BDNF-Mediated Trophic Support of Striatal Neurons in the R6/2 Mouse Model of Huntington's Disease. *Front Cell Neurosci, 10*, 37. doi:10.3389/fncel.2016.00037

Nonnenmacher, M., & Weber, T. (2011). Adeno-associated virus 2 infection requires endocytosis through the CLIC/GEEC pathway. *Cell Host Microbe, 10*(6), 563-576. doi:10.1016/j.chom.2011.10.014

Nonnenmacher, M., & Weber, T. (2012). Intracellular transport of recombinant adeno-associated virus vectors. *Gene Ther, 19*(6), 649-658. doi:10.1038/gt.2012.6

Oumesmar, B. N., Vignais, L., & Baron-Van Evercooren, A. (1997). Developmental Expression of Platelet-Derived Growth Factor α-Receptor in Neurons and Glial Cells of the Mouse CNS. *The Journal of Neuroscience, 17*(1), 125-139. doi:10.1523/jneurosci.17-01-00125.1997

Paré, D., Smith, Y., Parent, A., & Steriade, M. (1988). Projections of brainstem core cholinergic and non-cholinergic neurons of cat to intralaminar and reticular thalamic nuclei. *Neuroscience, 25*(1), 69-86. doi:10.1016/0306-4522(88)90007-3

Parievsky, A., Moore, C., Kamdjou, T., Cepeda, C., Meshul, C. K., & Levine, M. S. (2017). Differential electrophysiological and morphological alterations of thalamostriatal and corticostriatal projections in the R6/2 mouse model of Huntington's disease. *Neurobiol Dis, 108*, 29-44. doi:10.1016/j.nbd.2017.07.020

Pasquale, G. D., Davidson, B. L., Stein, C. S., Martins, I., Scudiero, D., Monks, A., & Chiorini, J. A. (2003). Identification of PDGFR as a receptor for AAV-5 transduction. *Nature Medicine, 9*(10), 1306-1312. doi:10.1038/nm929

Pearson, T. S., Gupta, N., San Sebastian, W., Imamura-Ching, J., Viehoever, A., Grijalvo-Perez, A., . . . Bankiewicz, K. S. (2021). Gene therapy for aromatic L-amino acid decarboxylase deficiency by MR-guided direct delivery of AAV2-AADC to midbrain dopaminergic neurons. *Nat Commun, 12*(1), 4251. doi:10.1038/s41467-021-24524-8

Pietropaolo, S., Delage, P., Cayzac, S., Crusio, W. E., & Cho, Y. H. (2011). Sex-dependent changes in social behaviors in motor pre-symptomatic R6/1 mice. *PloS one, 6*(5), e19965. doi:10.1371/journal.pone.0019965

Pillay, S., Meyer, N. L., Puschnik, A. S., Davulcu, O., Diep, J., Ishikawa, Y., . . . Carette, J. E. (2016). An essential receptor for adeno-associated virus infection. *Nature, 530*(7588), 108-112. doi:10.1038/nature16465

Pla, P., Orvoen, S., Benstaali, C., Dodier, S., Gardier, A. M., David, D. J., . . . Saudou, F. (2013). Huntingtin acts non cell-autonomously on hippocampal neurogenesis and controls anxiety-related behaviors in adult mouse. *PloS one, 8*(9), e73902. doi:10.1371/journal.pone.0073902

Pla, P., Orvoen, S., Saudou, F., David, D. J., & Humbert, S. (2014). Mood disorders in Huntington's disease: from behavior to cellular and molecular mechanisms. *Frontiers in Behavioral Neuroscience, 8*. doi:10.3389/fnbeh.2014.00135

Powell, S. K., Rivera-Soto, R., & Gray, S. J. (2015). Viral expression cassette elements to enhance transgene target specificity and expression in gene therapy. *Discov Med, 19*(102), 49-57.

Ramaswamy, S., & Kordower, J. H. (2012). Gene therapy for Huntington's disease. *Neurobiology of Disease, 48*(2), 243-254. doi:https://doi.org/10.1016/j.nbd.2011.12.030

Ramaswamy, S., McBride, J. L., Han, I., Berry-Kravis, E. M., Zhou, L., Herzog, C. D., . . . Kordower, J. H. (2009). Intrastriatal CERE-120 (AAV-Neurturin) protects striatal and cortical neurons and delays motor deficits in a transgenic mouse model of Huntington's disease. *Neurobiol Dis, 34*(1), 40-50. doi:10.1016/j.nbd.2008.12.005

Rangone, H., Humbert, S., & Saudou, F. (2004). Huntington's disease: how does huntingtin, an anti-apoptotic protein, become toxic? *Pathol Biol (Paris), 52*(6), 338-342. doi:10.1016/j.patbio.2003.06.004

Rawlins, M. D., Wexler, N. S., Wexler, A. R., Tabrizi, S. J., Douglas, I., Evans, S. J., & Smeeth, L. (2016). The Prevalence of Huntington's Disease. *Neuroepidemiology, 46*(2), 144-153. doi:10.1159/000443738

Reddy, P. H., Williams, M., Charles, V., Garrett, L., Pike-Buchanan, L., Whetsell, W. O., . . . Tagle, D. A. (1998). Behavioural abnormalities and selective neuronal loss in HD transgenic mice expressing mutated full-length HD cDNA. *Nature Genetics, 20*(2), 198-202. doi:10.1038/2510

Reiner, A., Albin, R. L., Anderson, K. D., D'Amato, C. J., Penney, J. B., & Young, A. B. (1988). Differential loss of striatal projection neurons in Huntington disease. *Proc Natl Acad Sci U S A, 85*(15), 5733-5737. doi:10.1073/pnas.85.15.5733

Reiner, A., & Deng, Y. P. (2018). Disrupted striatal neuron inputs and outputs in Huntington's disease. *CNS Neurosci Ther, 24*(4), 250-280. doi:10.1111/cns.12844

Reiner, A., Dragatsis, I., & Dietrich, P. (2011). Genetics and neuropathology of Huntington's disease. *Int Rev Neurobiol, 98*, 325-372. doi:10.1016/b978-0-12-381328-2.00014-6

Reiner, A., Shelby, E., Wang, H., Demarch, Z., Deng, Y., Guley, N. H., . . . Faull, R. L. (2013). Striatal parvalbuminergic neurons are lost in Huntington's disease: implications for dystonia. *Mov Disord, 28*(12), 1691-1699. doi:10.1002/mds.25624

Reiner, A., Veenman, C. L., Medina, L., Jiao, Y., Del Mar, N., & Honig, M. G. (2000). Pathway tracing using biotinylated dextran amines. *J Neurosci Methods, 103*(1), 23-37.

Roux, P. P., Bhakar, A. L., Kennedy, T. E., & Barker, P. A. (2001). The p75 Neurotrophin Receptor Activates Akt (Protein Kinase B) through a Phosphatidylinositol 3-Kinase-dependent Pathway. *Journal of Biological Chemistry, 276*(25), 23097-23104. doi:10.1074/jbc.m011520200

Roux, P. P., Colicos, M. A., Barker, P. A., & Kennedy, T. E. (1999). p75 neurotrophin receptor expression is induced in apoptotic neurons after seizure. *J Neurosci, 19*(16), 6887-6896.

Sadikot, A. F., Parent, A., & François, C. (1992). Efferent connections of the centromedian and parafascicular thalamic nuclei in the squirrel monkey: a PHA-L study of subcortical projections. *J Comp Neurol, 315*(2), 137-159. doi:10.1002/cne.903150203

Sadikot, A. F., Parent, A., Smith, Y., & Bolam, J. P. (1992). Efferent connections of the centromedian and parafascicular thalamic nuclei in the squirrel monkey: a light and electron microscopic study of the thalamostriatal projection in relation to striatal heterogeneity. *J Comp Neurol, 320*(2), 228-242. doi:10.1002/cne.903200207

Sadikot, A. F., & Rymar, V. V. (2009). The primate centromedian-parafascicular complex: anatomical organization with a note on neuromodulation. *Brain Res Bull, 78*(2-3), 122-130. doi:10.1016/j.brainresbull.2008.09.016

Samadi, P., Boutet, A., Rymar, V. V., Rawal, K., Maheux, J., Kvann, J. C., . . . Sadikot, A. F. (2013). Relationship between BDNF expression in major striatal afferents, striatum morphology and motor behavior in the R6/2 mouse model of Huntington's disease. *Genes Brain Behav, 12*(1), 108-124. doi:10.1111/j.1601-183X.2012.00858.x

Samaranch, L., Blits, B., San Sebastian, W., Hadaczek, P., Bringas, J., Sudhakar, V., . . . Bankiewicz, K. S. (2017). MR-guided parenchymal delivery of adeno-associated viral vector serotype 5 in non-human primate brain. *Gene Ther, 24*(4), 253-261. doi:10.1038/gt.2017.14

Samaranch, L., Sebastian, W. S., Kells, A. P., Salegio, E. A., Heller, G., Bringas, J. R., . . . Bankiewicz, K. S. (2014). AAV9-mediated Expression of a Non-self Protein in Nonhuman Primate Central Nervous System Triggers Widespread Neuroinflammation Driven by Antigen-presenting Cell Transduction. *Molecular Therapy, 22*(2), 329-337. doi:10.1038/mt.2013.266

Samulski, R. J., & Muzyczka, N. (2014). AAV-Mediated Gene Therapy for Research and Therapeutic Purposes. *Annu Rev Virol, 1*(1), 427-451. doi:10.1146/annurev-virology-031413-085355

Saudou, F., Finkbeiner, S., Devys, D., & Greenberg, M. E. (1998). Huntingtin Acts in the Nucleus to Induce Apoptosis but Death Does Not Correlate with the Formation of Intranuclear Inclusions. *Cell, 95*(1), 55-66. doi:https://doi.org/10.1016/S0092-8674(00)81782-1

Savolainen, M., Emerich, D., & Kordower, J. H. (2018). Disease Modification Through Trophic Factor Delivery. *Methods Mol Biol, 1780*, 525-547. doi:10.1007/978-1-4939-7825-0_24

Schulte, J., & Littleton, J. T. (2011). The biological function of the Huntingtin protein and its relevance to Huntington's Disease pathology. *Curr Trends Neurol, 5*, 65-78.

Shear, D. A., Dong, J., Gundy, C. D., Haik-Creguer, K. L., & Dunbar, G. L. (1998). Comparison of intrastriatal injections of quinolinic acid and 3-nitropropionic acid for use in animal models of Huntington's disease. *Prog Neuropsychopharmacol Biol Psychiatry, 22*(7), 1217-1240. doi:10.1016/s0278-5846(98)00070-0

Shen, S., Bryant, K. D., Brown, S. M., Randell, S. H., & Asokan, A. (2011). Terminal N-linked galactose is the primary receptor for adeno-associated virus 9. *J Biol Chem, 286*(15), 13532-13540. doi:10.1074/jbc.M110.210922

Sil, S., Periyasamy, P., Thangaraj, A., Chivero, E. T., & Buch, S. (2018). PDGF/PDGFR axis in the neural systems. *Mol Aspects Med, 62*, 63-74. doi:10.1016/j.mam.2018.01.006

Simmons, D. A. (2017). Modulating Neurotrophin Receptor Signaling as a Therapeutic Strategy for Huntington's Disease. *J Huntingtons Dis, 6*(4), 303-325. doi:10.3233/jhd-170275

Skaper, S. D. (2008). The biology of neurotrophins, signalling pathways, and functional peptide mimetics of neurotrophins and their receptors. *CNS Neurol Disord Drug Targets, 7*(1), 46-62. doi:10.2174/187152708783885174

Smith, R., Chung, H., Rundquist, S., Maat-Schieman, M. L., Colgan, L., Englund, E., . . . Li, J. Y. (2006). Cholinergic neuronal defect without cell loss in Huntington's disease. *Hum Mol Genet, 15*(21), 3119-3131. doi:10.1093/hmg/ddl252

Smith, Y., Galvan, A., Ellender, T. J., Doig, N., Villalba, R. M., Huerta-Ocampo, I., . . . Bolam, J. P. (2014). The thalamostriatal system in normal and diseased states. *Front Syst Neurosci, 8*, 5. doi:10.3389/fnsys.2014.00005

Smith, Y., Raju, D. V., Pare, J. F., & Sidibe, M. (2004). The thalamostriatal system: a highly specific network of the basal ganglia circuitry. *Trends Neurosci, 27*(9), 520-527. doi:10.1016/j.tins.2004.07.004

Sonntag, F., Bleker, S., Leuchs, B., Fischer, R., & Kleinschmidt, J. A. (2006). Adeno-associated virus type 2 capsids with externalized VP1/VP2 trafficking domains are generated prior to passage through the cytoplasm and are maintained until uncoating occurs in the nucleus. *J Virol, 80*(22), 11040-11054. doi:10.1128/jvi.01056-06

Srivastava, A., Lusby, E. W., & Berns, K. I. (1983). Nucleotide sequence and organization of the adeno-associated virus 2 genome. *J Virol, 45*(2), 555-564. doi:10.1128/jvi.45.2.555-564.1983

Stael, S., Miller, L. P., Fernández-Fernández Á, D., & Van Breusegem, F. (2022). Detection of Damage-Activated Metacaspase Activity by Western Blot in Plants. *Methods Mol Biol, 2447*, 127-137. doi:10.1007/978-1-0716-2079-3_11

Strand, A. D., Baquet, Z. C., Aragaki, A. K., Holmans, P., Yang, L., Cleren, C., . . . Jones, K. R. (2007). Expression profiling of Huntington's disease models suggests that brain-derived neurotrophic factor depletion plays a major role in striatal degeneration. *J Neurosci, 27*(43), 11758-11768. doi:10.1523/jneurosci.2461-07.2007

Tabebordbar, M., Lagerborg, K. A., Stanton, A., King, E. M., Ye, S., Tellez, L., . . . Sabeti, P. C. (2021). Directed evolution of a family of AAV capsid variants enabling potent muscle-directed gene delivery across species. *Cell, 184*(19), 4919-4938.e4922. doi:10.1016/j.cell.2021.08.028

Tanaka, T., Saito, H., & Matsuki, N. (1997). Inhibition of GABAA synaptic responses by brain-derived neurotrophic factor (BDNF) in rat hippocampus. *J Neurosci, 17*(9), 2959-2966. doi:10.1523/jneurosci.17-09-02959.1997

Torres-Cruz, F. M., César Vivar-Cortés, I., Moran, I., Mendoza, E., Gómez-Pineda, V., García-Sierra, F., & Hernández-Echeagaray, E. (2019). NT-4/5 antagonizes the BDNF modulation of corticostriatal transmission: Role of the TrkB.T1 receptor. *CNS Neurosci Ther, 25*(5), 621-631. doi:10.1111/cns.13091

Túnez, I., Tasset, I., Pérez-De La Cruz, V., & Santamaría, A. (2010). 3-Nitropropionic acid as a tool to study the mechanisms involved in Huntington's disease: past, present and future. *Molecules, 15*(2), 878-916. doi:10.3390/molecules15020878

Underwood, C. K., Reid, K., May, L. M., Bartlett, P. F., & Coulson, E. J. (2008). Palmitoylation of the C-terminal fragment of p75NTR regulates death signaling and is required for subsequent cleavage by γ-secretase. *Molecular and Cellular Neuroscience, 37*(2), 346-358. doi:10.1016/j.mcn.2007.10.005

Velier, J., Kim, M., Schwarz, C., Kim, T. W., Sapp, E., Chase, K., . . . DiFiglia, M. (1998). Wild-Type and Mutant Huntingtins Function in Vesicle Trafficking in the Secretory and Endocytic Pathways. *Experimental Neurology, 152*(1), 34-40. doi:https://doi.org/10.1006/exnr.1998.6832

Vilar, M. (2017). Chapter Four - Structural Characterization of the p75 Neurotrophin Receptor: A Stranger in the TNFR Superfamily. In G. Litwack (Ed.), *Vitamins and Hormones* (Vol. 104, pp. 57-87): Academic Press.

Von Bartheld, C. S., Byers, M. R., Williams, R., & Bothwell, M. (1996). Anterograde transport of neurotrophins and axodendritic transfer in the developing visual system. *Nature, 379*(6568), 830-833. doi:10.1038/379830a0

Walker, F. O. (2007). Huntington's disease. *Lancet, 369*(9557), 218-228. doi:10.1016/s0140-6736(07)60111-1

Wang, J., Bastle, R. M., Bass, C. E., Hammer, R. P., Jr., Neisewander, J. L., & Nikulina, E. M. (2016). Overexpression of BDNF in the ventral tegmental area enhances binge cocaine self-administration in rats exposed to repeated social defeat. *Neuropharmacology, 109*, 121-130. doi:10.1016/j.neuropharm.2016.04.045

Wang, J. H., Gessler, D. J., Zhan, W., Gallagher, T. L., & Gao, G. (2024). Adeno-associated virus as a delivery vector for gene therapy of human diseases. *Signal Transduct Target Ther, 9*(1), 78. doi:10.1038/s41392-024-01780-w

Watakabe, A., Ohtsuka, M., Kinoshita, M., Takaji, M., Isa, K., Mizukami, H., . . . Yamamori, T. (2015). Comparative analyses of adeno-associated viral vector serotypes 1, 2, 5, 8 and 9 in marmoset, mouse and macaque cerebral cortex. *Neuroscience Research, 93*, 144-157. doi:https://doi.org/10.1016/j.neures.2014.09.002

Watson, F. L., Heerssen, H. M., Bhattacharyya, A., Klesse, L., Lin, M. Z., & Segal, R. A. (2001). Neurotrophins use the Erk5 pathway to mediate a retrograde survival response. *Nature Neuroscience, 4*(10), 981-988. doi:10.1038/nn720

Xiao, Y., Muhuri, M., Li, S., Qin, W., Xu, G., Luo, L., . . . Gao, G. (2019). Circumventing cellular immunity by miR142-mediated regulation sufficiently supports rAAV-delivered OVA expression without activating humoral immunity. *JCI Insight, 5*(13). doi:10.1172/jci.insight.99052

Xie, J., Xie, Q., Zhang, H., Ameres, S. L., Hung, J. H., Su, Q., . . . Gao, G. (2011). MicroRNA-regulated, systemically delivered rAAV9: a step closer to CNS-restricted transgene expression. *Mol Ther, 19*(3), 526-535. doi:10.1038/mt.2010.279

Xie, Q., Ma, H., Chen, X., Zhu, Y., Ma, Y., Jalinous, L., . . . Xie, J. (2022). *Endogenous human SMN1 promoter-driven gene replacement improves the efficacy and safety of AAV9-mediated gene therapy for spinal muscular atrophy (SMA) in mice.* Paper presented at the Human Gene Therapy.

Yano, H., Lee, F. S., Kong, H., Chuang, J.-Z., Arevalo, J. C., Perez, P., . . . Chao, M. V. (2001). Association of Trk Neurotrophin Receptors with Components of the Cytoplasmic Dynein Motor. *The Journal of Neuroscience, 21*(3), RC125-RC125. doi:10.1523/jneurosci.21-03-j0003.2001

Zhou, X. F., & Rush, R. A. (1996). Endogenous brain-derived neurotrophic factor is anterogradely transported in primary sensory neurons. *Neuroscience, 74*(4), 945-951. doi:10.1016/0306-4522(96)00237-0

Ziemlińska, E., Kügler, S., Schachner, M., Wewiór, I., Czarkowska-Bauch, J., & Skup, M. (2014). Overexpression of BDNF Increases Excitability of the Lumbar Spinal Network and Leads to Robust Early Locomotor Recovery in Completely Spinalized Rats. *PloS one, 9*(2), e88833. doi:10.1371/journal.pone.0088833

Zincarelli, C., Soltys, S., Rengo, G., & Rabinowitz, J. E. (2008). Analysis of AAV Serotypes 1–9 Mediated Gene Expression and Tropism in Mice After Systemic Injection. *Molecular Therapy, 16*(6), 1073-1080. doi:https://doi.org/10.1038/mt.2008.76

Zuccato, C., & Cattaneo, E. (2009). Brain-derived neurotrophic factor in neurodegenerative diseases. *Nat Rev Neurol, 5*(6), 311-322. doi:10.1038/nrneurol.2009.54

Zuccato, C., Ciammola, A., Rigamonti, D., Leavitt, B. R., & et al. (2001). Loss of Huntingtin-mediated BDNF gene transcription in Huntington's disease. *Science, 293*(5529), 493-498. Retrieved from

https://proxy.library.mcgill.ca/login?url=https://www.proquest.com/scholarly-journals/loss-huntingtin-mediated-bdnf-gene-transcription/docview/213574642/se-2?accountid=12339

https://mcgill.on.worldcat.org/atoztitles/link?sid=ProQ:&issn=00368075&volume=293&issue=5529&title=Loss+of+Huntingtin-mediated+BDNF+gene+transcription+in+Huntington%27s+disease&spage=493&date=2001&atitle=Loss+of+Huntingtin-mediated+BDNF+gene+transcription+in+Huntington%27s+disease&au=Zuccato%2C+Chiara%3BCiammola%2C+Andrea%3BRigamonti%2C+Dorotea%3BLeavitt%2C+Blair+R%3Bet+al&id=&isbn=

Zuccato, C., Marullo, M., Conforti, P., MacDonald, M. E., Tartari, M., & Cattaneo, E. (2008). Systematic assessment of BDNF and its receptor levels in human cortices affected by Huntington's disease. *Brain Pathol, 18*(2), 225-238. doi:10.1111/j.1750-3639.2007.00111.x

Zuccato, C., Valenza, M., & Cattaneo, E. (2010). Molecular mechanisms and potential therapeutical targets in Huntington's disease. *Physiol Rev, 90*(3), 905-981. doi:10.1152/physrev.00041.2009